TECHNOLOGY DEPT.

PUBLIC LIBRARY
MAR 10 1941
DETROIT

JOURNAL OF APPLIED PHYSICS

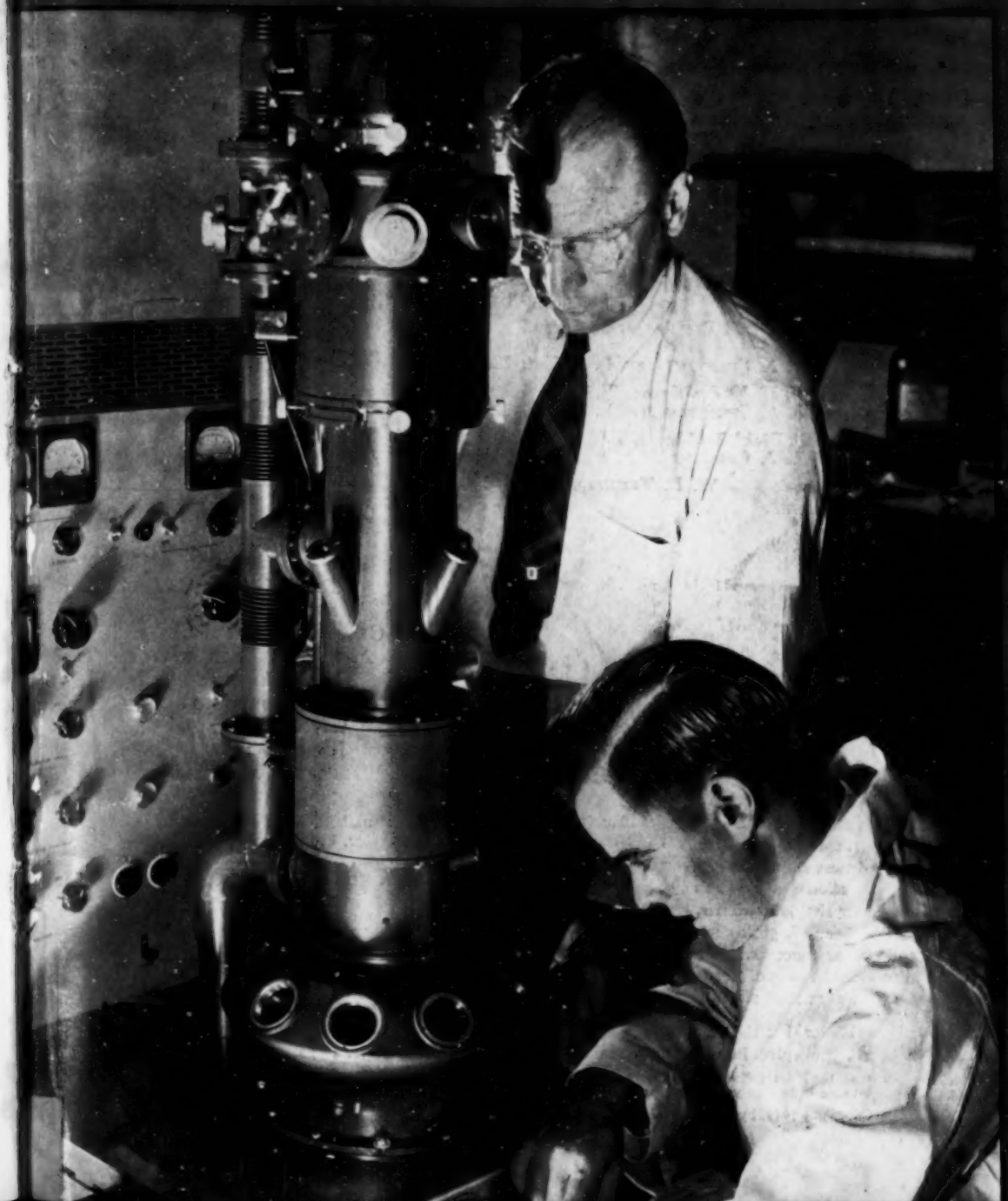

MARCH
1941
Vol. 12 No. 3

New Electron Microscope Magnifying up to 100,000 Diameters

Courtesy RCA Manufacturing Company, Inc.

JOURNAL
OF
APPLIED PHYSICS

MARCH, 1941 Vol. 12, No. 3

In This Issue

	Page
Research and Defense Preparation	169
Theory of the Plastic Properties of Solids. II. FREDERICK SEITZ AND T. A. READ	170
Contributed Original Research	
X-Ray Study of the Changes that Occur in Aluminum During the Process of Fatiguing RAYMOND G. SPENCER AND J. WALLACE MARSHALL	191
Use of the Radioactive Properties of Thorium for a Quantitative Study of Phagocytosis F. A. MAXFIELD AND O. A. MORTENSEN	197
***p*H Determinations on Sludge of Particulate Carbonaceous Materials and Ash Discharged in the Atmosphere by Fuel Burning Sources** S. BLOOMENTHAL AND I. A. DEUTCH	202
Some Useful X-Ray Data EUGENE W. PIKE	206
Cathode Spot Initiation on a Mercury Pool by Means of an External Grid MARK A. TOWNSEND	209
Effect of X-Rays on the Breakdown Strength and Flashover Voltage of Certain Dielectrics ERIC A. WALKER	215
Electromagnetic Waves in Transformer Coils Treated by Maxwell's Equations REINHOLD RÜDENBERG	219
Steady-State Solutions of Electromagnetic Field Problems. I. Forced Oscillations of a Cylindrical Conductor J. A. STRATTON AND L. J. CHU	230
Steady-State Solutions of Electromagnetic Field Problems. II. Forced Oscillations of a Conducting Sphere J. A. STRATTON AND L. J. CHU	236
Steady-State Solutions of Electromagnetic Field Problems. III. Forced Oscillations of a Prolate Spheroid L. J. CHU AND J. A. STRATTON	241
Relaxation of Metals at High Temperatures W. E. TRUMPLER, JR.	248
Engineering Defense Training Program	254
Letter to the Editor	
On the Resistance to the Uniform Motion of a Solid Through a Viscous Liquid JOHN T. BURWELL, JR.	257
In Every Issue	
Here and There	187
Contributors to This Issue	189
New Books	190
Calendar of Meetings	258
Index to Advertisers	vi

BOARD OF EDITORS

ELMER HUTCHISSON,
Editor

Associate Editors

FRANCIS BITTER
W. F. BUSSE
ROBLEY D. EVANS
MORRIS MUSKAT
B. E. WARREN
J. B. WHITEHEAD

Publication of the American Institute of Physics

ADMINISTRATIVE STAFF

HENRY A. BARTON,
Director

MADELINE M. MITCHELL,
Publications Manager

JOHN T. TATE,
Adviser on Publications

GOVERNING BOARD

PAUL E. KLOPSTEG,
Chairman
GEORGE B. PEGRAM,
Secretary
KARL T. COMPTON
WHEELER P. DAVEY
FLOYD A. FIRESTONE
HARVEY FLETCHER
R. C. GIBBS
ARTHUR C. HARDY
GEORGE R. HARRISON
A. STUART HUNTER
H. R. LILLIE
A. G. WORTHING
W. B. RAYTON
JOHN T. TATE
WALLACE WATERFALL

The JOURNAL OF APPLIED PHYSICS, published monthly at Prince and Lemon Sts., Lancaster, Pa., is devoted to physics in its role as the science basic to other natural sciences and to the arts and industries. Previous to 1937 this publication was known as PHYSICS. It aims to be of service not only in physical laboratories, but also in the laboratories of industrial, chemical, geological, geophysical, meteorological, radio, and similar concerns. The JOURNAL OF APPLIED PHYSICS publishes editorials, news of physicists and reviews, as well as technical papers of applied physics.

Manuscripts should be submitted to Elmer Hutchisson, Editor, University of Pittsburgh, Pittsburgh, Pennsylvania.

Subscriptions and orders for back numbers should be addressed to Prince and Lemon Streets, Lancaster, Pa. or to the American Institute of Physics, 175 Fifth Avenue, New York, N. Y.

SUBSCRIPTION PRICE

	U. S. AND CANADA	ELSEWHERE
To members of scientific societies	$5.00	$5.70
To all others	7.00	7.70

Single copies are $.70 each.

Changes of address and proofs should be addressed to the Publications Manager.

Advertising rates supplied on request. Orders, advertising copy and cuts should be sent to the American Institute of Physics.

Entered as second class matter at the Post Office at Lancaster, Pennsylvania, under the Act of March 3, 1897.
Accepted for mailing at the special rate of postage provided for in the Act of February 28, 1925, authorized May 2, 1932.

Copyright 1941, by the American Institute of Physics.

Under salt water for an hour this Type K Potentiometer (arrow) was returned to the factory for repair. Restored to its original accuracy, it is again in use.

Water-Soaked Potentiometer Restored to Full Accuracy

When the flood subsided after the New England hurricane of 1938, the men at the Marine Biological Laboratory, Woods Hole, Mass., began to take stock of the damage. To their disappointment, they found that one of their Type K Potentiometers, used to calibrate ammeters, voltmeters and wattmeters, had been under salt water for an hour. Corrosion soon began to appear, and the potentiometer seemed a total loss.

After a thorough inspection, however, some resistors were replaced, and salt deposits thoroughly removed from the top plate and case. The reconditioned instrument is again in use, at its original accuracy.

EARLY TYPE K TURNS UP

In addition to the calibrating potentiometer, there's another interesting Type K at the Laboratory . . . serial number 10141 . . . purchased in 1908 by a power company. Where it has been since, and how it got to Woods Hole, is a lost story. But even after 32 years, this Type K is still in first-class mechanical condition. And electrically, the initial stability of its resistors has increased with age. It stands as a tribute to the skill and care of the instrument makers of another generation.

Some of these men are still working at L&N with modern materials and, with this unique background of experience, today's instruments can be expected to serve even longer.

CONDENSED CATALOG

Type K Potentiometers are described in Catalog E-50B(3), sent on request.

Jrl Ad E(14)

110 RESISTANCE STANDARDS GUARD L&N ACCURACY

Stock Instruments Used in Making And Calibrating Other Equipment

L&N's working standards of resistance are checked against other L&N resistors used as primary standards. Working and primary standards are identical to stock instruments except for these periodic records of resistance.

There are 92 working standards of resistance at L&N . . . 18 primary standards. Working units are checked against primary units every 4 months. Primary units are certified at the National Bureau of Standards every year. Resistance of all is very constant. In practically every case the variation from year to year is well within the limit of error of the comparison.

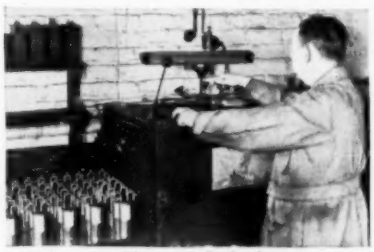

Checking working standards in a constant (±0.1 C) temperature chamber at the L&N plant, Phila., Pa. Switches are turned and standards moved by rods projecting through the chamber.

Used in calibrating every L&N instrument, these standards are typical of the constancy of L&N equipment in general. Many other L&N instruments are also used as primary and working standards. All are described in Catalog E which will be sent on request.

LEEDS & NORTHRUP COMPANY, 4978 STENTON AVE., PHILA., PA.

LEEDS & NORTHRUP

Measuring Instruments · Telemeters · Automatic Controls · Heat Treating Furnaces

Precise Measurements of Frequency with G-R Measuring Equipment

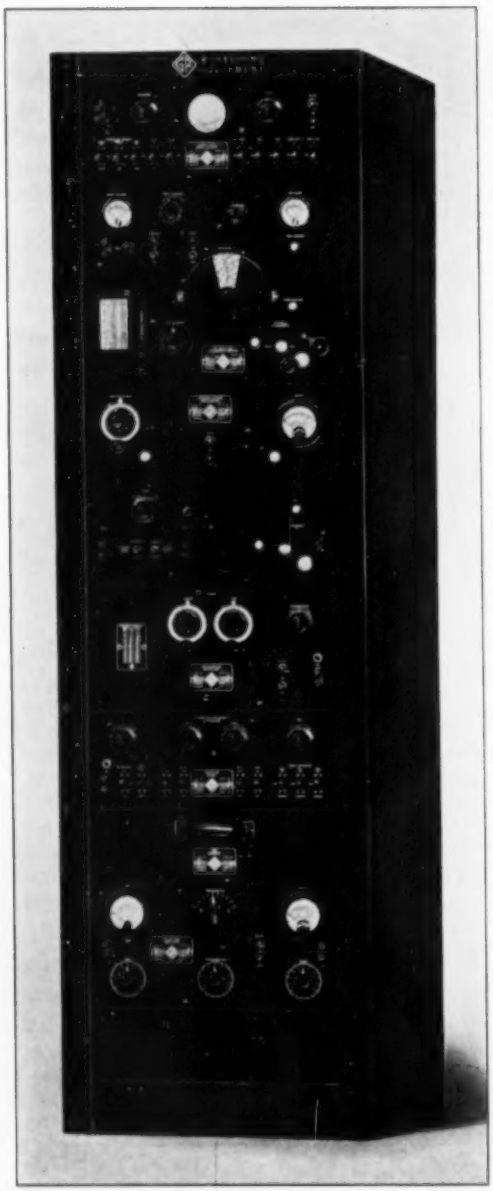

FROM THE G-R PRIMARY STANDARD OF FREQUENCY, fundamental frequencies of 50, 11, 10, 9, 1 and 0.1 kilocycles are obtained. By means of harmonic frequency multipliers in the primary standard, a large number of harmonics of each of these frequencies are available, also, at the output terminals of the standard.

For the precise measurement of frequencies in terms of these standard frequencies, suitable auxiliary and interpolation equipment is needed. The G-R Frequency Measuring Equipment assembly, with the Primary Standard of Frequency, makes possible the accurate, direct, precision measurement of *any* frequency from a few cycles up to 25 megacycles, or higher if external receivers are used.

The units comprising the measuring equipment are as follows:

Heterodyne Frequency Meter covering the range of 100 kc to 5,000 kc in sixteen steps. Sufficient harmonic output is obtained to produce beats in a high-frequency receiver operating at 30 Mc or higher. For many measurements, sufficient accuracy is obtained through use of direct-reading finder and interpolation dials on the heterodyne frequency meter.

Interpolation Oscillator which is a direct-reading, linear-scale audio-frequency oscillator covering frequencies between 0 and 5,000 kc. It is used to measure the audio-frequency differences between the unknown frequency (or a submultiple thereof) and a standard 10-kc harmonic. When the difference is very small, use is made of the 9–11 kc standard harmonics to avoid measurements with very low audio frequencies.

Heterodyne Detector with plug-in coils covering the range from 25 kc to 25 Mc. This detector is used to obtain beats between the standard and the unknown radio frequencies.

Regenerative Selective Amplifier which is used to select any multiple of 1 kc between 1 and 10. This amplifier is particularly useful when the cathode-ray Comparison Oscilloscope is used in calibrations in the upper audio-frequency and lower radio-frequency ranges.

Comparison Oscilloscope with 100-cycle and 1,000-cycle smoothing filters, networks for obtaining circular sweeps at these frequencies, and switches for connecting units of the frequency standard and measuring equipment to the oscilloscope.

The assembly is housed in a steel cabinet and includes a built-in loud-speaker. Permanent shielded connecting cables between the measuring equipment and the Primary Standard and for all interconnections between units of the measuring assembly are furnished. All connections for actual measurements are made by suitable switching on the centralized coupling panel, through which the standard and unknown sources and the various measuring instruments are connected. Suitable power supplies for a-c operation from 115–230 volts and 50–60 cycle mains are individually built in each instrument. GENERAL RADIO COMPANY, Cambridge, Massachusetts.

MANUFACTURERS of PRECISION LABORATORY APPARATUS

Journal
of
Applied Physics

Volume 12 March, 1941 Number 3

Research and Defense Preparation

HISTORIANS looking back a hundred years from now will be able to make a much more objective evaluation of the trying times which we are passing through than we are able to do now. Yet one can be fairly sure that, on the red side of the ledger sheet, will appear the large loss of life (unfortunately from the ranks of those most physically fit), the permanent injuries and diseases of those engaged in combat and those enslaved in concentration camps, the stifling of intellectual freedom, and finally the destruction of great masterpieces of art and architecture. The destruction of battleships, airplanes, and other implements of war will probably not be an important item since these would become obsolescent in any case. Even the prodigious waste of labor in manufacturing these implements hardly constitutes a net loss because it is difficult to prove that busy men obtain less satisfaction out of life than those who have a great deal of leisure time. It may easily be that even the great destruction of buildings now going on will be placed on the profit side of the ledger because in the place where this destruction now stands new streets, modern and more efficient buildings will grow up. There is one item that is sure to be on the profit side; that is the research which the intense competition of war time has forced upon us. *Research like time itself always goes forward and its results still stand in peace as well as in war.*

Professor J. C. Hunsaker brought this point out very forcefully in his paper at the Christmas meeting of the American Association for the Advancement of Science on progress in the aeronautical industry. He discussed the possibility of applying much of the research now going on to the improvement of commercial airplanes. For instance, the use of the spectroscope in the study of the nature of combustion has led to greater power-over-weight ratios for engines that will aid planes used for non-military purposes as much as those in military service. The principles needed to design planes that can take off with heavy bombing loads may be applied with only small modification in peace times as well as in war times. Our increase in knowledge of aerodynamics will lead to improved wing sections with a greater "lift to resistance" ratio and thus lead to improved civil planes. Perhaps even such controversies as air cooling *vs.* liquid cooling will be settled by the research forced upon us by war conditions.

The gist of this entire discussion can be summed up in a few words. *The truly useful result of all our defense effort is the additional knowledge gained from the increased research program.* Let us make sure that this important fact is not forgotten by those setting up budgets for national defense.

For April

Special Issue on Applied Nuclear Physics

***Applications of Nuclear Physics*, by ROBLEY D. EVANS**

***Separation and Use of Stable Isotopes*, by HAROLD C. UREY**

***Biological Effects of Ionizing Radiations*, by G. FAILLA**

Also abstracts of papers presented at the Conference on Applied Nuclear Physics

Theory of the Plastic Properties of Solids. II[1]

BY FREDERICK SEITZ

Randal Morgan Laboratory of Physics, University of Pennsylvania, Philadelphia, Pennsylvania

AND

T. A. READ*

Westinghouse Research Laboratories, East Pittsburgh, Pennsylvania

Part A. Single Crystals

2. THE THEORY OF SLIP (CONTINUED)

IN the first installment of this series, we outlined the basic facts concerning the plastic properties of single crystals and proceeded with a discussion of the theories of slip. It was found that the theory of dislocations provided the most plausible mechanism of the slip process suggested thus far, and it was pointed out that the experiments on internal friction in single crystals can be given a good qualitative interpretation in terms of this mechanism. We shall now proceed to test this theory further by considering its application to other topics surrounding the slip process.

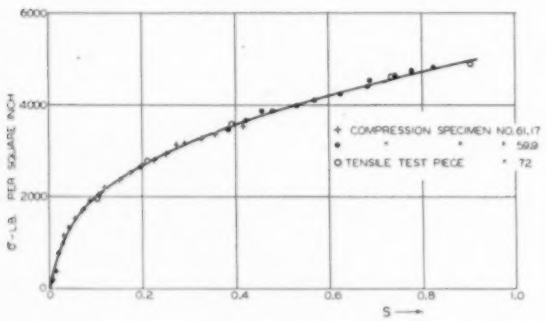

FIG. 19. Stress-strain curves for aluminum obtained in compression and tension. (After Taylor.) The experimental values coincide for both types of deformation. The ordinate is stress and the abscissa strain.

e. Work hardening

The critical shearing stress for a given specimen is strongly dependent upon the amount of previous slip that has taken place within it. This hardening influence of cold work is shown strikingly by conventional stress-strain diagrams in which the critical shearing stress is plotted as a function of the strain. Curves of this type are usually obtained in practice by placing a single crystal under tension or compression and observing the stress required to produce plastic flow for a wide range of extension or compression, suitable correction being made for the change in dimensions of the specimen and orientation of the slip planes in relating the applied load to the actual shearing stress. Stress-strain curves of this type are shown in Fig. 19 for aluminum[2] and in Fig. 20 for sodium chloride[3] and silver chloride.

In order to appreciate the features of this change let us consider the general behavior of a

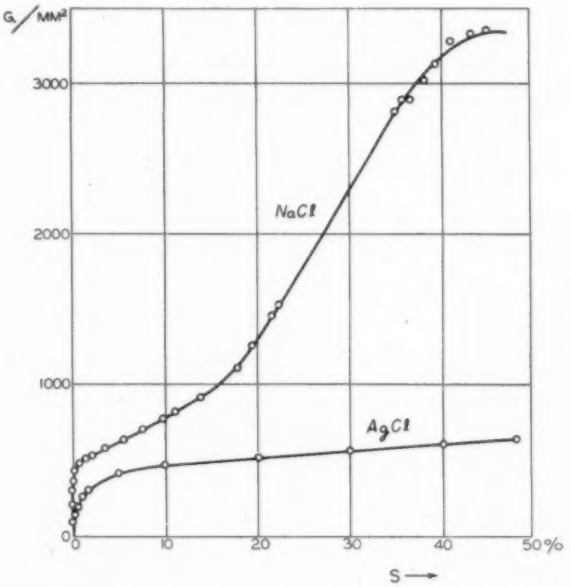

FIG. 20. Stress-strain curves for sodium chloride (upper curve) and silver chloride (lower curve). (After Stepanow.) The ordinate is stress; the abscissa is strain.

[1] The first installment appeared in the previous issue of this journal (February, 1941).

* Westinghouse Research Fellow.

[2] G. I. Taylor, Proc. Roy. Soc. **145**, 388 (1934).

[3] A. W. Stepanow, Physik. Zeits. Sowjetunion **8**, 25 (1935).

typical specimen during an extension test. Starting with the virgin material, which we shall assume to be well annealed, we find that there is a region of stress in the immediate vicinity of the origin of its stress-strain curve in which the material behaves elastically. This range extends up to values of the order of 10^7 dynes/cm^2, as we have seen previously, or over about one-fiftieth of the entire range of ordinate shown in Figs. 20 and 21. If the crystal is extended beyond its Hooke's law range to a point such as A in Fig. 21, it does not return to its original length when the stress is relieved, but retains practically all of its extension. Generally speaking, there is a new elastic stress-strain region about the new length. This region usually extends over a larger range of stress than in the virgin material, as is shown in the figure, for plastic flow does not begin until the stress approximately reaches the value A. Similarly, if the material is further extended to B by additional slip, it will possess a new elastic range about the new length for a still wider region of stress. Thus cold work

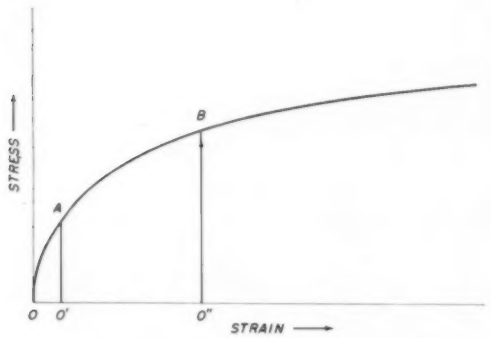

FIG. 21. Behavior of a crystal during straining. In the virgin state, its elastic range covers a region of stress near the origin too small to be shown; after plastic flow to A, obtained by stressing, the crystal retains an amount of strain corresponding to O', when the stress is relieved. The range of stress in which Hooke's law is valid is $O'-A$. Similarly, after extension to B, the strain O'' is retained and the new range of elasticity corresponds to $O''-B$. Lines such as $O'-A$ and $O''-B$ have a slight forward slope corresponding to Hooke's law.

increases the range in which the material is elastic. Within practical limits, the actual values of the elastic constants of pure materials do not seem to be altered as a result of extension.

Taylor[2] has pointed out that in many simple metals the part of the stress-strain diagram nearest the origin can be fitted with a parabolic

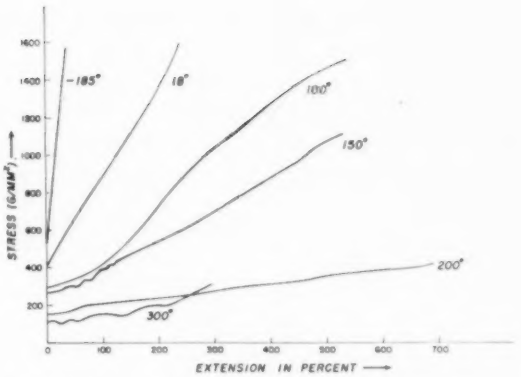

FIG. 22. Stress-strain curves in zinc at various temperatures. Equation (1) does not appear to be valid in any of these cases. (After Boas and Schmid.)

curve corresponding to the equation

$$S^2 = a\sigma,$$

where S is the strain, σ is the stress and a is a constant. The case of aluminum, shown in Fig. 19 is an excellent example of this type. There appear to be exceptions to this rule, however, such as the case of zinc illustrated[4] in Fig. 22, in which the stress strain curves are practically linear over a range of temperature. Figure 23 shows that the parabolic type of curve is valid in aluminum over a wide range of temperature,[5] so that the difference between the curve for the two metals seems to be due to some underlying difference in the materials.

It is interesting to note that more extensive straining can be produced by compression than by extension since the tensile strength for rupture is ultimately reached in a tension experiment. Thus compression strains of fifty have been attained by Taylor[6] in copper, whereas extensions of much more than ten are rare. Work hardening continues to the rupture point in tension tests; however, the critical shearing stress reaches a maximum value in compression tests after approximately tenfold compression has occurred and then remains constant. Thus about the same degree of work hardening is achieved for both kinds of strain in single crystals.

[4] W. Boas and E. Schmid, Zeits. f. Physik **61**, 767 (1930); **64**, 845 (1930).
[5] W. Boas and E. Schmid, Zeits. f. Physik **71**, 703 (1931).
[6] G. I. Taylor and W. Farren, Proc. Roy. Soc. **111**, 529 (1926); **116**, 16, 39 (1927).

An interpretation of work hardening on the basis of dislocation theory was first given by Taylor,[2] who pointed out that dislocations are surrounded by a stress field and hence should exert forces on one another. A straightforward investigation on the basis of elasticity theory

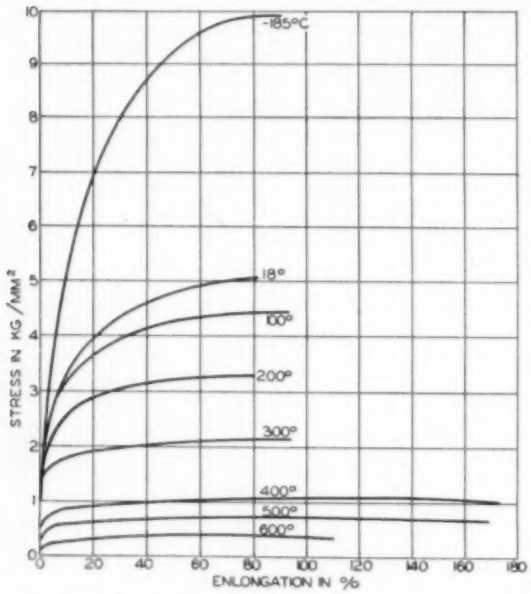

FIG. 23. Stress strain diagrams for aluminum at various temperatures. All of these are parabolic, at least near the origin.

shows that at distances not too near the center of a long line dislocation the stress components fall off as the inverse first power of the distance from the line of dislocation. The angular variation of the stress field[7] is shown in Figs. 24a, b, c and d. The first of these illustrates the shearing stress in planes parallel to that in which the dislocation travels, the second shows the shearing stress in planes orthogonal to these and parallel to the axis of the dislocation line, whereas the third and fourth illustrate, respectively, the tensile stresses in the same planes. The angular variable in all of these polar plots is the azimuthal angle in the plane normal to the line of the dislocation (Fig. 25), that is, the plane shown in Figs. 8, 9, 10 and 12. Figures 24a and 24b are identical because of the relation $\sigma_{xy}=\sigma_{yx}$ between the shear components. Thus the shearing stresses are largest in the forward direction lying in the actual slip plane, decrease to zero in the direction normal to this plane, and reverse their sign in the next two quadrants. Similarly the tensile stress in planes parallel to the slip plane is zero in the slip plane, has a maximum in one direction normal to the slip plane and a minimum in the other, and so forth. Thus a dislocation lying in any direction from the given dislocation except

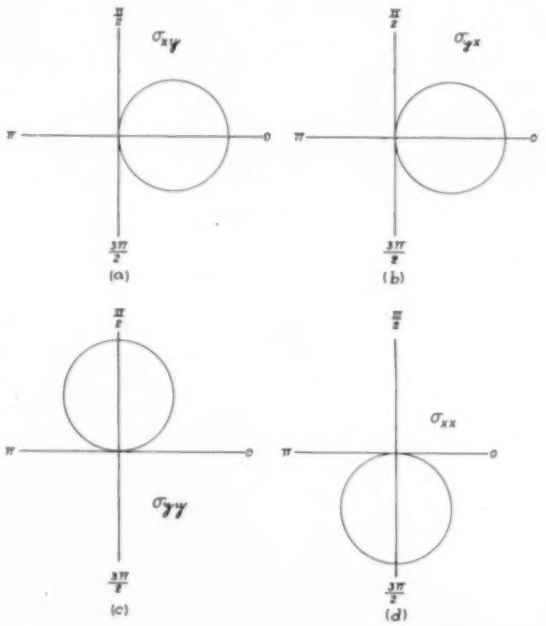

FIG. 24. Polar plots of the angular variation of stresses about a dislocation. The polar angle lies in a plane normal to the line of the dislocation and is oriented in the manner shown in Fig. 25; that is, the compressed part of the dislocation is above the slip plane and the extended part is below. (a) is the shearing stress in planes parallel to the slip plane, whereas (b) is the shearing stress in planes orthogonal to these and parallel to the axis of the dislocation line. (c) and (d) show, respectively, the tensile stresses in the same planes.

along the 90° and 180° azimuths is subject to a shearing stress.

For the present we shall confine the discussion to dislocations traveling in parallel planes and extending in the same directions. Simple con-

[7] The mathematical equations for the stresses about a dislocation in an infinite isotropic medium are, in terms of the coordinate axes of Fig. 25,

$$\sigma_{xx}=-\sigma_{yy}=c\frac{y}{x^2+y^2},$$

$$\sigma_{xy}=\sigma_{yx}=c\frac{x}{x^2+y^2},$$

where $c=G\lambda/\pi$, in which λ is the relative slip distance near the center of the dislocation and G is the rigidity modulus of the solid.

siderations show that like dislocations, in the sense of Fig. 9, repel one another and unlike ones attract. Hence unlike dislocations traveling in the same planes and having parallel lines would tend to get as close together as possible, that is to be on the same normal plane. For this reason, it is possible to form stable lattice-like arrays of positive and negative dislocations analogous to the lattices of positive and negative charges occurring in ionic crystals such as rock-salt (Fig. 26). Taylor investigated the properties of such lattices of dislocations under external shearing stresses and showed that even if the isolated dislocations would move under zero stress in an undeformed lattice, the lattice of dislocations will not shear unless the stress exceeds a critical value dependent upon the density of dislocations.

It is easy to see from dimensional reasoning that this critical shearing stress will increase as the square root of the density of dislocations in a plane normal to their length. As we mentioned above, the shearing stress between two dislocations drops off as the inverse first power of the distance between them, whereas the density N in the plane cutting across the dislocation lines drops off as the inverse second power of the average distance between neighboring dislocations in the lattice. Thus the shearing stress σ_c required to overcome the interaction forces should vary as the square root of the density:

$$\sigma_c = cN^{\frac{1}{2}}, \qquad (1)$$

where c is a constant. Taylor has shown that c has the value

$$c = \alpha G\lambda,$$

where G is the rigidity modulus of the solid, λ is the distance of slip produced by passage of one dislocation through a crystal, and α is a constant near unity depending on the precise arrangement of dislocations.

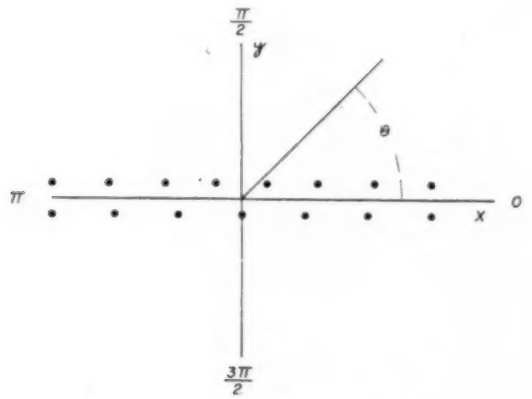

FIG. 25. The coordinate system chosen in Fig. 24.

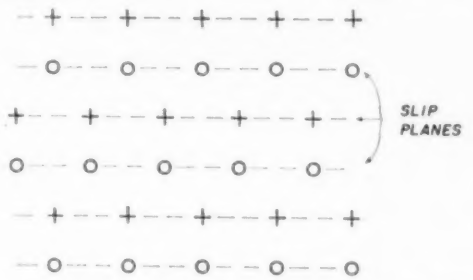

FIG. 26. A stable array of dislocations. (After Taylor.) The negative dislocations are indicated by circles, the slip planes by dashes.

With these facts in mind, Taylor suggested the following picture of the hardening process:

1. Dislocations of opposite types are generated at block boundaries in approximately equal numbers, and move into the crystal blocks under the action of the stress.

2. They do not pass entirely through the blocks, but become stuck, perhaps as a result of their mutual interaction, and form a more or less regular lattice structure.

3. As the number of dislocations increases, the shearing stress required to make them move becomes higher and higher and the material hardens in accordance with Eq. (1).

Now if the dislocations are more or less uniformly distributed throughout all blocks, it is clear that the strain produced as a result of their generation and motion will be proportional to their density. Thus, according to Taylor's picture, the critical shearing stress should vary as the square root of the strain S. Using more quantitative reasoning, Taylor has derived the following relation:

$$\sigma = kG(\lambda S/L)^{\frac{1}{2}}, \qquad (2)$$

where k is a constant of the order unity related to c in (1), and L is the linear dimension of a block.

As we saw above, this type of relation is in excellent agreement with the type of stress-strain

curve found in certain metals, such as aluminum, and in the salts sodium chloride and silver chloride. In fact, by fitting Eq. (2) to the curve for aluminum, in the manner shown in Fig. 27, Taylor has found that the best value of L is about $5.3 \cdot 10^{-4}$ cm, which, in order of magnitude, is the value we should expect from other evidence concerning the size of mosaic blocks.

A close analysis of the derivation of Eq. (2) shows that an essential condition for this parabolic type of relation is that the relative spacing of dislocations in the directions parallel and normal to the slip plane remain fixed during the slip process. It turns out that σ would increase more rapidly with S if the spacing normal to the slip plane decreased more rapidly than that parallel to the slip plane, and, in fact, a linear connection between stress and strain could readily be obtained by assuming the proper relation between the two spacings. Thus cases such as zinc, in which the parabolic law is not valid (Fig. 22), do not necessarily imply that Taylor's basic concept of the hardening process is incorrect.

In any event, Taylor's theory gives rise to a number of questions on which it seems worth while to speculate. These are as follows:

1. Is the length of a fully formed dislocation also of the dimensions of a block? If so, there are two problems: First, that of explaining what occurs at the boundary of two blocks in a region where a dislocation ends; and second, that of explaining the fact that slip bands often run completely around a specimen as though slip took place through a plane.

If neighboring blocks are joined together nearly as firmly as parts of individual blocks, as we must assume at present, it follows that the atoms at the end of a dislocation that terminates at a block boundary will encounter resistance to motion from the atoms in the neighboring block. Moreover, one block will exert shearing stresses on its neighbors if a dislocation moves in it and not in the others, these stresses being such as to oppose the motion. The second type of stress obviously will be greatly reduced if dislocations are present in the neighboring blocks and move more or less simultaneously. A partial reduction will occur even if dislocations do not run continuously from one block to another; however, it will be greatest if they do.

The resistance encountered by the end atoms during the motion of a dislocation provides the most serious obstacle to the assumption that fully formed dislocations terminate at block boundaries. It is a matter of observation[8] that extensive shearing strain can occur in a fraction of a second for stresses of the same magnitude as those shown in Figs. 19 and 22. According to Taylor's picture of the shear process, this implies that a dislocation can move 10^{-4} cm in a fraction of a second. Now the time τ required for an atom impeded by barrier to jump from one equilibrium position to another is determined in order of magnitude by the equation.

$$\tau = \frac{1}{\nu} \exp(\epsilon/kT),$$

where $\nu \sim 10^{13}$ sec.$^{-1}$ is the oscillation frequency of the atom and ϵ is the activation energy required to surmount the barrier. Thus the

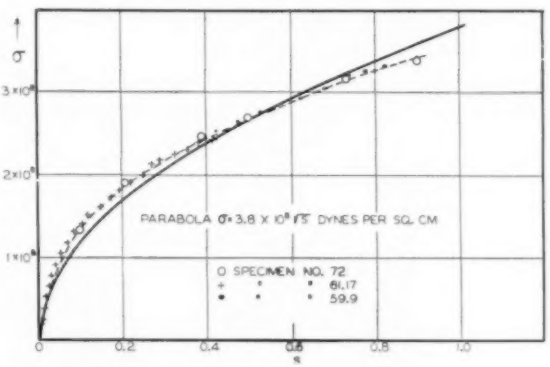

FIG. 27. Comparison of the observed stress-strain curve of aluminum and that obtained from Taylor's theory with $L = 5.3 \cdot 10^{-4}$ cm. The ordinate is expressed in units of dynes/cm².

minimum time T required to jump 10^4 atomic distances is

$$T = 10^{-9} \exp(\epsilon/kT) \text{ sec.}$$

If this is to be less than 1 at room temperature, it is necessary that ϵ be less than 0.5 ev. We may conclude either that fully grown dislocations

[8] M. Manjoine and A. Nadai, Proc. A. S. T. M. (summer meeting 1940), have shown for example, that normal stress-strain curves may be obtained for iron in 10^{-3} sec.

run through many blocks, or that they terminate at block boundaries and are impeded at the end points by very small barriers.

The fact that slip planes often appear to run throughout the crystal specimen is readily explained if dislocations pass through the entire specimen. However, the actual width of slip bands is not known because of the finite resolving power of microscopes. Thus the observed results would be equally well explained if the dislocations were much shorter and were distributed throughout a lamellar region a hundred or so atoms broad parallel to the slip plane.

2. Why are slip bands separated by finite distances? This problem is important not only because we are interested in explaining the origin of slip bands, but also because the density of dislocations in the regions where slip occurs should be higher than the mean values used in deriving Eq. (2) if slip is highly localized in separate planar regions.

The facts concerning our knowledge of slip bands seem to be as follows:

(a) Slip bands are spaced by distances of the order of 1μ at ordinary temperatures in highly worked material. This conclusion seems to be agreed upon by a number of independent investigators.[9] It also seems to be established as a general rule that this spacing increases with increasing temperature.

(b) The spacing between bands is random. This point does not seem to be generally accepted by all investigators. For example, Straumanis[10] has claimed that the spacings in zinc are integer multiples of a constant; however, extensive and apparently trustworthy results of Gough and Cox[11] indicate that the spacing is random in silver.

The fact that definite slip bands occur at all seems to imply that dislocations cannot be generated with equal ease at all points in the specimen. From our present viewpoint, it is only natural to conclude that the regions of easiest nucleation are those where the most stress magnification occurs. Now we pointed out in Part *c* of this section that only very large stress magnifications of the order of 10^3 would be sufficient to make the process of nucleation independent of temperature. There is no reason at present for concluding that magnifications of this size ordinarily occur; however, even much smaller concentrations would have an important influence on the rate of nucleation by lowering the barrier for formation to a fraction of its height.

Two reasonable connections between the slip bands and weak spots occur to one:

(a) In the first place it is possible that each slip band is formed by dislocations generated at a single spot. In this event, fully formed dislocations would necessarily extend continuously through many blocks, and, contrary to Taylor's hypothesis, would move through more than one block when slip occurs. It is not necessary to assume that all dislocations generated by a single weak spot lie in the same atomic plane, for it is possible that the region of stress magnification extends over a number of planes. However, it is necessary to assume that dislocations of opposite sign are generated at the weak spot and move in opposite directions in a static experiment. This implies, in turn, that a lattice of positive and negative dislocations of the type postulated by Taylor cannot form so that the problem of hardening would require an entirely different solution.

One of the advantages of this picture is that it provides a ready explanation of the fact that the glide planes do not come closer than 1μ in spite of the fact that larger and larger stresses must be employed to produce slip as work hardening proceeds, for it may be assumed that all of the weak spots are employed in the fully worked solid.

(b) A number of spots of varying degrees of weakness occur on each block and are distributed more or less at random throughout the specimen. Slip nuclei may be generated at all of these weak spots, but a slip band occurs only if a number of very weak spots happen to lie very nearly in the same plane parallel to the slip plane. In this event, slip occurs initially in many parts of this planar region causing a concentration of

[9] See for example the discussion by E. Schmid and W. Boas in *Kristallplastizität* (Springer, Berlin, 1935); C. F. Elam, *The Distortion of Metal Crystals* (Oxford University Press, 1935).

[10] M. Straumanis, Zeits. f. Krist. **83**, 29 (1932).

[11] H. J. Gough and H. L. Cox, J. Inst. Metals **14**, 71 (1931).

stress in the remainder, which, in turn, aids in the generation and motion of dislocations in these regions. In this picture, the dislocations in a given slip plane can be generated at many points so that both positive and negative kinds will pass in neighboring planes and interfere in the manner postulated by Taylor, and Taylor's theory of hardening can be applied.

In either of these pictures the strain is not uniform throughout the specimen, for practically no slip occurs in the regions between bands. If d is the unknown thickness of a band and D is the average spacing between bands, the actual strain S_a within the slip band is related to the average strain S, obtained from direct measurement of the change in shape of the specimen, by the equation

$$S_a = DS/d.$$

Now the S appearing in Eq. (2) should be the actual strain in the slip band since this quantity determines the density of dislocations in these regions, according to Taylor's picture. Thus we seem obliged to rewrite Eq. (2) in the form

$$\sigma = kG(\lambda DS/Ld)^{\frac{1}{2}}.$$

D is the order of 1μ, but d, being below the resolving power of optical microscopes, presumably can vary from 0.1μ to an atomic distance. In the first of these extremes the estimate of L is still about 10^{-4} cm, but in the second it must be assumed that dislocations move through many blocks if Taylor's theory is valid.

It is possible, of course, that submicroscopic changes take place within the regions between the obvious slip bands and make the arguments leading to the revision of Eq. (2) invalid. In this connection, it would be interesting to know whether or not the hardness in regions between slip bands, as measured by an indentation method such as the Brinell or Vickers methods, increases during slip. If so, it might be concluded that submicroscopic slip occurs in these regions.

3. Figures 22 and 23 show that the stress-strain curves for zinc and aluminum change in going from room temperature to liquid-air temperature, the initial slopes becoming more steep. It is remarkable, however, that extensions of the order of a hundred percent may be obtained at low temperatures, for we should not expect temperature fluctuations to be sufficient to allow the dislocations to elongate in a reasonable length of time if our picture of their formation is correct. Even more remarkable is the fact that similar elongations have been produced in cadmium at liquid hydrogen temperatures (20°K) in a few seconds.[4] Figure 28 shows the manner in which the initial slope of the stress-strain curve for cadmium varies with temperature. A similar curve has been obtained for zinc. It is interesting to note that this slope increases very rapidly just below room temperature and then flattens again below liquid-air temperature. This result seems to be relatively insensitive to the rate at which the strain occurs and indicates that the low temperature mechanism of slip contains features essentially different from those of the high temperature mechanism. The temperature changes occurring in cubic crystals such as aluminum and copper do not seem to have been investigated as thoroughly as those for the hexagonal metals.

If our previous picture of the formation of dislocations is correct, we apparently must conclude that the slip at very low temperatures is caused by dislocations already formed. In this event, the work hardening occurring at low temperatures originates in the fact that dislocations become stuck at lattice imperfections. For plausibility, these conclusions evidently require that some of the dislocations formed at room temperature remain in spite of annealing. The fact that slight handling of crystals at room temperature gives a measurable internal friction

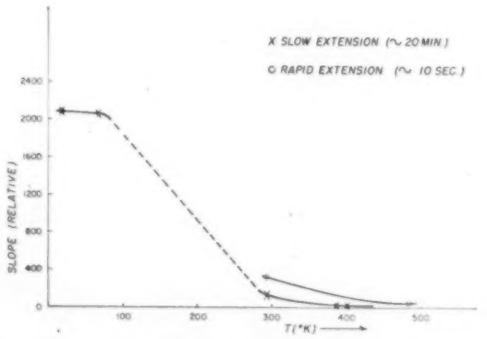

FIG. 28. The initial slope of the stress-strain curves for cadmium as a function of temperature. The ordinate is expressed in relative units. (After Boas and Schmid.)

presumably shows that this assumption is not unreasonable. As we shall see in the next part of this section, independent estimates indicate that there are about 10 dislocations per atomic plane in a block in the work-hardened state. If one ten-thousandth of this number are present in the annealed state, an extension of 100 would be attained if each dislocation moved 10^{-2} cm. Thus we apparently must picture the slip process at low temperatures as occurring by the motion of a comparatively small number of dislocations through large distances. This conclusion evidently favors the viewpoint that block boundaries do not seriously limit the motion and extension of dislocations, and hence favors the possibility that fully formed dislocations extend through many blocks.

The possibility that dislocations are formed and are set in motion entirely as a result of the action of applied stresses must not be left out of mind. A picture of this type evidently is not easy to justify on the basis of the model of a dislocation we have been employing, but the conclusions of the preceding paragraph would bear considerable revision if justification were found.

It is interesting to note in passing that the existence of a stress field extending for large distances about an isolated dislocation in the interior of a solid implies that the energy of such a dislocation is not all localized in the few atoms at its center, or that part is distributed throughout large regions of the solid. It is not difficult to show[12] that a slip nucleus or a line dislocation near a surface do not have a similar extended stress field so that their energies are localized in the atoms near the center of the dislocated regions. It follows that as an isolated dislocation moves from the surface to the interior the elastic energy of the system gradually increases, the additional energy being supplied by the applied stresses. When many dislocations are present and form a stable lattice of the type discussed by Taylor, their mutual interaction energy is related to a decrease in the extended stress rather than to a decrease of the energy of the comparatively small number of atoms near the center of dislocations.

f. The energy increase associated with work hardening

It is found experimentally that the internal energy of solids is raised during work hardening. The most careful measurements of this energy have been made by Taylor and Quinney,[13] who found that the maximum increase attainable is of the order of magnitude 1 cal./gram for a number of metals. This energy may be measured in several ways, the most reliable results being obtained by measuring the difference between work input and heat output during straining and by measuring the heat evolved when a specimen is heated to temperatures sufficiently high to remove the effects of work hardening. It is found that the stored energy increases with the amount of cold work during the initial stages of straining and reaches a saturation value when the critical shearing stress approaches a constant value, as occurs in compression. This limiting value is attained most readily by torsion and compression, the values reached during tension tests with polycrystals being considerably less, presumably because fracture occurs before the same degree of strain is reached. The circular points in Fig. 29 show the percentage ratio of the stored energy to the work done on specimens of copper during torsion tests, the abscissa being proportional to the torsion strain. The triangular points are similar results obtained from extension tests. Values of the maximum stored energy are given in Table III for several metals.

TABLE III. *Values of the maximum energy stored during work hardening. (The values are expressed in cal./gram.)*

ALUMINUM	COPPER	IRON	NICKEL	BRASS
1.1	0.5	1.2	0.78	0.49

We naturally must look for the source of this increased internal energy in the increased imperfection of the crystals. The two most likely

[12] This subject is being made the topic of an extensive investigation by J. S. Koehler, Bull. Am. Phys. Soc. **15**, 21A (1940).

[13] G. I. Taylor and H. Quinney, Proc. Roy. Soc. **143**, 307 (1934); **163**, 157 (1937). Earlier work in tension was carried out by G. I. Taylor and W. Farren, Proc. Roy. Soc. **107**, 422 (1925).

possibilities are the distortion of blocks, which is responsible for broadening of the x-ray diffraction lines of crystals, as we saw in the Part *b* of this section, and the number of dislocations. Cogliotti and Sachs,[14] and later Boas,[15]

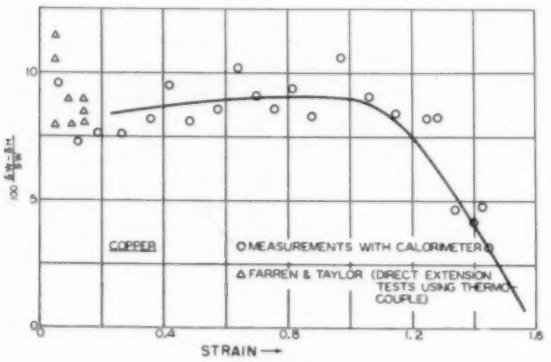

FIG. 29. The percentage ratio of the stored energy to the mechanical work done on copper specimens during cold work. (After Taylor and Quinney). The triangles refer to tension tests and the circles to torsion tests in which much greater straining is possible. The abscissa is proportional to the strain. The falling portion of the curve implies the stored energy reaches a saturation value.

pointed out that the distortion of the blocks is not sufficiently large to account for more than a very small fraction of the stored energy. Thus Dehlinger and Kochendörfer[16] have found that the percentage distortion of lattice constant in the most highly cold-worked metals is of the order of 0.1, which corresponds to an elastic energy of about 10^{-2} cal./gram. Apparently we must conclude that the stored energy is to be associated with dislocations. This assumption is reasonable since the number of dislocations should increase with cold work according to Taylor's theory of hardening.

If we make this assumption we may readily estimate the density of dislocated atoms in an approximate fashion. We saw previously that it is reasonable to suppose that the energy of a dislocation per atomic distance along its length is about 1 ev, or 10^{-12} erg. Since the stored energy is of the order of magnitude 10^9 ergs per mol (one mol contains 6.10^{23} atoms), it follows that about one atom in a thousand is near the center of a dislocation in a highly worked specimen. This is in good qualitative agreement with the number that we would estimate directly from Taylor's picture of the hardening process. If an average dislocation moves a distance of 10^4 atoms, as is assumed in Taylor's theory, and if the strain at maximum hardening is about ten, there must be ten dislocations per atomic plane in each block in the hardened crystal. Hence about one atom in a thousand must be near the center of a dislocation.[17]

Excellent corroborating evidence for the conclusion that the energy of cold work is to be associated with defects extending over atomic dimensions has apparently been obtained by Hengstenberg and Mark and by Brindley[18] and his co-workers. As we pointed out in the previous installment (Part *b* of this section) the principal influence on the x-ray diffraction patterns of defects of atomic size is a decrease in the intensity of the diffracted line because of incoherent scattering by the defects. Brindley and coworkers have found that the intensity of diffraction lines of metals actually decreases with increased cold working and Boas[15] has shown that the elastic energies associated with the atomic displacements derived from their results are of the same order of magnitude as the observed stored energies. This does not prove that the defects are dislocations, of course, but provides additional support for the picture that defects of atomic size play a primary role in the hardening process.

An interesting and critical experiment on the mechanism of slip at low and high temperatures

[14] V. Cogliotti and G. Sachs, Zeits. f. Physik **74**, 647 (1932).

[15] W. Boas, Zeits. f. Krist. **96**, 214 (1937); **97**, 354 (1937). Other papers on this topic are: G. R. Stibitz, Phys. Rev. **52**, 619 (1937); F. E. Haworth, Phys. Rev. **52**, 613 (1937); G. W. Brindley and P. Ridley, Proc. Roy. Soc. **50**, 501 (1938).

[16] This work is surveyed in a review article by U. Dehlinger and A. Kochendörfer, Zeits. f. Metall. **31**, 231 (1939).

[17] A fraction of one dislocated atom per thousand normal atoms corresponds to a density of dislocation lines of about 10^{12} per cm². W. F. Brown, Phys. Rev. **58**, 736 (1940), has derived the same density from an investigation of the manner in which the magnetization of highly worked materials approaches saturation. The writers are indebted to Professor Brown and Dr. R. Smoluchowski for discussions of this point.

[18] H. Hengstenberg and H. Mark, Zeits. f. Physik **61**, 435 (1930); Zeits. f. Elektrochemie **37**, 524 (1931); G. W. Brindley and F. W. Spiers, Phil. Mag. **20**, 882 (1933); G. W. Brindley and P. Ridley, Proc. Roy. Soc. **50**, 501 (1938); **51**, 432 (1939); Phil. Mag. **21**, 778 (1936); Proc. Roy. Soc. **52**, 117 (1940).

would be provided by measurements of the energy stored during cold work at very low temperatures. If the supposition, made in the previous part of this section, that a comparatively small number of dislocations are responsible for slip at low temperatures, as compared with the situation assumed by Taylor at high temperatures, we should expect striking differences in the ratio of stored energy to work done in low temperature and high temperature cases.

Simple estimates, based on a comparison of the work done during hardening and thermal data for metals, show that sufficient heat is produced during extensive hardening to melt about 5 percent of the material in the cases listed in Table III. Thus if straining actually occurs in very narrow slip bands, it is conceivable that local melting would be produced if the strain occurred in a time short compared with that for thermal equilibrium to be reached. Unfortunately, the time for equilibrium appears to be too short for melting actually to be observable. For example, if the slip bands are 500A wide, the time required for thermal equilibrium is of the order of 10^{-10} second.

g. Resoftening

The effect of work hardening may be undone by appropriate heat treatment. Apparently this resoftening takes place to some extent at all temperatures above absolute zero, but it may be greatly accelerated by heating. Thus zinc resoftens in the course of several days at room temperature, whereas the rate is negligibly small at liquid-air temperatures. It is common in practical work to designate the lowest temperature at which softening takes place at a practically interesting rate, such as a day or a week, the *recovery temperature*. This is defined to within an ambiguity of twenty degrees or so depending upon the range of time in which recovery is expected. Just above the temperature at which resoftening is first observable in a practical sense, a change in crystalline texture of worked specimens occurs. This effect, which is known as *recrystallization*, will be discussed later in connection with polycrystals. Since the temperatures at which recrystallization begins have been tabulated for a large number of materials and since this temperature marks an upper limit to a range of about thirty degrees or so in which resoftening can occur without change in texture, we list the values[19] of the recrystallization temperature for the polycrystalline form of several metals in Table IV.

TABLE IV. *Recrystallization temperatures of several metals. (These temperatures mark the upper limit of the range in which resoftening can occur without change in texture. The values are expressed in degrees centigrade and are only approximate.)*

aluminum	150	nickel	620
cadmium	50	platinum	470
copper	200	silver	200
gold	200	tantalum	1020
iron	450	tin	0
lead	0	tungsten	1210
magnesium	150	zinc	15

Karnop and Sachs[20] have shown in the cases of aluminum and copper that the recrystallization temperature is higher in single crystals than in polycrystals, for which the values in Table IV are valid. Thus recrystallization occurs only at about 600°C in single crystals of aluminum. Resoftening, however, occurs at far lower temperatures, in the range below the recrystallization temperature for highly worked polycrystals given in Table IV. It is to be noted that in less severely cold-worked specimens recrystallization takes place at temperatures higher than those given in Table IV.

Figure 30 shows stress-strain curves for zinc obtained at room temperature under two different sets of experimental conditions. In the case corresponding to Fig. 30a the specimen was given a succession of fifty-percent extensions, the load removed for a "rest period" of about one minute between the extensions. In the second case, the extensions were identical, but the rest period was increased to a day. It is clear that the first period of rest was not sufficiently long for very extensive resoftening to occur, whereas softening was almost complete after the second. The dotted curves in the figures show the yield stress calculated from the original critical shearing stress of the specimen. The yield stress varies as a result of reorientation

[19] Taken from the article by R. S. Archer, *A. S. M. Handbook*, (1939), p. 198.

[20] R. Karnop and G. Sachs, Zeits. f. Physik **42**, 283 (1927).

of the specimen during extension. The observed value agrees closely with this calculated one at the start of each run in case *b*.

The phenomena of resoftening would seem to be closely connected with the time dependence of the type of internal friction discussed in Part *d* of this section (previous installment), for the variations take place in comparable periods of time in both cases. On the basis of dislocation theory, we are tempted to conclude that above the recovery temperature dislocations introduced into the crystals during straining diffuse out and thereby reduce the solid to its virgin state. This exodus should be accompanied by a decrease in internal friction, at least in the later stages when the number of dislocations has become so small that they do not interfere with one another appreciably, since there are fewer centers to dissipate the vibrational energy. Such a decrease actually occurs, as we saw previously in the case of zinc.

It seems worthwhile to speculate on some of the details of the process by which dislocations diffuse out of crystals. In the first place, it is possible that dislocations move about primarily as a result of thermal agitation, just as atoms diffuse as a result of thermal motion. On the other hand it is possible that the motion is produced as a result of stress acting on the dislocations and that thermal fluctuations play a role only insofar as they furnish the activation energy required to get the dislocation past obstacles that impede very small regions along the line of the dislocation. It will be recalled that in Part *c* of this section we inferred that temperature plays a similar role in the process of elongation of a dislocation. Concerning the possible origin of stresses in the second case, we noted at the end of Part *e* of this section that the elastic energy of a solid increases as a dislocation moves from the surface to the interior. This implies that the solid exerts stresses on the dislocation of such a sign as to force it to the surface.[12] The force on an isolated dislocation may be estimated roughly in the following way. If we have a dislocation at a distance x from the surface, the requisite boundary conditions may be approximately satisfied by assuming that there is a dislocation of opposite sign at a distance $-x$ on the other side of the surface. This "image" dislocation exerts a shearing stress of magnitude

$$G\lambda/2\pi x \qquad (3)$$

(see footnote 7 for notation) on the given dislocation. The quantity (3) is about 10^7 dynes/cm^2 for a dislocation midway in a block and should be sufficient to drive an isolated dislocation out of an otherwise perfect crystal if our views concerning the ease with which dislocations may move is correct. Naturally the required stress is larger when there are many dislocations present; however, we may visualize the process as taking place in such a way that dislocations near the surface which are under greater stress, according to Eq. (3), move out first and the others then follow in succession.

Equation (3) is valid, of course, in the case in which dislocations are produced at block boundaries, or in the interior of blocks, in pairs of opposite sign which move in opposite directions. In this case the image dislocation is replaced by a real one.

Thus estimates based on (3) indicate that dislocations will tend to move out of blocks when the temperature is sufficiently high to provide the activation energy for getting by localized obstacles. The assumption that this actually is

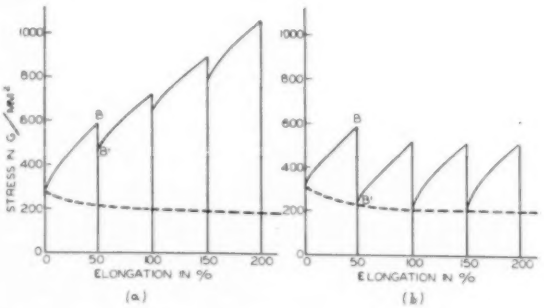

FIG. 30. Stress-strain curves for zinc at room temperature in cases in which the specimen was allowed to rest during successive elongations. In case (a) the rest time is about a minute and in case (b) it is 24 hours. (After Haase and Schmid.)

the mechanism requires, however, that we accept some of the details of Taylor's picture concerning the distances that dislocations move from the places where they are generated and it seems worthwhile to consider further the possibility that they would wander about as a result of thermal agitation even if no stresses were present.

In the first place, let us assume that the dislocation runs through only a single block. If we use the model of a dislocation considered in Part *c* (Figs. 8, 9, 10 and 12), we must conclude that one part of a given line dislocation cannot readily move ahead of the remainder since a large amount of energy would be required to break the line into two parts. Now, exclusive of any friction the atoms at the end of the dislocation may encounter when the dislocation moves, the activation energy required for motion of a line 10^4 atoms long from one equilibrium position to another will be a small fraction of an electron volt if our assumption concerning the low critical shearing stress is correct. Thus the only obstacle in the way of rapid thermal diffusion of dislocations, aside from end friction, is the question of whether it is probable that all atoms in the line can move in phase so as to jump simultaneously from one equilibrium position to the next. Apparently there is no difficulty arising from

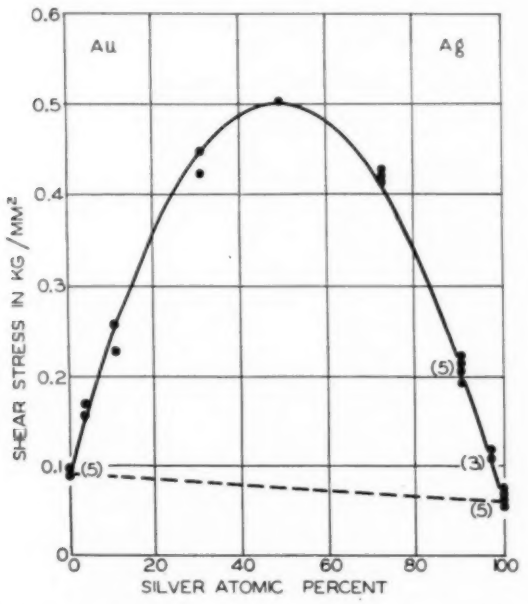

FIG. 31. The critical shearing stress of a sequence of silver-gold alloys as a function of composition. These metals are miscible in all proportions. (After Sachs and Weerts.)

this source, for if one atom in the dislocation gains sufficient energy to take the entire dislocation to the next equilibrium position, and is moving in the proper direction, it will be able to drag the others with it because of the close coupling between atoms in the dislocation. In this respect a dislocation 10^4 atoms long is analogous to a particle undergoing Brownian motion in air or in a liquid. The only difference

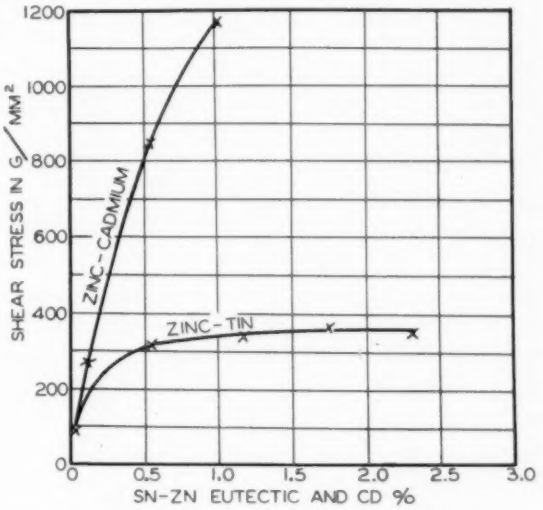

FIG. 32. The critical shearing stress of a sequence of zinc-cadmium and zinc-tin alloys. At 250°C somewhat more than 1.5 weight percent of cadmium is soluble in zinc, whereas at the same temperature less than 0.1 weight percent of tin will dissolve in zinc. These results illustrate the fact that soluble impurities have a greater influence than insoluble ones. (After Rosbaud and Schmid.)

between the two cases appears to lie in the fact that a dislocation requires an activation energy for motion between equilibrium positions.

Naturally, if the barrier encountered by end atoms is very large, the rate of diffusion will be cut. However, we have already seen from other evidence, discussed in Part *e*, that the assumption that dislocations terminate at block boundaries requires that the barriers at these points be very low.

If dislocations are very long, running through many blocks, their natural rate of diffusion will be correspondingly decreased; however, it does not seem permissible to draw any definite conclusions concerning their mobility without more quantitative information concerning their properties.

h. The hardening influence of impurities

The influence of impurity content on the critical shearing stress of metals is shown in Figs. 31, 32 and 33. The first of these[21] shows

[21] G. Sachs and J. Weerts, Zeits. f. Physik **62**, 473 (1930).

the variation in critical shearing stress in a sequence of silver-gold alloys that were carefully annealed before measurements were made. The striking features of these results are the fact that the hardness of solid solutions is greater than that of the pure metals and that the variation in hardness is a simple function of composition. This increased hardness of alloys as compared to pure metals is, of course, partly responsible for their wide use. The second of these figures[22] illustrates the relative increase in hardness of zinc-cadmium and zinc-tin alloys. Cadmium is soluble at 250°C to the extent of about 1.5 weight percent in the first of these alloys, whereas less than 0.1 weight percent of tin is soluble in zinc. This case provides an illustration of the general rule that the hardening effect of a soluble impurity is greater than that of an insoluble one. Figure 33 shows the effect of very slight traces of silver impurity on the critical shearing stress of extremely pure mercury. The results were obtained by Greenland[23] on single crystals of mercury that was carefully purified by distillation. It is very interesting to note that these results indicate that impurity contents as low as 10^{-7} or 10^{-8} have a measurable effect on the hardness.

In this connection, it is interesting to note the influence on hardness of different atoms present in the same atomic percentage. Figure 34 shows[24] the Brinell hardness of a number of copper alloys, per atomic percent of the dissolved metal, as a function of the relative difference in sizes of the dissolved atom and the copper atom. Although the Brinell hardness is not a direct measure of the critical shearing stress, we may assume that the two increase together. Figure 34 then indicates that dissolved atoms have a greater hardening influence the greater the fractional difference in the diameters of the solvent and solute atoms. An approximately linear relation of the type of Fig. 34 is also valid in a sequence of lead alloys.[24]

The interpretation of the hardening influence of impurities or alloying elements on the basis of the theory of dislocations is not entirely apparent, particularly in cases such as mercury in which very small atomic fractions seem to be effective. Since soluble impurities have a greater influence than insoluble ones, we may conclude that the effect occurs primarily within the volume of the crystals rather than at their surface or at block boundaries. Moreover, since there is a simple relation between hardening and atomic size, it seems reasonable to suppose that the effect is related to the distortion of the lattice by the alloying atoms. Now it is clear that these atoms will compress or expand the surrounding lattice in a way depending upon whether their size is larger or smaller than that of the normal atoms. In either case, the impurity atom will be the center of a more or less spherically symmetrical stress field. This radially symmetric compressional or tensional field varies with the distance r from the center of the impurity atom in the manner[25]

$$\sigma_r = 4Gfa^3/r^3, \quad \sigma_\theta = -4Gfa^3/r^3, \tag{4}$$

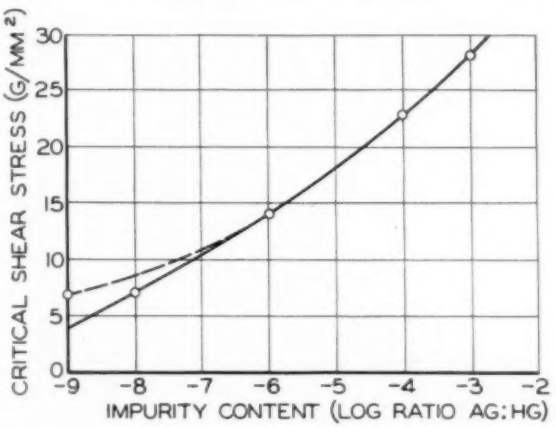

FIG. 33. The critical shearing stress of single crystals of very pure mercury containing small amounts of silver. (After Greenland.) The results were obtained at about −60°C, which is only about 23° below the freezing point. Work hardening does not occur at this temperature so that the specimens were not sensitive to previous handling.

where σ_r is the stress in the radial direction and σ_θ is that in the angular direction, G is the shear modulus, which is about 10^{11} dynes/cm², f is the relative difference in radii of the solute and solvent atoms, and a is the atomic radius, which

[22] P. Rosbaud and E. Schmid, Zeits. f. Physik **32**, 197 (1925).
[23] K. M. Greenland, Proc. Roy. Soc. **163**, 28 (1937).
[24] A. L. Norbury, Trans. Faraday Soc. **19**, 586 (1924).

[25] See for example, A. E. H. Love, *The Mathematical Theory of Elasticity* (Cambridge University Press, 1927), p. 142. The present discussion follows closely that employed by Mott and Nabarro in connection with precipitation hardening, discussed in the next part of this section.

is usually about $1.5 \cdot 10^{-8}$ cm. The shearing stress in any plane may be computed from this by projecting the tension stress in the plane. In passing by this stressed region, a dislocation will be acted upon by a shearing stress having an azimuthal variation of the type shown in Fig. 35, that is, the dislocation will be retarded on one side of the 90° azimuth and will be accelerated on the other. In either case, it will experience greater difficulty in passing the atom, so that the critical shearing stress should increase, just as in the case in which there are other dislocations present to impede the ease of motion.

This picture is in qualitative agreement with the fact that the hardness is a maximum for 50–50 composition in an ideal substitutional alloy, for the amount of inhomogeneity should then be a maximum, at least in disordered substitutional alloys. It seems to face some difficulty, however, in interpreting the hardening in very pure mercury, although the following argument indicates that such an interpretation may be within the scope of the theory.

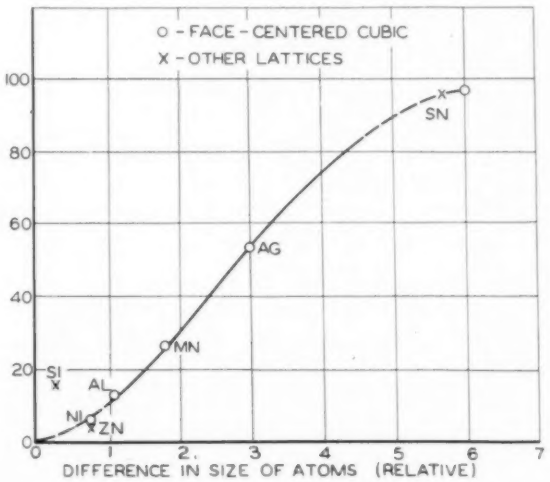

FIG. 34. Relation between the relative increase in hardness and the fractional difference in sizes of the solvent and solute atoms for a number of copper alloys containing 0.1 atom percent of alloying metal. (After Norbury.) The abscissa is the difference in atomic volume of solvent and solute. This difference is proportional to the difference in atomic radii.

To begin with let us consider the case in which the crystal is at absolute zero of temperature so that thermal fluctuations do not play a role. The radius of the cylinder about a line dislocation 10^4 atoms long in which there is one silver atom when the concentration of silver atoms is about 10^{-7} is 50A. Thus at an average position each dislocation encounters a shearing

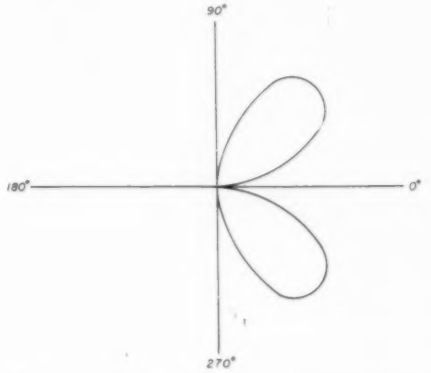

FIG. 35. The variation in shearing stress with azimuthal angle about an impurity atom. The shearing stress is measured in a system of parallel planes and at distances equally spaced from the impurity atom.

stress of about 10^6 dynes/cm^2 extending over a region approximately fifty atoms square. Unless the applied stress is sufficient to compensate for this stress arising from the impurity atom, the dislocation will become stuck. It is interesting to note that the observed critical shearing stress in the relatively pure mercury is of this order of magnitude.

Now the work required to push the dislocation past this difficult spot may be shown to be of the order of 10^{-13} erg or 0.1 ev. This barrier is sufficiently small that we should expect the dislocation to diffuse past it readily even at dry ice temperatures. It is possible, however, that speeds of migration of the type required for observation of slip in Greenland's measuring apparatus required that the applied stress be sufficient to neutralize the retarding stress arising from impurities.

If dislocations are considerably longer than 10^{-4} cm, the average distance from an impurity atom to a dislocation should be much smaller than 50 atom distances and the resisting stress should increase. Measurements of the critical shearing stress of the mercury crystals at temperatures sufficiently low that thermal activation is unlikely should provide a direct measure of the mean stress encountered by dislocations and hence should furnish an indirect method of estimating their length.

One of the consequences of the foregoing reasoning is that the critical shearing stress should be proportional to the three-halves power of the concentration of impurities for small concentrations. This may be seen from the fact that the square of the radius of the cylinder about a dislocation containing one impurity atom varies inversely as the concentration of the impurity atoms, whereas the stress about the impurity atom varies inversely as the cube of the distance, according to Eq. (4). It is impossible to tell from Figs. 31 and 32 whether or not a law of this type is valid for very small concentrations. Greenland's results, shown in Fig. 33, seem to require a more complicated dependence upon concentration. This work, however, is open to the objection that silver is only slightly soluble in mercury and it is not proved that the silver atoms are randomly distributed in the crystals on which the measurements were made.

In addition, it is interesting to note that the previous reasoning predicts that the critical shearing stress should vary linearly with the relative difference in atomic radii of the impurity and solvent atoms. This is in reasonable accord with Fig. 34 and with results for lead described by Norbury.

i. Precipitation hardening

In many alloy systems the solubility limits of given phases decrease with decreasing temperature. Thus copper is soluble in aluminum to the extent of 4.1 percent at 500°C, whereas the solubility is less than 0.5 percent at room temperature. For this reason perfectly homogeneous crystals of aluminum containing several percent of copper are stable at elevated temperatures, but become thermodynamically unstable when cooled near room temperature. It is found in many such cases that precipitation of the dissolved metal proceeds in the course of hours or days at room temperature and that this precipitation is accompanied by hardening of the alloy. The dynamics of this precipitation process are fairly complex and will not be reviewed here.

An analysis of the theoretical factors entering into the problem have been given by Mott and Nabarro.[26] They point out that the precipitated material usually has an atomic volume different from that of the homogeneous alloy, so that the lattice becomes strained in the vicinity of the precipitate (see Fig. 36). This straining implies that there are regions about the precipitate where the shearing stress is unfavorable for the passage of dislocations, just as in the case of impurity atoms discussed in the previous part of this section. In fact, Eqs. (4) may be employed to describe the stress field about a spherical particle of precipitated material. Using reasoning of this type, Mott and Nabarro have shown that in the case of spherical particles, the critical shearing stress is given roughly by the equation

$$\sigma = Gfr,$$

where G is the shear modulus for the matrix, f is the fraction by which the linear dimensions of the precipitated particle is changed by the compressing action of the matrix, and r is the ratio of amount of precipitate to matrix.

j. Multiple gliding

When slip is taking place in a given set of parallel planes in a crystal of high symmetry there usually are symmetrically equivalent planes which may be regarded as latent slip planes. Thus if slip is occurring in one set of (111) planes in a face-centered cubic metal there are three latent systems of easiest slip. During the process of slip it frequently happens[27] that, as a result of reorientation of the specimen, the shearing stress in one of the latent slip planes becomes larger than that in the actual slip planes. Accumulated evidence for face-centered cubic crystals of the pure metals indicates that hardening occurs in the latent slip planes at about the same rate as in the actual slip planes, for gliding will occur in the first system just as soon as the shearing stress becomes larger than in the actual slip planes. On the other hand, evidence for slip in the (101) planes of tin indicates that the latent slip planes harden more rapidly than the actual planes, that is, slip occurs in the latent system only after the

[26] N. F. Mott and N. F. R. Nabarro, Proc. Phys. Soc. **52**, 86 (1940); N. F. R. Nabarro, Proc. Phys. Soc. **52**, 90 (1940); Proc. Roy. Soc. **175**, 519 (1940).

[27] The topic of multiple gliding is discussed in the books by Elam and by Schmid and Boas (see reference 9).

shearing stress in these planes has become much larger than that in the actual system. Similar results have been found by Elam[27] in single crystals of copper-zinc and copper-aluminum alloys.

The relationship between hardening in actual and latent slip planes is not very simple when viewed in terms of the model of dislocations we have been considering. To begin with, let us consider a hypothetical cubic case in which the planes of easiest slip are three systems equivalent to (100), and let us assume that the specimen contains a uniform distribution of dislocations which can move in the x direction and which extend along the y direction, so that when they move the slip planes are $x-y$ planes and the slip direction is parallel to the x axis. Now because of the relation $\sigma_{ij}=\sigma_{ji}$ between the components of shear stress, it follows that the average shearing stress encountered by one of these dislocations as a result of the presence of the others is the same as that encountered by a dislocation which moves in the direction of the z axis and extends along the y axis. Thus, using Taylor's picture of the hardening mechanism, we should expect hardening to proceed as rapidly in the $y-z$ planes for slip in the z directions as in the $x-y$ planes for slip in the x direction, after slip has started in the second system. On the other hand, dislocations which move in the z direction and extend in the x direction should encounter no shearing stress because of the presence of the other types of dislocations, and we should not expect the $x-z$ slip planes to harden at the same rate as the others. Although this is not a practical case, it does indicate that we shall meet difficulties in attempting to understand the hardening of latent planes in the face-centered cubic crystals in terms of Taylor's mechanism and line dislocations of the type we have been treating. In fact it would appear that the observation that all planes harden equally is explicable only if the distortion induced by the dislocations associated with the primary slip process has the same cubic symmetry as the lattice; this does not seem to be conceivable in terms of the concepts we have been using.

It is possible, of course, that the rule stated above for the hardening of latent slip planes in pure face-centered cubic crystals is based on insufficient evidence and that all latent planes do not harden equally. In this event, additional experimental work on the point would be of great value.

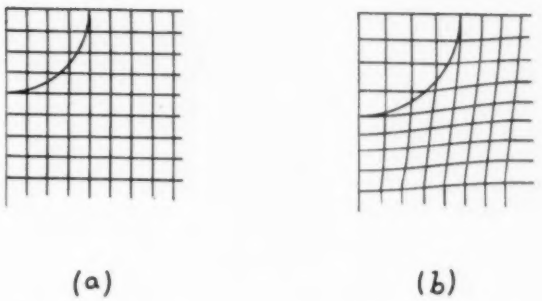

FIG. 36. Schematic representation of the strain about an inclusion of precipitate in a precipitation hardened alloy. (After Mott.) (a) Situation occurring if the atomic volume of the precipitate is the same as that of the solvent. (b) Actual situation at equilibrium in a case in which the atomic volume of the precipitate is larger than that of the solvent.

A discussion of the cases of pure tin and the copper alloys, in which the latent planes harden more rapidly than the others, does not seem in order until the more simple one of pure cubic metals is understood.

k. Asterism

Although a crystal that has been uniformly strained by slip remains a single crystal, in principle, its x-ray diffraction patterns show striking changes that are indicative of internal distortion. In particular, it is found that the Laue x-ray pattern, which is obtained by sending a beam of continuous radiation through the system, consists of radial streaks or bands instead of sharp spots, as in an unstrained single crystal. This streaking is generally called asterism.[28] The appearance of asterism implies that the crystallographic planes which reflect particular wave-lengths of the incident beam, and thereby give Laue spots, are bent as a result of the straining. It is not possible to say whether or not this bending is accompanied by fragmentation.

It has been pointed out by a number of

[28] See for example, Schmid and Boas, and Elam, reference 9; W. G. Burgers, Proc. Int. Conf. in Physics 139 (1934); E. N. da C. Andrade, Proc. Phys. Soc. **52**, 1 (1940).

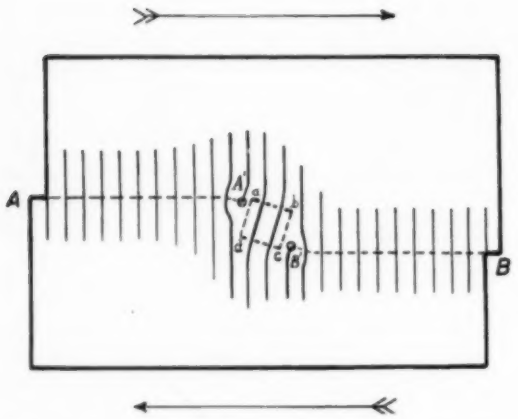

FIG. 37. Origin of asterism on basis of Burger's picture. The material between dislocations is distorted as a result of the stresses about dislocations.

workers that the distortion of the Laue pattern can be explained by assuming that the bending of planes takes place about an axis lying in the slip plane and normal to the slip direction, the angle of bending varying statistically over a finite range. However, there is no conclusive evidence concerning the size of the bent regions or their positions relative to the planes on which slip has occurred.

Barrett and Levenson[29] have pointed out that cold-worked crystals frequently exhibit narrow bands on either side of which the crystallographic orientation is slightly different. They have suggested that the disorientation associated with those *distortion bands* is the seat of asterism.

Burgers[30] has suggested that the warping of the lattice is directly connected with the presence of dislocations in a manner such as that shown in Fig. 37. This hypothesis awaits more extensive confirmation. In disagreement with it appears to be the fact, observed by Karnop and Sachs[20] in aluminum strained by 15 percent, that extensive resoftening does not appreciably affect the asterism.

It was recently shown by Andrade and Chow[31] that the asterism changes its character when the crystal is heated sufficiently, for the continuous streaks appear to coagulate into spots extending along the line of the streak. This result seems to imply that, as a result of heating, the bent material changes its orientation to one of several arrangements bearing a fixed relationship relative to the bulk of the crystal. Since the original rotated material is presumably the most highly distorted in the crystal, it is reasonable to suppose that it is thermodynamically unstable and that the reorientation accompanying heating is associated with a transition to a more stable state. It is also natural to suggest that the newly oriented material is identical with the nuclei responsible for recrystallization (see Part *g*), but this possibility has not yet been subject to careful experimental investigation.

[29] C. S. Barrett, Trans. A. I. M. E. **135**, 296 (1939); C. S. Barrett and L. H. Levenson, Trans. A. I. M. E. **135**, 327 (1939).

[30] J. M. Burgers, Proc. Phys. Soc. **52**, 23 (1940).

[31] E. N. da C. Andrade and Y. S. Chow, Proc. Roy. Soc. **175**, 290 (1940).

Here and There

Rockefeller Foundation Grant

The following statement is an excerpt from the Minutes of the November meeting of the Executive Committee of the Governing Board of the American Institute of Physics:

"The American Institute of Physics has for several years been greatly indebted to the Rockefeller Foundation for encouragement and financial assistance in developing a well-rounded and normally self-sustaining publication program in the field of physics. A drastic decline in foreign dues and subscription income caused by the war in Europe has now threatened to cancel the gains which have been made. In response to the Institute's appeal on this account, the Foundation has generously granted the sum of $20,000 to assist the Institute to adjust the publication program to the new circumstances.

"Therefore, be it resolved: That the Executive Committee express for the Institute its full appreciation of this timely and generous assistance and convey to the Rockefeller Foundation an assurance of the gratitude of physicists."

★

New Electron Microscope

Details of a more effective and simplified model of the RCA electron microscope were discussed recently before a convention of the Institute of Radio Engineers in New York City, by James Hillier of the RCA Research Laboratories. A section of the new model is shown on the cover of this issue; Dr. V. K. Zworykin, under whose direction the instrument was designed and constructed, is shown standing beside it; while James Hillier, co-developer, sits at the controls. The electron microscope is capable of magnifying objects up to 100,000 times and has therefore far-reaching possibilities in virtually every field of medical and industrial research. RCA's first electron microscope, announced early last year, was designed primarily for use by electrical experts and physicists; the new model is smaller and better adapted for use in general medical and chemical laboratories since it may be operated by any competent laboratory worker.

Despite its radical design improvements, Mr. Hillier said, the new microscope yields nothing in operating efficiency to the earlier model. The new instrument, housed in a steel cabinet, is completely self-contained and is ready for operation when plugged into an ordinary light socket, according to Mr. Hillier. It is not affected by magnetic fields set up by other electrical equipment, as was the earlier model, nor is it disturbed by ordinary room vibrations. An important feature is an ingenious "submarine lock" arrangement for changing specimens in the evacuated chamber of the instrument without admitting air. A number of viewing windows are provided through which several persons can study specimens at the same time.

The RCA electron microscope operates very much like an ordinary light microscope, except that instead of glass lenses and light, it utilizes a stream of electrons propelled at high speed through a series of magnetic coils, Mr. Hillier explained. "Commercial possibilities for the electron microscope, even in such an all-important field as national defense (where it may be used to improve materials and processes) led to the development of this simpler instrument," he said. "We are now engaged in producing the new microscope for use in leading educational and commercial research laboratories throughout the country."

★

Book on "Temperature—Its Measurement and Control"

It was announced last year that a book on "Temperature—Its Measurement and Control in Science and Industry" was in preparation to make permanently available the valuable papers presented at a symposium on this subject sponsored by the American Institute of Physics with the cooperation of the National Bureau of Standards and the National Research Council, held in New York. This monumental volume will be ready for distribution about the middle of February. The original papers have been carefully edited by authorities in their fields. They have also been rearranged, supplemented and exhaustively indexed. All phases of temperature are covered in great detail. By special arrangement, the book is to be published by the Reinhold Publishing Corporation, 330 West 42nd Street, New York City, at a list price of $11.00 per copy. A valuable Appendix of 25 reference tables is also included and this may be purchased separately bound for $1.00 per copy. With introductory material and indexes, the volume runs to 1375 pages. It will be especially valuable for chemists, teachers, physicists, biologists, medical men, metallurgists, geologists, electrical, mechanical and refrigerating engineers, and plant-operating officials.

★

Honor Parole

According to a wireless dispatch to *The New York Times*, Dr. Paul Langevin, formerly Professor of Experimental Physics at the College de France, who had been detained in the Cherche Midi prison in Paris, has received an honor parole. His release was ordered for reasons of health. Professor Langevin was deprived of his professorship because of his political activities.—*Science.*

★

Holder of 52 Patents Cited

Dr. C. Guy Suits, 35-year-old physicist who was named assistant to the Director of the General Electric Research Laboratory in October, has been chosen as one of the outstanding young men of 1940 in the annual selection of Durward Howes, editor of *America's Young Men*, a biographical work. Dr. Suits, a graduate of the University of Wisconsin, has 52 patents and credit for creating the hottest flames ever made by man. These were electric arcs twice as hot as the surface of the sun.

Dublin Institute for Advanced Studies

The founding of the Dublin Institute for Advanced Studies, by an act of the Oireachtas, in October, was announced in a recent issue of *Nature*. For the present it consists of two schools, the School of Celtic Studies and the School of Theoretical Physics. The Institute will provide facilities for advanced studies and research in special branches of knowledge, according to the announcement, and for the publication of the results of such studies, irrespective of whether or not they have originated from the Institute. Moderate fees will be charged, but a limited number of scholarships are available.

The scope of the School of Theoretical Physics is described as "the investigation of the mathematical principles of natural philosophy and their application to the sciences in which they obtain." The first senior professor appointed to the School of Theoretical Physics is Professor E. Schrödinger, formerly of the University of Graz.

★

University of Michigan Honors Retiring Professor

Professor Harrison M. Randall, Chairman of the Department of Physics of the University of Michigan has retired after forty years of service in the University, according to a recent note in *Science*. In his honor East Physics Hall is to be known as the Harrison M. Randall Laboratory of Physics, the regents of the University have announced. Dr. Randall has been appointed Henry Russel lecturer for 1940–41. This award goes to the faculty member judged to have attained the highest scholastic distinction during the year.

★

Many-Valued Logics

Seven years ago a physicist, Dr. F. Zwicky of the California Institute of Technology, declared that he thought it would be easier to explain the atom if he could use a many-valued logic instead of the usual two-valued logic. By a many-valued logic he meant one which denies the principle of *reductio ad absurdum*. This new logic states that, instead of the two possibilities, "so" and "not so," there are n possibilities. When n is small, there might be a chance of saying what the possibilities are. For instance, when n is six, the possibilities might be "certainly so," "probably so," "possibly so," "possibly not so," "probably not so," and "certainly not so." Even the most precise and clear-cut statement may fall into any one of n possible cases, according to the new theory.

Systematic work has been done on the problem of the development of many-valued logics by a number of workers, and a survey report of their findings was presented by Professor J. Barkley Rosser of Cornell University at the November meeting of the American Mathematical Society held at Wayne University, Detroit, Michigan. The principal result, according to Professor Rosser's statements, is the discovery that a many-valued logic proves to be much more complicated than anyone expected. In a three-valued logic, for instance, there are 256 distinct meanings of the simple word, "and"; in a four-valued logic there are 14,348,907 distinct meanings of the same word. All this complication makes things hard for the mathematician, but allows more freedom for the physicist. Imagine, proponents of the theory point out, how many possible kinds of atoms a physicist could make out of electrons *and* protons with 256 kinds of "and" to choose from, and how much more chance he'd have of finding one that worked the way it ought to!

★

Sanitizing Service

"Protecto-Ray Bathrooms" is the term applied to a new and exclusive service of sanitizing bathrooms in the Hotel New Yorker in New York City, according to Frank L. Andrews, the hotel's president. A special Protecto-Ray machine has been developed by the hotel in conjunction with the General Electric Lighting Laboratory in Nela Park, Cleveland. It is a specially constructed portable unit on wheels with ultraviolet ray equipment of high intensity which, the announcement states, destroys all bacteria, germ life and fungi known as athlete's foot. These machines, fifty of which are in use in the hotel, are operated by the regular maids. After each bathroom is cleaned upon the departure of a guest, a Protecto-Ray machine is wheeled into the bathroom and turned on for a minimum of ten minutes, regulated by an automatic timing device. The bathroom door is then sealed with Cellophane, assuring the next guest that the bathroom is thoroughly sanitary.

★

Mathematical Biophysics

The table of contents of the March issue of the *Bulletin of Mathematical Biophysics*, edited by N. Rashevsky and published by the University of Chicago Press, includes the following articles:

Some Remarks on the Movement of Chromosomes During Cell Division, by N. RASHEVSKY;
On Reinforcement and Interference Between Stimuli, by G. YOUNG;
Studies in the Mathematical Biophysics of Discrimination and Conditioning. I, by H. D. LANDAHL;
Cellular Forms and Movements, by A. S. HOUSEHOLDER.

★

Spectrographic Analysis Conference

A second Midwest Conference on Spectrographic Analysis will be held in the Kent Chemical Laboratory at the University of Chicago on Saturday, March 29, according to an announcement received from that Laboratory. Because of the growing importance of absorption spectroscopy, the announcement states, this year's conference will be held in two divisions, one dealing with emission spectra, the other with absorption spectra. The former is being organized by W. C. Pierce, of the University of Chicago, and the latter by Elmer Miller, of the University of Minnesota. Further information and copies of the final program may be obtained from either of these men.

Contributors to This Issue

J. W. Marshall

Raymond G. Spencer, Professor and Head of the Department of Physics at Albion College, Albion, Michigan, has been making x-ray studies of static and cyclic stressing of metals for the last several years. He received his Ph.D. degree from the University of Chicago in 1932.

J. Wallace Marshall is a graduate student at the University of Michigan. He received his B.A. and M.A. degrees in 1938 and 1939 from Albion College, Albion, Michigan, and remained at that institution for one year as research assistant in the Physics Department.

R. G. Spencer

I. A. Deutch

Isador A. Deutch has been a mechanical engineer in the Department of Smoke Inspection and Abatement, Chicago, since 1926; he took part in the Air Pollution Study of Chicago made in 1938–40. Mr. Deutch received the B.S. degree in Chemical Engineering at the Armour Institute of Technology in 1925.

O. A. Mortensen received his M.D. degree from the University of Wisconsin in 1929 and served his internship at the Kansas City Research Hospital. Dr. Mortensen joined the faculty of the University of Wisconsin in 1930 as an instructor in anatomy. He is now Associate Professor of Anatomy there.

O. A. Mortensen

Sidney Bloomenthal

Sidney Bloomenthal joined, in 1940, the staff of the Automatic Electric Company, Division of the Associated Telephone and Telegraph Corporation, Chicago. Since receiving his Ph.D. degree from the University of Chicago in 1939, Dr. Bloomenthal has worked with RCA, the U. S. War Department, the University of Chicago, and the Chicago Department of Smoke Inspection and Abatement.

Mark A. Townsend received his B.S. degree in 1936 from the Texas Technological College and his M.S. in 1937 from the Massachusetts Institute of Technology. Following his graduation he was employed by the General Electric Vapor Lamp Company. In 1939 he was transferred to the Lamp Development Laboratory of the General Electric Company in Cleveland.

M. A. Townsend

W. E. Trumpler, Jr.

J. A. Stratton received his S.B. degree in 1923 and his S.M. degree in 1925 from the Massachusetts Institute of Technology. In 1927 he obtained the Sc.D. degree in physics at the Technische Hochschule in Zürich. Since 1928 Dr. Stratton has been a member of the faculty of the Massachusetts Institute of Technology.

William E. Trumpler, Jr., was graduated from Lehigh University in 1937 with a B.S. degree in mechanical engineering. He has since been engaged in steam turbine design for the Westinghouse Electric and Manufacturing Company.

J. A. Stratton

The following contributors have received mention in earlier issues of the *Journal of Applied Physics:*

L. J. Chu, p. 580, Vol. 9, No. 9, 1938.
Frederick A. Maxfield, p. 580, Vol. 9, No. 9, 1938.
Thomas A. Read, p. 128, Vol. 12, No. 2, 1941.
Reinhold Rüdenberg, p. 693, Vol. 11, No. 10, 1940.
Frederick Seitz, p. 128, Vol. 12, No. 2, 1941.
Eric A. Walker, p. 710, Vol. 11, No. 11, 1940.

New Books

Physical Chemistry of High Polymeric Systems

H. MARK, Adjunct Professor of Organic Chemistry, Polytechnic Institute of Brooklyn, New York, New York. Volume 2 of *High Polymers*. Pp. 345+vii, Figs. 99, 16×23½ cm. Interscience Publishers, Inc., 215 Fourth Ave., New York, 1940. Price $6.50.

Except for minor changes and additions, this book is a translation of the author's recently published *Allgemeine Grundlagen der hochpolymere Chemie*, the first volume of Meyer and Mark's *Hochpolymere Chemie. Ein Lehr- und Handbuch für Chemiker und Biologer.*

Physical and physico-chemical methods of value for studying relationships between composition and structure and between structure and properties are, with few exceptions, the same for high polymeric systems as for systems containing only small molecules. However, because the experimental and theoretical complications are generally much greater when high polymers are being studied, a combination of different methods must frequently be employed—and even then a thoroughly satisfactory interpretation of the experimental data is often impossible. It, therefore, becomes advisable for anyone studying the physical chemistry of systems containing high polymers to have as thorough an understanding as possible of the capabilities and limitations of the various conceivably applicable research methods. Hence this book was written —not primarily to summarize the present state of knowledge concerning the physical chemistry of high polymers, but to provide a sound basis for future progress in this field, as well as for the critical evaluation of past work.

The author has done a remarkably fine job in combing the literature for significant articles, in critically extracting from them their essential points, and in presenting these briefly, yet clearly and understandably, in their proper perspective relative to each other.

The treatment in most of the book is nonmathematical, although the fundamental equations related to the more important phenomena and methods are given and the language of the calculus is used fairly extensively in the treatment of such subjects as osmotic phenomena, solubility, viscosity and polymerization kinetics. Many references are included to the more important papers and books in the fields covered, thus directing the reader to appropriate sources for details of the mathematical and experimental methods, further applications, etc. The choice of material for the numerous tables and figures is excellent.

The first chapter, "The geometry of molecules," contains sections dealing with x-ray and electron diffraction, polarizability and dipole moments, and the Kerr effect. The second chapter, "The internal motions of molecules," presents mainly some results of band spectrum and specific heat studies. The "Primary and secondary valence" chapter is a discussion of intra- and intermolecular forces. In the chapter on "Crystal structure, lattice forces and chemical structure of the unit cell," crystals are classified, first on the basis of the interatomic forces involved, then on the basis of their symmetry. "Molecular arrangement in liquids and the investigation of minute crystals" deals with x-ray methods for studying such systems. The chapter on "The behavior of mixtures" presents a condensed thermodynamic treatment of mixtures, with especial regard to such properties as osmotic pressure and solubility, in addition to an admirable discussion of the viscosity of liquids and solutions. In the final chapter, "Kinetic phenomena in high polymer chemistry," diffusion phenomena and the kinetics of the formation and degradation of long-chain molecules are considered.

In conclusion, the reviewer is glad to recommend this volume, not only to those whose chief interest is in the high polymer field, but also to those interested in correlating the properties of *low* molecular weight substances with their structures.

M. L. HUGGINS
Eastman Kodak Company

The Story of Superfinish

ARTHUR M. SWIGERT, JR. Pp. 672, Figs. 720, 16×23½ cm. Lynn Publishing Company, Detroit, 1940. Price $5.00.

This book describes a recently-developed process for producing commercially fine finishes on machine surfaces of any shape, which hitherto could be approached in quality only by expensive lapping processes. The new process employs a random abrasive action which geometrically develops a smooth true surface by eliminating the surface points and projection above the bearing or contact surface.

EUGENE PERKINS
University of Pittsburgh

Handbook of Physics and Chemistry

24th Edition. Pp. 2564, 12½×18½ cm. Chemical Rubber Publishing Company, Cleveland, Ohio, 1940. Price $3.50.

Every year this important handbook becomes bigger and better. The physicist, in particular, will be interested in the sections on mathematical constants; physical constants in the fields of heat, sound, electricity, light, and specific gravity; and in the tables of elements and their properties. In the present edition, 7 pages are devoted to induced radioactivities.

A 31-page index makes most of this material readily available. The handbook is well-bound and costs less than one-seventh cent per page.

Contributed Original Research

An X-Ray Study of the Changes That Occur in Aluminum During the Process of Fatiguing

RAYMOND G. SPENCER AND J. WALLACE MARSHALL
Albion College, Albion, Michigan

(Received November 1, 1940)

Carefully prepared test bars of 17S–T aluminum alloy have been fatigued; x-ray diffraction patterns of each specimen were taken at intervals as fatiguing progressed. Approximately thirty different test bars have been studied. Seven series of diffraction patterns, corresponding to seven different specimens, are reproduced and discussed in this paper. This study shows that (1) fatigue failure of 17S–T aluminum is always preceded by fatigue damage which is detectable by the use of x-ray diffraction patterns; (2) nearly all of the detectable changes occur in the last stages of fatiguing and consist of rotation of grains, introduction of strains in some of the crystallites, and fragmentation of some of the crystallites; (3) these changes do not occur when the specimen is fatigued below its endurance limit, but always occur prior to failure when it is fatigued above the endurance limit; (4) failure is probably intercrystalline rather than intracrystalline in character.

INTRODUCTION

A LARGE percentage of the very large number of experimental studies of fatiguing of metals consists merely of subjecting the samples to repeated cycles of stress and recording the number of cycles required to cause failure. These data yield the so-called $S-N$ curves which indicate a more or less accurate endurance limit and give, with rather poor accuracy, the number of cycles required to cause failure at a given stress, but give no information at all about what happens within the sample to cause it to fail or what physical changes, if any, precede failure. At stresses much above the endurance limit the number of cycles required to produce failure of different specimens of the same material varies over wide limits. For example, one can say that different specimens of the same material, fatigued in exactly the same manner at the same stress, will fail after being subjected to somewhere between two and three million cycles of stress.

Fatiguing of metals might be expected to cause any one, or all, of the following reactions: (1) rotation or reorientation of some of the crystallites, which may or may not be a preferred orientation, (2) a warping of some of the crystallites which would represent a strained condition with consequent lattice distortion, (3) fragmentation of some of the crystallites and (4) a gradual weakening and consequent breaking of the intercrystalline bonds. Under suitable conditions, any one of the above-mentioned reactions, except (4), will produce a corresponding and detectable change in the x-ray diffraction pattern. If the nature of the specimen in its original conditions is such that the diffraction lines consist of a row of separate spots, fragmentation would produce a larger number of spots, rotation of a crystallite would change the position of the corresponding spot, and lattice distortion of a crystallite would cause the corresponding spot to become blurred. Fragmentation of sufficient extent would cause the spots to coalesce. Lattice distortion in a specimen which has crystallites small enough to produce uniform, solid diffraction lines would cause the lines to widen and decrease in intensity. It should be pointed out that, while most of the changes that one would expect to take place within the metal when it is fatigued cause changes in the diffraction pattern, it is not always possible to be sure which of the possible reactions has affected the pattern. For example, if the specimen has small grains of the order of magnitude of 10^{-4} cm, either further fragmentation or lattice distortion would cause the diffraction lines to broaden and it would be difficult to distinguish between the two.

Since any reasonable understanding of the causes of fatigue failure awaits a knowledge of the changes within the specimen which precede failure, it is not surprising to note that several investigators have attempted to study these changes by using x-ray diffraction methods. Charles S. Barrett[1] has given a critical review of the literature up to 1936, including a rather complete bibliography. Gough and Wood[2–4] have published a series of papers on x-ray studies of both cyclic and static stresses in ferrous metals and conclude, among other things, that fatiguing of steel below the endurance limit has no appreciable effect on the crystalline structure, that fatigue failure is preceded by definite and detectable changes in crystalline structure, and that failure due to static and cyclic stressing is preceded by the same changes in structure. Wever and Möller[5] point out the rather obvious fact that there is a marked difference in the response of the specimen from place to place on its surface due to cyclic stressing. They followed the practice of etching a small spot on the surface of the specimen and assumed that the maximum damage would occur at this spot. The specimen was locked in the x-ray camera so that this etched spot was always irradiated. They conclude that they can differentiate between safe and unsafe stresses. Wever, Hemple and Möller[6] conclude that fatigue damage can be detected by x-ray methods in the case of cold-worked steel. Barrett[1,7] has studied both steels and aluminum alloys. He states that, in general, it is not possible to distinguish between safe and unsafe stresses from x-ray diffraction patterns. He also states that the changes in the diffraction patterns reveal cold work due to fatigue, not necessarily fatigue damage, and that cold work may take place at stresses both above and below the endurance limit. Cold work, of course, does not necessarily weaken the specimen. One of the authors[8] has shown that x-ray methods can be used to distinguish between safe and unsafe stresses in malleable iron and to reveal the progressive changes that occur in the metal when it is stressed above its endurance limit. His studies show that these changes do not occur when malleable iron is stressed below its endurance limit. Kies and Quick[9] have worked with 25S aluminum alloy and conclude that x-ray diffraction patterns do not reveal any significant structural changes due to fatigue stressing of the alloy.

Materials Used and Preparation of the Specimens

17S–T aluminum alloy, specially prepared bars of which were kindly furnished by Mr. D. W. Smith of the Aluminum Company of America, were used in all of the tests described in this paper. The 17S–T ingot was hot rolled to $\frac{3}{4}$ of an inch diameter. This rod was then cold-worked to 0.625 of an inch diameter, straightened and heat treated at 950°F. The samples were handled in such manner that no internal strains could have been introduced into them prior to the time that they were put into the fatiguing machine. Mr. Smith states that 17S–T aluminum alloy has a tensile strength of 61,400, a yield strength of 39,000 and an endurance limit at 500,000,000 cycles of 15,000 pounds per square inch. The endurance limit of the specimens as we prepared them is about 2000 pounds per square inch less than this.

Each specimen was machined to one-half inch diameter. A constriction of circular contour was then machined near one end. The smallest diameter of this constriction was $\frac{3}{8}$ of an inch. The last half-dozen cuts of the lathe tool when machining the constriction were about 0.0005 of an inch in depth. The specimen was then polished with fine aloxite cloth. Finally, the specimen was etched to remove any crystallites which might have been strained during the process of machining and polishing, and to remove any finely powdered aluminum and abrasive dust which

[1] Charles S. Barrett, Trans. A. S. M. E. **25**, 1115–1143 (1937).
[2] H. J. Gough and W. A. Wood, Proc. Roy. Soc. **A154**, 510–539 (1936).
[3] H. J. Gough and W. A. Wood, Proc. Roy. Soc. **A165**, 358–371 (1938).
[4] H. J. Gough and W. A. Wood, Proc. Inst. Mech. Eng., London **141**, 175–185 (1939).
[5] F. Wever and H. Möller, Naturwiss. **25**, 449–453 (1937).
[6] F. Wever, M. Hemple and H. Möller, Archiv f. Eisenhuttenwesen **11**, 313–318 (1937–38).
[7] Charles S. Barrett, Metals and Alloys **8**, 13–21 (1937).
[8] Raymond G. Spencer, Phys. Rev. **55**, 991–994 (1939).
[9] J. A. Kies and G. W. Quick, Report No. 659, National Advisory Committee for Aeronautics (1939).

might have been imbedded in the surface. Specimens with etched surfaces, of course, have a lower endurance limit than polished surfaces. However, crystallites which have been broken up or strained by machining and polishing must be removed from the surface or the results will be confusing. A study of surfaces prepared in this manner will reveal what changes occur due to fatiguing not confused by strains or fragmentation of crystallites which have been produced by other processes before fatiguing has started.

The Camera

A circular camera was used. The film was on the circumference and the part of the specimen which was irradiated was in the center of the circle. The collimating system was so designed that a large number of well-defined spots appear in each line. The x-ray beam struck the specimen in the middle of the constriction on its minimum circumference at a point which was subjected to the maximum stress. However, it must be noted that the x-ray beam did not necessarily strike at the point of maximum strain or where the first fatigue crack would start.

Iron *K*-alpha x-rays were used. This soft radiation penetrated a comparatively short distance into the specimen and gave large deviations of the diffracted beams. Both of these conditions have advantages for this type of work. Each diffraction pattern contains lines from the 111, 100, 110, and 311 sets of planes and the second-order lines from the 111 and 100 sets of planes. The angle of deviation of the second-order diffracted beam from the 100 planes is roughly 145 degrees.

The specimens were fatigued in an ordinary rotating beam machine in our laboratory. They were removed from the machine at intervals as fatiguing progressed so that diffraction patterns could be made. The camera was so designed that a specimen could be removed and replaced in the same position. Thus, the same area was irradiated each time an exposure was made. If, after the specimen was broken, it was found that the fracture passed through this area, it was put in the camera in a slightly different position so that the x-ray beam struck it a small distance away from the edge of the fracture. When diffraction patterns were made after a specimen was broken, the x-ray beam was never permitted to strike the specimen so that any part of it struck a fatigue crack or the edge of a fracture. (Except, of course, when we wished to study the structure of the fractured surface. The x-ray beam was then directed upon the face of the fracture.) Under these conditions, we think it is logical to assume that the damage revealed by the diffraction patterns taken after failure occurred prior to failure, rather than to assume that the damage was caused by the breaking of the specimen. To test this assumption we took diffraction patterns at different places on the circumference adjacent to the edge of the fracture of some of the specimens after they had broken. We found that in some positions very marked damage was revealed, in others only slight damage was indicated, and sometimes a position was found where no damage at all was revealed. For example, Fig. 4(E) shows a place adjacent to the fracture where very marked damage had occurred; Fig. 4(F) shows another position on the circumference adjacent to the fracture where only slight damage was revealed. If the act of rupturing caused the damage indicated, this damage should have occurred at all positions adjacent to the fracture. Whenever we made a survey of different positions on the circumference of a broken specimen, we always found one position where very marked damage was indicated, and other positions where little or no damage was revealed. We assume that the fracture which caused the specimen to fail started on the side of the specimen where the marked damage was indicated. It seems obvious that the damage revealed in the diffraction patterns occurred prior to failure and was the cause of failure. Since, as will be pointed out later, failure follows very soon after detectable damage occurs, the probability that a specimen could be removed from the fatiguing machine at the right time, prior to failure, for this damage to be evidenced in the diffraction pattern is very small. Nevertheless, a few specimens were removed at the proper time to have damage revealed prior to failure. The diffraction patterns of specimen No. 7 show clearly that detectable damage occurred before failure.

FIG. 1. X-ray diffraction patterns from specimen No. 1. Stress 11,000 lb./sq. in. (A) before fatigue. (B) after 1000 cycles. (C) 5,000,000. (D) 17,000,000. (E) 23,000,000. (F) 60,000,000.

RESULTS

Specimen No. 1 was fatigued at a stress of 11,000 lb./sq. in., which is approximately 2000 lb./sq. in. below the endurance limit. Figure 1(A) is the diffraction pattern taken before fatiguing started, (B) after 1000 cycles, (C) after 5,000,000 cycles, (D) after 17,000,000 cycles, (E) after 23,000,000 cycles, and (F) after 60,000,000 cycles. The specimen did not break. The spots in the lines of these patterns are sharp and clear and show no changes with increasing fatigue. Even after 60,000,000 cycles the diffraction pattern is unchanged.

Specimen No. 2 was fatigued at a stress of 16,500 lb./sq. in. Figure 2(A) is the diffraction pattern taken before fatiguing started, (B) after 1000 cycles, (C) after 1,200,000 cycles, (D) after 7,500,000 cycles, (E) after the sample had broken, and (F) at a different place on the circumference after the sample had broken. The specimen broke after 8,200,000 cycles. Only very slight changes occurred in the diffraction patterns until sometime after the specimen had undergone 7,500,000 cycles of stress. All the changes indicated in (E) and (F) took place sometime during the last 700,000 cycles.

Specimen No. 3 was fatigued at a stress of 22,700 lb./sq. in. Figure 3(A) is the diffraction pattern taken before fatiguing started, (B) after 1000 cycles, (C) after 1,500,000 cycles, (D) after 2,200,000 cycles, (E) after 2,500,000 cycles, and (F) after 2,800,000 cycles after the specimen had broken. (E) indicates that no appreciable damage had occurred up to that time, but (F) indicates very marked changes. These changes must have taken place sometime during the last 300,000 cycles.

Specimen No. 4 was fatigued at a stress of 27,500 lb./sq. in. Figure 4(A) is the diffraction pattern taken before fatiguing started, (B) after 1000 cycles, (C) after 640,000 cycles, (D) after 744,000 cycles, (E) after the specimen had broken at 760,300 cycles, and (F) at a different place on the circumference after the specimen had broken. Here again, nearly all of the fatigue damage occurred in the last stages of fatiguing, in fact, nearly all the damage indicated by (E)

FIG. 2. X-ray diffraction patterns from specimen No. 2. Stress 16,500 lb./sq. in. (A) before fatigue. (B) after 1000 cycles. (C) 1,200,000. (D) 7,500,000. (E) and (F) 8,200,000.

took place during the last 16,000 cycles. (F) indicates much less damage than (E), which shows that different areas of a specimen subjected to the same stress may respond very differently. This shows that x-ray studies of fatiguing are probably misleading, if arrangements are not made to have the x-ray beam survey the same area each time a diffraction pattern is made.

Specimen No. 5 was fatigued at a stress of 30,000 lb./sq. in. Figure 5(A) is the diffraction pattern taken before fatiguing started, (B) after 1000 cycles, (C) after 440,000 cycles, (D) after the specimen had broken at 560,500 cycles, and (E) at a different place on the circumference after the specimen had broken. In this case, marked changes in crystalline structure evidently took place during the first few cycles of fatiguing. (B) taken after only 1000 cycles indicates some fatigue damage. Fatigue damage increased steadily until failure occurred. No other specimen that we fatigued responded in this manner. It was first thought that this behavior might be due to the relatively high stress at which the specimen was run and that the response was due to plastic flow or cold work of the surface as Barrett contends. To check this

possibility, several other specimens were run at the same and higher stresses, but in all of these cases practically all of the fatigue damage occurred in the last stages of fatiguing. For example, see Fig. 6.

Specimen No. 6 was fatigued at a stress of 32,000 lb./sq. in. Figure 6(A) is the diffraction pattern taken before fatiguing started, (B) after 1000 cycles, (C) after 69,500 cycles, (D) after 153,000 cycles (E) after the specimen had broken at 181,300 cycles, and (F) at a different place on the circumference of maximum stress after the specimen had broken. Here again, the detectable fatigue damage took place in the last stages of fatiguing.

Specimen No. 7 was fatigued at a stress of 26,000 lb./sq. in. Figure 7(A) is the diffraction pattern taken before fatiguing started, (B) after 600,000 cycles, (C) after 700,000 cycles, (D) after the specimen had broken at 725,000 cycles, and (E) is a diffraction pattern taken with the x-ray beam incident upon the broken end. (C) indicated that definite, detectable damage had occurred prior to failure. Since neither (C) nor (D) indicates the marked damage that is often revealed, it is probable that more damage

FIG. 3. X-ray diffraction patterns from specimen No. 3. Stress 22,700 lb./sq. in. (A) before fatigue. (B) after 1000 cycles. (C) 1,500,000. (D) 2,200,000. (E) 2,500,000. (F) 2,800,000.

would have been revealed at some other position on the circumference if a survey of the entire circumference had been made.

DISCUSSION AND CONCLUSIONS

Although diffraction patterns for only seven specimens are shown in this paper, at least thirty different specimens were studied. The fatigue stresses for the seven specimens discussed here vary from 2000 lb./sq. in. below the endurance limit to stresses of more than two and one-half times the endurance limit. In all instances except one, specimen No. 5, nearly all of the detectable fatigue damage occurred in the last stages of fatiguing. Since no other specimen of the thirty studied responded as did No. 5, we feel that its behavior is due to some unknown, spurious condition. We think that it is permissible, logical and necessary to neglect it in drawing general conclusions. It is included here only for the sake of scientific completeness. Anyone who reads this paper may attach whatever significance to it that he wishes.

Distortion of various types within a crystallite would cause an increase in the size of its corresponding spot in the diffraction pattern. Increase in size of some of the spots due to this cause is evident. However, some of the large spots which we found, we think, cannot be due to distortion. If the increase in spot size is due to distortion, the density of the spot should decrease, partly due to the fact that the diffracted x-rays are distributed over a larger area on the film. Some of the spots increase in size and, also, in density. This is exactly what one would expect if two crystallites should rotate so that their spots coalesce. These large, dense spots do not occur until the specimen is near failure.

The suddenness with which failure follows detectable damage is of considerable interest. Detectable fatigue damage indicates that failure is imminent. It does not seem reasonable to assume that the cyclic stresses cause no damage within the metal until failure is almost reached and then the incidence of damage sets in. It seems to us highly probable that the specimen is damaged in some way in the early stages of fatiguing, but that this damage is not revealed

FIG. 4. X-ray diffraction patterns from specimen No. 4. Stress 27,500 lb./sq. in. (A) before fatigue. (B) after 1000 cycles. (C) 640,000. (D) 744,000. (E) and (F) 760,000.

in the diffraction patterns. Since the diffraction patterns show very slight or no change until failure is imminent, this early damage, if it occurs, cannot consist of fragmentation of crystallites or introduction of strains into them. If the failure of the specimen is due to intercrystalline rather than intracrystalline failure, we would expect the type of response that is observed. Any weakening of the intercrystalline bonds would not be evident in the diffraction patterns. Nothing would be evident until some of these bonds gave way and the crystallites started to rotate and to slide over one another. This would cause the strains and fragmentation which are evidenced in the diffraction patterns just prior to failure.

We feel that our studies warrant the following conclusions: (1) Fatigue failure of 17S–T aluminum alloy is always preceded by fatigue damage which is detectable by x-ray methods. (2) Nearly all of the detectable damage occurs

FIG. 5. X-ray diffraction patterns from specimen No. 5. Stress 30,000 lb./sq. in. (A) before fatigue. (B) after 1000 cycles. (C) 440,700. (D) and (F) 560,500.

in the last stages of fatiguing and consists of rotation of some of the grains, introduction of strains into some of the crystallites, and fragmentation of some of the crystallites. (3) These changes do not occur when the specimen is fatigued below its endurance limit. (4) Repeated cyclic stresses gradually weaken the intercrystalline bonds which cause the metal to fail.

Conclusion No. 1 does not agree with Kies and Quick[9] who state that no significant changes due

FIG. 6. X-ray diffraction patterns from specimen No. 6. Stress 32,000 lb./sq. in. (A) before fatigue. (B) after 1000 cycles. (C) 69,500. (D) 153,000. (E) and (F) 181,300.

FIG. 7. X-ray diffraction patterns for specimen No. 7. Stress 26,000 lb./sq. in. (A) before fatigue. (B) after 600,000 cycles. (C) 712,000. (D) 735,000. (E) from broken end.

to fatiguing are apparent from their diffraction patterns. However, for every one of our specimens that failed, diffraction patterns revealed the fact that marked fatigue damage at some position on the circumference of maximum stress had preceded failure. Barrett[1] does not agree with conclusion No. 3. However, we are convinced that our experimental evidence justifies this conclusion. We do not argue that the experimental evidence proves conclusion No. 4. This conclusion, however, is consistent with the experimental facts and it seems difficult to explain them without it.

ACKNOWLEDGMENTS

It is a pleasure to acknowledge that this study was made possible by grants of money by the Trustees of the Horace H. Rackham and Mary A. Rackham Fund.

Use of the Radioactive Properties of Thorium for a Quantitative Study of Phagocytosis

F. A. MAXFIELD
Department of Electrical Engineering, University of Wisconsin, Madison, Wisconsin

AND

O. A. MORTENSEN
Department of Anatomy, University of Wisconsin, Madison, Wisconsin

(Received October 28, 1940)

Use has been made of the radioactive properties of colloidal thorium dioxide, intravenously injected into rabbits, to study the functional capacity of the reticulo-endothelial cells for phagocytosis. A mathematical analysis of the problem is presented which indicates that when the system is not overloaded, the foreign material should be removed from the blood according to the relation

$$n = n_0 e^{-at} + \frac{b}{2a} n_0 e^{-bt}.$$

Here $a \gg b$ and n is the number of particles remaining in the blood at any time t. Experiments on 13 rabbits substantiate this prediction. With a standard injection of 1 cc of colloidal thorium dioxide per kilogram of body weight, n decreases according to three distinct exponential relations. The system is apparently overloaded initially, but after n decreases to about one-sixth its initial value (at $t=0$), the fraction of the amount of material present that is removed in unit time increases and the rest of the curve follows the predicted relation. The fact that the system is initially overloaded was checked by the use of smaller amounts of thorium. In all cases more than 99 percent of the thorium was removed from the blood stream within 6 or 8 hours after the injection. The technique reported here should serve as a basis for testing many theories of phagocytosis now largely based on deduction.

THE extensive use of artificially radioactive elements such as radio-phosphorus and radio-sodium as tracers in studies of the chemical processes involved in plant and animal metabolism is well known. However, the possibility that long-lived naturally radioactive elements can be used in studying other physiological processes such as phagocytosis apparently has not been fully explored. The disadvantages usually presented against the use of naturally radioactive elements are that they do not enter into the normal chemical reactions of the body and that the cumulative effect of their radiations are harmful to the tissues over a period of time. Colloidal thorium is, however, a very satisfactory substance for a quantitative study of phagocytosis because it is readily taken up by the phagocytic cells and the relative amount in the circulating blood, at any time, can be determined from its radioactive properties. Intravenous injections of colloidal thorium dioxide have been used in clinical x-ray studies for the past ten years, and in the dosage of 1 cc per kilogram the radioactivity is apparently insufficient to produce harmful effects.

When such a colloidal material is injected into the blood stream, it is removed by cells collectively known as the reticulo-endothelial system. These cells are most numerous in the liver, spleen, bone marrow and lymph nodes but in addition are widely distributed in the connective tissues of the body. Obviously the functional activity of such a widely distributed group of cells is difficult to study. It was apparent, however, that the ability of these cells to remove colloidal thorium from the circulating blood would serve as a functional test of the reticulo-endothelial system. Therefore, a measured amount of thorium dioxide was injected into the blood stream of rabbits and the decrease in the radioactivity of blood samples taken at selected intervals was determined.

It is not difficult to estimate the type of results that should be expected in an experiment of this sort. Since the total mass of particulate matter injected into the blood stream is relatively

small and since the dimensions of a colloidal particle are extremely small, even in comparison to the dimensions of an individual cell, phagocytosis probably takes place almost immediately on the contact of a particle with a phagocytic cell. Furthermore, the capacity of a cell for further phagocytosis is probably not appreciably affected by the ingestion of successive particles until the mass of material taken up by an individual cell is of the order of a few percent of the total cell volume. These are not unreasonable assumptions since histological examination of portions of the liver show that individual cells take up literally millions of the colloidal particles even when relatively small doses of colloidal material are used. This is based on the fact that the colloidal particles of thorium dioxide are too small (diameter order of 10^{-6} cm) to be observed with an ordinary microscope even at the highest magnification but agglomerates of the thorium dioxide (diameter order of 10^{-4} cm) can be easily distinguished in the interior of individual cells a few hours after an injection.

Although we have postulated that phagocytosis takes place as soon as a particle makes contact with a phagocytic cell, it is evident that only a small percentage of the particles present actually disappear from the blood stream in a given small interval of time, for the trajectories of the individual particles are of the same order of magnitude as the diameters of the particles themselves and most of their motion is due to the motion of the supporting fluid, the blood. Thus we can assume that the removal of an individual particle is purely a matter of chance since only those particles are removed that are carried into contact with phagocytic cells by the blood stream. It is evident, then, that on this basis the fraction of the total number of particles present that is removed in a given short interval of time is constant.

It may be necessary to postulate also that some of the particles are only temporarily removed from the blood stream and that a fraction of these temporarily removed particles is continually being reintroduced into the blood stream. The possibility of temporary removal is a valid assumption since it has been demonstrated that some of the reticulo-endothelial cells of the liver and spleen, after they have phagocyted particulate material, leave their fixed abode on the walls of the sinusoids and enter the circulating blood. The majority of such circulating phagocytes are arrested in the capillaries of the lung but doubtless a smaller number reach the peripheral blood. Furthermore, because of the very small size of the colloidal particles and the fact that the blood has a finite viscosity and its velocity is very small adjacent to the cell boundaries, some of the thorium dioxide may be temporarily stored in pericapillary fluid spaces and on the surface of the general endothelium. That thorium dioxide so removed from the blood may later re-enter the circulation is distinctly probable.

Let us say, then, that α represents the fraction of the amount of thorium dioxide present that is disappearing permanently in unit time and that β represents the fraction of the amount present that is disappearing temporarily in unit time. To take account of the reappearance of these latter particles in the blood stream, we can let γ represent the fraction of the amount temporarily removed that is reappearing in the blood stream in unit time. Then, if we assume that initially n_0 particles of thorium dioxide are injected into the blood and that at any time, t, there are n particles still present in the blood while n_1 are permanently phagocytized and n_2 are temporarily removed from the circulating blood, we can represent the variation of n with time by two first-order differential equations.

$$dn_1/dt = \alpha n$$
$$dn_2/dt = \beta n - \gamma n_2.$$

Here the first equation simply states that since α is the fraction of the amount of thorium dioxide present that is disappearing permanently in unit time, αn is the instantaneous rate at which particles are permanently phagocytized. Similarily the second equation states that the instantaneous rate at which particles are collecting in regions which will subsequently reintroduce the thorium into the blood stream is given by the difference of the rate at which thorium dioxide particles are accumulating in these regions, βn, and the rate at which these temporarily removed particles are reappearing in the blood stream, γn_2. As in the case of the

first equation, the rate at which particles are disappearing into a temporary abode is proportional to the number of particles available for phagocytosis, n, the proportionality constant being simply β. Similarly the rate at which thorium dioxide particles are reappearing in the blood stream is proportional to the number of particles which have been temporarily removed n_2, the proportionality constant being γ. By combining the above equations to eliminate n, we can get two second-order differential equations for the variation of n_1 and n_2 with time.

$$\frac{d^2n_1}{dt^2}+(\alpha+\beta+\gamma)\frac{dn_1}{dt}+\alpha\gamma n_1=\alpha\gamma n_0,$$

$$\frac{d^2n_2}{dt^2}+(\alpha+\beta+\gamma)\frac{dn_2}{dt}+\alpha\gamma n_2=0.$$

If α, β, and γ are true constants (a reasonable assumption under the conditions of the problem) the solution of these equations yields the following value for n.

$$n=n_0-n_1-n_2$$

or

$$n=[A+\tfrac{1}{2}]n_0e^{-kt}-[A-\tfrac{1}{2}]n_0e^{-ht},$$

where

$$A=\frac{\alpha+\beta-\gamma}{2((\alpha+\beta+\gamma)^2-4\alpha\gamma)^{\frac{1}{2}}}$$

$$h=\tfrac{1}{2}(\alpha+\beta+\gamma)-\tfrac{1}{2}((\alpha+\beta+\gamma)^2-4\alpha\gamma)^{\frac{1}{2}}$$

and

$$k=\tfrac{1}{2}(\alpha+\beta+\gamma)+\tfrac{1}{2}((\alpha+\beta+\gamma)^2-4\alpha\gamma)^{\frac{1}{2}}.$$

Now if we assume that γ is small in comparison to α and β, we can easily simplify this solution to give the following value for n,

$$n=n_0e^{-at}+\frac{b}{2\alpha}n_0e^{-bt},$$

where

$$a=\alpha+\beta$$
$$b=\alpha\gamma/(\alpha+\beta)$$

and

$$b\ll a.$$

Thus, following an injection of a particulate substance into the blood stream, we might expect the number of particles present in the blood to decrease with time according to a rapidly varying exponential function initially when the first term is most important and then according to a less rapidly varying exponential function when the first term has dropped to a small value and the second term is the predominant one.

This analysis, of course, only can apply when the number of free particles in the blood is small enough so that the number of particles making contact with a single phagocytic cell at one time is a small number—perhaps one. If the amount of colloidal material in the blood is large or if the distribution of the colloidal material throughout the blood is non-uniform, as it must be immediately after an injection, the chance of an individual particle being removed in a given interval of time will be reduced and the rate at which particles are disappearing at any time will decrease. This condition will persist until enough phagocytosis has taken place to reduce the number of free particles in the blood to a value small enough to allow phagocytosis of all particles making contact with phagocytic cells. That is, the variation of n with time would only follow the above equation after a time interval long enough to allow for the decrease of n to the required value. Between the times $t=0$ and $t=t_1$, when this condition is reached, n would be given very closely by

$$n=n_0'e^{-ct},$$

where c is a smaller number than a in absolute value.

These relations were verified by a series of tests on 13 rabbits, as follows: Seven rabbits were given a standard intravenous injection of a colloidal suspension of 25 percent thorium dioxide in 20-percent dextrin (Thorotrast) in the amount of 1 cc per kilogram of body weight. Two rabbits received 0.25 cc per kilo of the 25-percent Thorotrast and two received 1 cc per kilo of 6 percent Thorotrast for a net dose of one-fourth the standard amount. Finally one rabbit received 0.5 cc per kilo of 25 percent Thorotrast and one received 2 cc per kilo of 6 percent Thorotrast for a net dose of one-half the standard amount. The six percent Thorotrast was used to determine whether a relative increase in the amount of dextrin for a given amount of thorium had any effect on phagocytosis. No difference in the results could be determined when equivalent amounts of thorium were used.

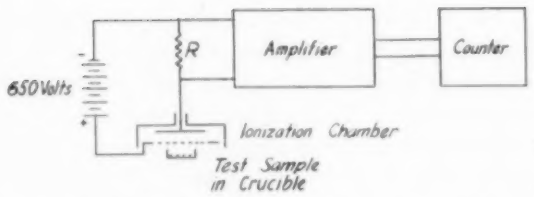

FIG. 1. Ionization chamber and linear pulse amplifier for testing alpha-ray activity.

Following the injections, a series of 2 cc blood samples were removed from each animal at various intervals ranging from 15 minutes to 10 hours. The blood samples were centrifuged and the red cells were discarded after being washed twice with normal saline solution and recentrifuged. Previous tests had shown that the amount of radioactive material discarded with the red cells was small in comparison to the total amount present and that discarding the red cells greatly simplified the reduction of the remaining material. The washings were added to the blood plasma and the total evaporated to dryness and charred. The residue was then transferred to a small ignition crucible and ignited over a Meker burner to remove the organic matter. After allowing the crucibles to cool, they were soaked overnight in separate jars each containing 400 cc of distilled water to remove the soluble salts still present. Finally the samples were again dried and then tested for their alpha-ray activity by means of an ionization chamber and linear pulse amplifier as indicated in the block diagram of Fig. 1. (The resistance R actually used was simply the leakage resistance from the grid of the first Western Electric 259B tube in the amplifier.) By following this procedure we were able to get initial counting rates of approximately 130 to 150 alpha-particles per minute with the largest dosage, while normal blood samples gave a counting rate, including the background in the counting circuit, of less than 0.3 count per minute.

Figures 2, 3 and 4 indicate the type of results obtained when the experimental counting rates were corrected for the counting rate obtained with normal blood samples. Figure 2 shows clearly the speed with which the circulating blood is freed of the particulate thorium dioxide after the injection of 1 cc per kilo of Thorotrast into a typical rabbit. About 85 percent of the particulate matter is removed in the first four hours after the injection and more than 99 percent is removed in five and one-half hours. The solid curve in this figure is obtained from the exponential lines of Fig. 3. Although the break in the curve is not particularly evident from the experimental data plotted in Fig. 2, it is distinctly visible when the data is plotted on semi-logarithmic paper as it is in Fig. 3. The close correspondence between the experimental points and the exponential relations is very striking. In all cases the deviations of experimental points from the exponential lines can be attributed to experimental error. It is clearly evident from Fig. 3 that the number of particles remaining in the blood decreases with time according to three distinct laws. This has been verified in all tests.

Figure 4, which summarizes all the tests made with the standard injection of 1 cc per kilogram of body weight, shows that the counting rate decreases along one exponential curve until it reaches the neighborhood of 20 to 25 counts per minute but beyond this point which may take anywhere from 190 to 410 minutes, depending on the animal, the fraction of the amount present that is disappearing from the blood

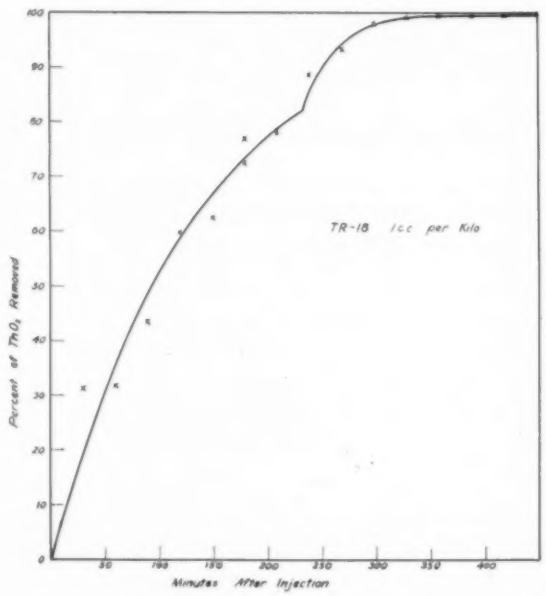

FIG. 2. Graph indicating the speed with which the circulating blood is freed of the particulate thorium dioxide after the injection of 1 cc per kilo of Thorotrast into a typical rabbit.

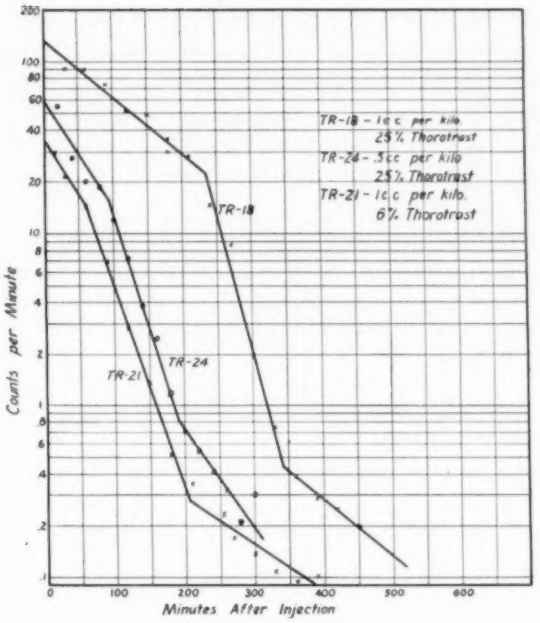

FIG. 3. Graph showing how the number of particles remaining in the blood decreases with time.

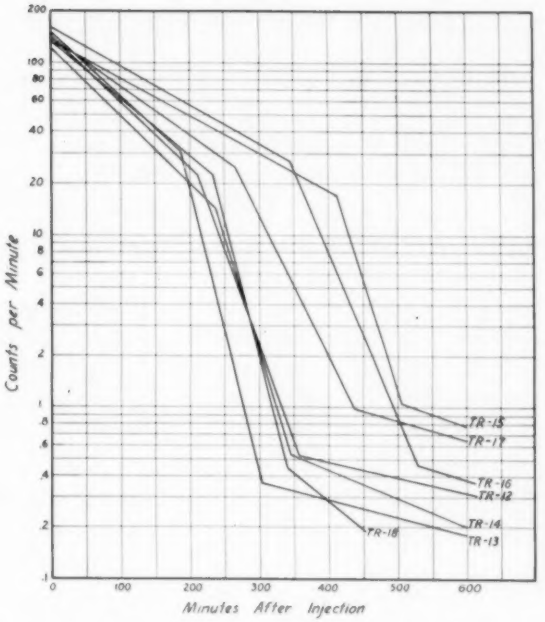

FIG. 4. Graph summarizing all tests made with 1 cc per kilo.

stream in unit time increases by a factor of 4 or 5 and the counting rate decreases along a steeper exponential curve. We can deduce from this that when the counting rate drops to approximately 23 counts per minute, the number of particles present in the blood stream has decreased to such a value that the number of particles striking an individual phagocytic cell in any given time interval is no longer more than the cell can ingest. Finally, there is a second break in the curve when the counting rate is somewhat less than one per minute and the fraction of the number of particles present that are disappearing from the blood in unit time decreases again. We can assume that from here on the number of thorium dioxide particles reintroduced into the blood stream has begun to be important in comparison with the number of particles still circulating in the blood. That is, the slope of the exponential curve as predicted by the equations above has been reduced by the reintroduction of thorium dioxide into the circulating blood. In any case, practically all of the thorium is removed in about 8 hours. With smaller doses (see Fig. 3) the thorium is removed in a correspondingly shorter time, for although the lower portions of the curves are all of essentially the same shape the initial amount of thorium introduced is much less and consequently the time necessary to reach a counting rate in the neighborhood of 20 per minute is considerably reduced. Because of the differences between individual rabbits, even of the same weight, the dose of 1 cc per kilo cannot be expected to lead to an exact comparison between the animals. However, the results show that the only apparent difference between the curves obtained with various rabbits is in the initial chance for removal. The first portion of the curves in Fig. 4 varied slightly in slope with individual rabbits but the other portions were all very nearly alike. Finally we can conclude that the experimental results verify, at least qualitatively, the assumptions made as to the mechanism of phagocytosis. Apparently, when the blood stream is not overloaded, the removal of particulate matter of colloidal size from the circulating blood depends solely on the chance that a particle is carried into contact with a phagocytic cell. When the blood stream contains more than the equivalent of about one-fifth or one-sixth of a cubic centimeter of Thorotrast per kilogram of body weight, however, the system can be considered to be overloaded and the fraction of the amount of particulate matter

present that is removed in unit time is considerably reduced.

Many functions have been assigned to the group of cells primarily concerned in this experiment. It is generally agreed, however, that one important function of the reticulo-endothelial system is the removal of any foreign material (including bacteria) from the circulating blood. In this manner the cells are an important factor in the defense mechanism of the body. Obviously quantitative measurements of the functional capacity of this widely distributed group of cells under varying conditions are important. Colloidal thorium dioxide should prove a good agent for such studies since it is specifically removed by the reticulo-endothelial cells and since its radioactive properties make it possible to determine easily the relative amount remaining in the circulating blood. The technique and the normal data recorded in this experiment should thus serve as a basis for testing in a more objective way this function of the reticulo-endothelial system.

We are indebted to Messrs. R. L. Guest, B. D. Lohmiller and B. E. Lambrecht who assisted in the preparation of the blood samples and in collecting the data. We also wish to acknowledge the assistance of the Wisconsin Alumni Research Foundation which through grants-in-aid made it possible to build the linear amplifier and obtain the animals and other supplies for this research.

*p*H Determinations on Sludge of Particulate Carbonaceous Materials and Ash Discharged in the Atmosphere by Fuel Burning Sources*

S. Bloomenthal† and I. A. Deutch
The University of Chicago and Chicago Department of Smoke Inspection and Abatement, Chicago, Illinois
(Received November 13, 1940)

*p*H measurements on sludge of particulate carbonaceous materials and ash were made with a vacuum tube potentiometer amplifier. Dust, precipitated out of flue gas of industrial fuel burning plants through the use of the series impinger, gives *p*H values of sludge in the range 2.5 to 5. Sludge of ash of coal used in these tests gives *p*H values in the range 7 to 11.5, depending upon the seam and locality in which the coal is mined. The results of this study may aid the "fingerprinting" of dust, responsible, in part, for atmospheric pollution in American cities.

I. Introduction

DURING the past fifty years, many cities of the middle west, where bituminous coal is the main fuel burnt, have been trying to reduce pollution of the atmosphere. Until recently, efforts were directed mainly to a reduction of visible smoke, the source of which can be readily determined. An observer, stationed on the roof of a tall building can watch the performance of hundreds of stacks, and notify violators of the smoke ordinance.

Recently, however, the attention of municipal authorities has been directed to contamination of the air by fuel burning plants that appear to be operating with clean chimneys. A reduction in the amount of visible smoke followed the introduction and acceptance by fuel users of the forced draft stoker, but the problem of excessive, tar-free particulate carbonaceous materials and ash often being discharged into and subsequently settling out of the atmosphere now confronts city authorities. There is a need for a positive method of linking carbonaceous materials and ash (either entrained in or settling out of the atmosphere) with the source. Simply stated there is a need for a method of "fingerprinting" dust.

This paper presents work done to date by the authors in attempting to find some easily measurable property of the chimney dust, which is also characteristic of the fuel burnt. The

* Paper presented at the Washington, D. C. meeting of the American Physical Society, April 25, 1940.

† Now with Automatic Electric Company (Division of Assoc. Tel. & Tel. Corp.), Chicago, Illinois.

success of Wiegand[1] in classifying types of gas carbon according to *p*H determined for the sludge suggested to the authors that similar measurements could be readily carried out on atmospheric contaminants. Wiegand found, for example, that "Peerless" or printing ink colloidal gas carbon, which is best milled in drying oils, has a sludge *p*H of 2.6 ($-\log_{10}[H]=2.6$). Deactivated rubber carbon sludge has a *p*H of 10.6, and this form of carbon is milled into rubber, which usually forms stable sols in alkaline media.

II. Composition of Coal Ash

Fieldner and his collaborators[2] have found significant differences in the chemical composition and softening point for ash obtained from fuel mined in various coal regions of the United States. The quantities of MgO, CaO, Na_2O and K_2O are variable in amount, and hence the alkaline properties of ash sludge ought to be more or less pronounced for different samples of coal. For an ash sample obtained from coal mined in the No. 3 Pocahontas bed in West Virginia, having a softening temperature of 2730°F there was 2.1 percent CaO, 0.9 percent MgO, 1.0 percent Na_2O and 0.4 percent K_2O present. For an ash sample obtained from coal mined in the No. 6 Franklin County, Illinois bed, having a softening temperature of 2320°F, there was 10.1 percent CaO, 1.6 percent MgO, 0.7 percent Na_2O and 0.8 percent CaO present.

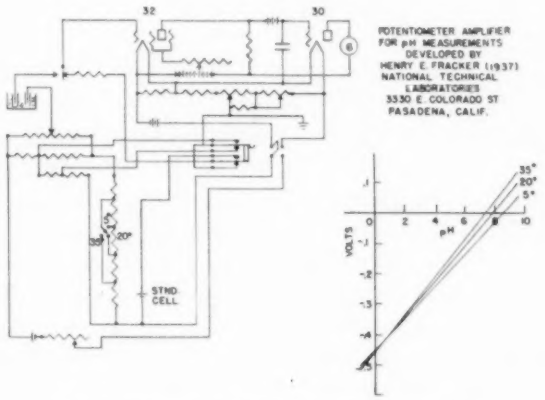
POTENTIOMETER AMPLIFIER FOR pH MEASUREMENTS DEVELOPED BY HENRY E. FRACKER (1937) NATIONAL TECHNICAL LABORATORIES 3330 E. COLORADO ST PASADENA, CALIF.
STND CELL
VOLTS
pH

Fig. 1. Vacuum tube potentiometer amplifier for *p*H measurements.

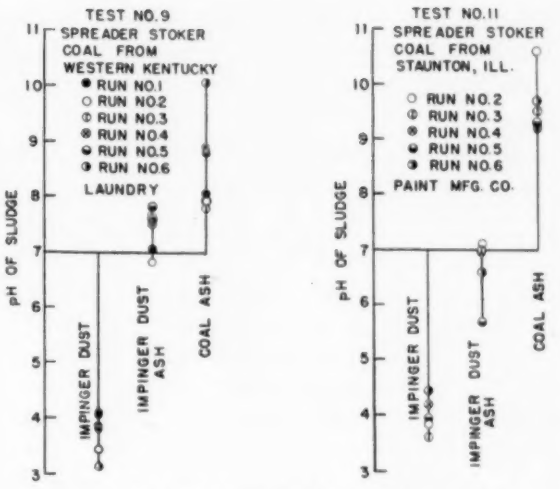

Fig. 2. *p*H values obtained for tests No. 9 and 11.

III. Method for Measuring *p*H of Sludge

The circuit diagram of a *p*H potentiometer amplifier of the type used in this work is shown in Fig. 1. Dr. P. Klopsteg of the Central Scientific Company sponsors this type of instrument, and it has a wide variety of extremely useful applications. Buffers effective at *p*H 3, 4, 7, 8 and 10 were prepared according to the tables of Clark and Lubs and were used to zero the instrument from time to time at a known *p*H value. The potential developed is balanced by the potentiometer circuit, which is arranged to take into account reversal of polarity. Balance is indicated by the vacuum tube amplifier and output meter arrangement. The instrument can be adjusted to compensate for changes in room temperature.

The sludge is prepared by boiling 0.28 gram of solid material in 10 cc of distilled water in a covered 100-cc beaker for fifteen minutes. The suspension is permitted to cool and settle, and about five cc of supernatent liquid is decanted. The sludge remaining is transferred to the five-cc beaker into which the glass and calomel electrodes are inserted. Before this procedure was fixed upon, a sample of Illinois coal ash was disintegrated in distilled water and the *p*H of the sludge determined at intervals during the boiling. The *p*H for sludge cooled to room temperature was 12.0, 12.1, 12.15 and 12.05 at 10, 100, 130 and 160

[1] W. B. Wiegand, Ind. Eng. Chem. **29**, 953 (1937); *Columbian Colloidal Carbons* (New York, 1938), p. 54.

[2] A. C. Fieldner, A. E. Hall and A. L. Feild, *Fusibility of Coal Ash and Determination of the Softening Temperature*, U. S. Bur. Mines Bull. 129 (1918); W. A. Selvig and A. C. Fieldner, *Fusibility of Ash from Coals of the United States*, *ibid.* 209 (1922).

minutes, respectively, after the start of boiling. The material was comminuted during the boiling with a stirring rod.

IV. Collection of Samples

The main project, of which this work is an outgrowth, involved a quantitative study of dust loading in flue gases from various types of industrial fuel burning equipment, and results of the survey have already been published in part.[3,4] Dust was precipitated out of the flue gas in a series impinger, which appeared to be suitable for the work because dust, rather than tarry smoke, is the material collected. In five hours of operation a sample in excess of 10 grams may be collected, sampling being performed at flue gas velocity. Four to six runs were usually made in each plant. The impinger liquid was poured through a 325-mesh screen in some cases to separate + and − sizes. The dust was collected in Alundum filtering crucibles. The amount of soluble material was determined by evaporating to dryness a 100-cc portion of the filtrate. A sample of coal used as fuel in each test was analyzed. When a dust collector was present in the plant, samples of dust retained in it during each run were collected. An attempt was made to obtain samples of dust settled outside of the boiler plant for comparison with that collected in the source.

V. *p*H Measurements

Measurements on *p*H of sludge of impinger dust, ash of impinger dust and ash of the coal used were made for each run of a test on flue gas dust loading in the survey. Figure 2 gives results for tests No. 9 and 11 on a laundry and paint manufacturing company boiler plant, respectively. Western Kentucky coal was used in the former test and coal from Staunton, Illinois, in the latter test. For run No. 6 of test No. 9, the coal was changed, with a consequent reduction in dust loading, and there remains some doubt as to its source. Impinger dust *p*H values in the range 3–4.5 indicate that a variable amount of SO_3 or

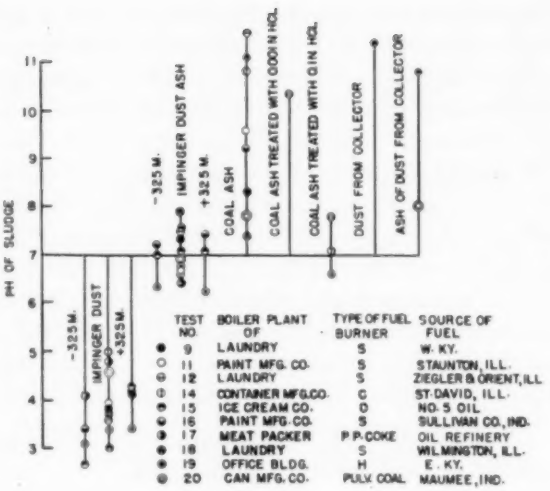

FIG. 3. *p*H values for sludge.

SO_2 may be adsorbed on the carbonaceous dust from the flue gas or liquid, depending upon the amount of sulphur in the coal used, the degree of subdivision of the dust or the action of the impinger in absorbing acid gases. Sludge of ash of impinger dust is nearly neutral because of the solvent action of the acid liquid in the impinger on the original dust entering it. The difference in sludge of ash of coal from western Kentucky and from Staunton, Illinois, is probably caused by a higher content of alkali and alkaline earth elements in Illinois coal.

All of the data obtained in the *p*H tests was plotted as in Fig. 2, but space does not permit all of the diagrams to be presented here. Averages were made for all runs of each test, and the data are shown in Fig. 3. In addition to *p*H tests on sludge of impinger dust, its ash, prepared without fusion, and that of the coal from which it is derived, tests were made on coal ash treated with 0.001*N* and 0.1*N* HCl, followed by ignition in order to find out why the impinger dust ash nearly always gives a lower *p*H value than the sludge of ash of the coal from which it is derived. In two cases, tests 18 and 20, samples were removed from a dust collector associated with the stack of the boiler plant. In the first case, a fresh water washer is used and ifi the second case a multiple baffle Bubar type collector is employed. Sludge of coal ash averaged 11.1 and 7.8 and sludge of ash of dust from the collector averaged 10.8 and 8.0, respectively, in these two cases.

[3] "Low cost flue dust sampler," Power **84**, 70 (April, 1940).
[4] Osborne Monnett, "Air pollution in Chicago," paper read before the Milwaukee meeting of the American Society of Mechanical Engineers, June, 1940.

The ash was unfused in both these tests, and hence the agreement is fairly good. The *p*H of sludge of dust from the collector for test No. 20 is 3.9. This value was found inconvenient for plotting in Fig. 3.

From the results of Fig. 3, it appears to be fairly certain that the −325-mesh dust has a sludge *p*H which is a few tenths of a unit lower than for the +325-mesh dust, probably because of greater surface area. A difference is not marked for *p*H of sludge of ash of this test. Intrinsic coal ash consists of mineral matter, much of which is present in the cell walls of plants prior to carbonization. Burning of the coarse particles, without fusion, brings about a finer state of division. In Fig. 3 *S* designates a spreader and *C* a chain grate type stoker. *O* designates an oil burner. *H* designates a combination with one boiler having forced draft and the second natural draft, both being hand fired.

Dust from an oil burner obtained in test No. 15, which is a mixture of lampblack and petroleum coke particles, gives a *p*H of 3.0 for the impinger dust sludge and slightly less for the −325-mesh fraction, which was separated in some runs. The ash was neutral. In test No. 17, where pulverized petroleum coke was used as fuel the *p*H for the impinger dust fell between 4 and 5, and that for the coke ash near to 11.3 (not shown in Fig. 3).

Significant differences in *p*H of sludge of ash of coal obtained from various localities are also shown in Fig. 3. Illinois coal gives the most alkaline sludge *p*H values, ranging from 9.2 to 11.5 units. The No. 6 seam is worked in many localities in Illinois. For the Maumee, Indiana, coal samples, where the No. 5 seam is probably worked, the *p*H for the coal ash sludge was much lower, falling near to 7.8. The fact that the ash remained unfused in the pulverized coal burning plant, probably indicates the absence of appreciable quantities of alkali or alkaline earth elements in the ash of the coal used in test No. 20. The sludge of ash of western Kentucky coal gave a *p*H value near to 8 and that of eastern Kentucky coal near to 7.3. If mixtures of coal from various seams were sampled, the *p*H of sludge of ash would fall between the *p*H values of the sludge of either constituent.

An attempt was made to correlate *p*H measurements on sludge of dust and its ash, collected by a Lake View housewife complainant, with similar determinations on combustion chamber dust and ash obtained from a nearby laundry equipped with a forced draft spreader type stoker, probably burning coal from northern Illinois. Values were 7.4 and 11.2 for the first two samples, and 11.4 and 11.7 for the last two samples, respectively. The similarity in *p*H values for sludge of the dust ash and of the ash of the coal used in the laundry was an aid in establishing a possible source of neighborhood atmospheric pollution.

VI. Summary

The use of the *p*H potentiometer amplifier in studies on atmospheric pollution is discussed and *p*H values are presented for sludge of dust and ash discharged in the atmosphere by modern industrial plants burning various types of mid-western coal as well as oil and pulverized petroleum coke. It is found that the ash of the dust obtained with the series impinger gives a sludge *p*H value which is lower than that for the ash of coal from which it is derived. However, a close correspondence is found between the *p*H of sludge of ash of dust precipitated in other types of dust collectors with the *p*H of sludge of the ash of coal from which the dust is derived. *p*H values for sludge of ash of coal from eight different coal mines are presented, and it is shown that such values for ash of Illinois coal are appreciably higher than for Kentucky coal. The use of *p*H measurements to aid in "fingerprinting" dust is discussed.

Assistance in the preparation of this report was supplied by Official W.P.A. Project 30051, sponsored by the Chicago Department of Smoke Inspection and Abatement, and co-sponsored by the Lewis Institute.

Some Useful X-Ray Data

EUGENE W. PIKE
Andrews and Perillo, Inc., Long Island City, New York
(Received September 23, 1940)

The measured mass absorption coefficients of Allen and Wrede for H, Be, C, N, O, F, Na, Al, Si, Cl and Br have been fitted to the "universal law"

$$\mu/\rho = a\lambda^n + c/(1+0.048/\lambda),$$

by least squares, and the values of a, n, and c tabulated. The energy distribution in the continuous x-ray spectrum in the range from 20 to 70 kv, as measured by Kirkpatrick and by Ulrey, has been recomputed, and presented graphically in a form which permits easy interpolation. The recomputation of Ulrey's data is described in some detail.

THE widening industrial use of x-rays in the range $0.2\text{A} < \lambda < 1.0\text{A}$ for the inspection of packaged foods and similar articles brings an increasing need for more complete and better organized tabular data on mass absorption coefficients and energy distributions in this range. The data presented below were assembled by the writer for his own use in problems of this kind, and have been extremely useful.

I. Mass Absorption Coefficients

The most extensive recent measurements of mass absorption coefficients are those of Allen,[1] and those of Kustner and his school, from whom Wrede[2] gives the most complete data. These two sets of data agree very well, and after excluding a few points obviously widely in error, they were combined. For interpolation purposes, the so-called "universal formula"

$$\mu/\rho = a\lambda^n + c/(1+0.048/\lambda) \qquad (1)$$

was used, fitted to the observed data by the method of least squares. Table I(A) gives the constants so obtained, and Table I(B) some interpolated values. The elements F and Si, marked by parentheses, have not been measured, and the constants were determined by interpolation on large accurate charts.

The constants so derived differ in several cases from those derived by Wrede;[2] a careful graphical check against the original data proves his values to be in error.

The single value for H in $(CH_2)_n$ is taken from Taylor.[3]

II. The Energy Distribution in the Continuous X-Ray Spectrum

The direct experimental measurements of this function are limited to the early and incomplete work of Kirkpatrick,[4] Dauvillier,[5] and Ulrey.[6] The former two agree very well over the range where Dauvillier's inadequate corrections for second-order reflection from the crystal do not prejudice his figures. Kirkpatrick's corrections are complete and accurate; his final result is "the intensity of x-radiation inside the bulb" of a tungsten target Coolidge tube. The target face

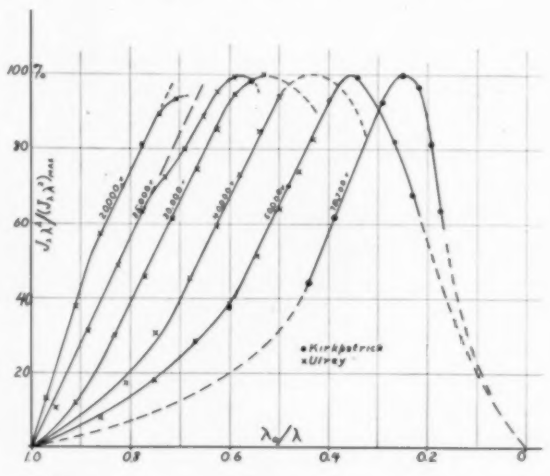

FIG. 1.

[1] S. J. M. Allen, *Handbook of Chemistry and Physics*, 22nd edition (Chemical Rubber Co., 1938), p. 1502.
[2] W. Wrede, Ann. d. Physik **36**, 684 (1939).
[3] E. G. Taylor, Phys. Rev. **20**, 709 (1920).
[4] P. Kirkpatrick, Phys. Rev. **22**, 37 (1923).
[5] A. Dauvillier, Ann. de physique **13**, 49 (1920).
[6] D. C. Ulrey, Phys. Rev. **11**, 401 (1918).

TABLE I(A).

ELEMENT	Be	C	N	O	(F)	Na
a	0.38	1.11	1.91	2.93	4.33	8.60
n	3.11	3.00	3.09	3.09	3.07	3.08
c	.188	.195	.20	.20	.20	.20

ELEMENT	Al	(Si)	S	Cl	Br ($\lambda<0.917$)	Br ($\lambda>0.917$)
a	13.9	16.9	25.7	30.6	201	26.6
n	3.01	3.00	2.99	2.96	2.71	2.80
c	.20	.21	.23	.23	—	—

TABLE I(B).

λ	H (H_2O)	H ($(CH_2)_n$)	C	N	O	(F)	Na	Al	(Si)	S	Cl	Br
0.28	0.39	—	0.195	0.207	0.228	0.258	0.341	0.471	0.55	0.77	0.903	6.35
.32	.39	—	.210	.228	.260	.305	.431	.619	.74	1.06	1.252	9.12
.36	.39	—	.228	.255	.301	.365	.546	.813	.97	1.42	1.69	12.9
.40	.39	—	.249	.286	.351	.439	.690	1.058	1.27	1.87	2.24	16.7
.44	.39	—	.274	.325	.412	.529	.868	1.357	1.63	2.43	2.91	21.45
.48	.43	—	.303	.371	.484	.637	1.078	1.71	2.06	3.09	3.72	27.4
.52	.43	—	.338	.425	.570	.765	1.32	2.12	2.56	2.87	4.64	34.1
.56	.43	—	.378	.488	.671	.914	1.62	2.60	3.16	4.77	5.72	42.4
.60	.43	—	.424	.561	.787	1.086	1.97	3.17	3.84	5.81	6.97	50.2
.64	.43	—	.476	.645	.921	1.28	2.36	3.81	4.62	7.00	8.40	59.8
.68	.43	—	.535	.741	1.074	1.51	2.81	4.54	5.51	8.35	10.0	70.5
.72	.44	.26	.601	.849	1.25	1.77	3.31	5.35	6.56	9.87	11.8	82.4
.76	.44	—	.675	.970	1.44	2.05	3.88	6.27	7.62	11.54	13.8	95.4
.80	.44	—	.757	1.106	1.66	2.37	4.52	7.29	8.85	13.4	16.0	110
.90	.45	—	.999	1.407	2.30	3.32	6.41	10.31	12.5	19.0	22.6	151
.917	—	—	—	—	—	—	—	—	—	—	—	159
												21
1.00	.45	—	1.303	2.10	3.12	4.52	8.79	14.1	17.1	26.0	30.8	26.6

was inclined at 45° to the electron beam, and the measurements were made in the direction of specular reflection of the beam from the target face.

Ulrey[6] used almost exactly the same experimental arrangement, but measured only the ionization current as a function of voltage and spectrometer setting. His description of the method used is so complete, however, that the necessary corrections may be computed, using a providential overlap with Kirkpatrick's work to determine the final parameters.

The plot of J_λ, the intensity, against λ for the various voltages used is shown in the lower graph of Fig. 2. The regularities of this system of curves are shown more strikingly in Fig. 1. Here the function $(\lambda^2 J_\lambda)/(\lambda^2 J_\lambda)_{max}$ is plotted in percent as a function of (λ_0/λ), where λ_0 is the short wave-length limit at the voltage in question. Considering the complexity of the processes involved, it is unlikely that there is any theoretical significance to these regularities, but they do facilitate interpolation. If the straight portions of the curves are prolonged, their intercepts with the axis of (λ_0/λ) form an almost linear progression with voltage, as is shown in the upper curve of Fig. 2.

The values of J_λ as a function of voltage and wave-length are given in Table II.

III. THE REDUCTION OF ULREY'S DATA

Ulrey measured simply the ionization current as a function of the spectrometer setting for several voltages. There are four major corrections to be applied to these data: (A) The efficiency of the ionization chamber. (B) The reflectivity of the crystal. (C) The absorption in materials such as the wall of the x-ray tube. (D) Second-order reflections from the crystal. These will be considered in order.

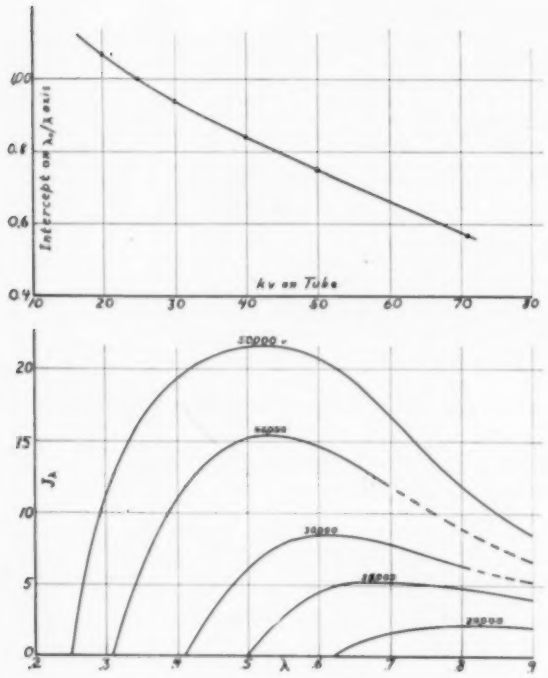

FIG. 2.

A. The efficiency of the ionization chamber

Ulrey's ionization chamber was 75 cm long and 7.5 cm in diameter, and contained air at atmospheric pressure, saturated with the vapor of ethyl bromide at 20°C. This amounts to 1.61 mg of Br, 0.95 mg of N, 0.49 mg of C, 0.24 mg of O, 0.09 mg of H, and 0.013 mg of A, per cc of gas. The x-ray beam was 1.8 cm high, and passed axially through the chamber.

Of the radiation entering the chamber, one part goes through, without being absorbed, while another part is converted into fluorescent bromine K radiation. Of this last, a portion escapes to the walls. The remainder of the original energy is transferred to photoelectrons which ionize the gas. Following Binks,[7] we assume that the energy expended per ion pair is essentially constant in this region, so that the ionization is a true measure of the total energy of the photoelectrons.

At any wave-length λ, the volume absorption coefficient β of the gas in the chamber can be computed from the known mass absorption coefficients in Table I. The portion of the original beam passing through the chamber unabsorbed is $\exp(-75\beta)$. The portion lost as fluorescent radiation can be estimated as follows:

In any element of volume, the energy absorbed from the beam in a wave-length interval $d\lambda$ will be $\beta J_\lambda dv d\lambda$. Of this energy, a fraction (β_k/β) will be expended in producing K ionization in bromine. (β_k can be computed as the difference between the absorption coefficient of bromine, and the L absorption extrapolated from the formula for ($\lambda > 0.917$) in Table I.) When a bromine atom is ionized in the K level by a quantum of wave-length λ, a fraction $(\lambda/1.03)$ of the energy of the photon is converted into bromine K radiation, the remainder goes into the primary photoelectron, or into soft radiation which does not reach the walls. Finally, only a fraction of this K radiation escapes to the walls. A numerical integration gives this fraction as 58 percent.

Combining all these, the efficiency of the chamber is

$$E=(1-\exp(-75\beta))(1-0.58\lambda\beta_k/1.03\beta). \quad (2)$$

This ranges from 0.48 at 0.28A to 0.74 at 0.48A, and back to 0.56 at 0.90A. It rises abruptly to 0.97 at the bromine K edge at 0.917A, and this discontinuity shows in Ulrey's original data, although it is smoothed away in his curves.

TABLE II.

λ	70.7 KV	51.4 KV	40 KV	30 KV	25 KV	20 KV
0.28	—	7.7	—	—	—	—
.32	—	13.8	1.9	—	—	—
.36	—	17.1	7.5	—	—	—
.40	41	19.5	11.0	—	—	—
.44	—	20.3	13.2	2.5	—	—
.48	—	21.2	14.5	5.2	—	—
.50	40.5	23	—	—	—	—
.52	—	21.6	15.4	6.9	1.26	—
.56	—	—	15.3	8.0	3.26	—
.60	35.5	21	14.9	8.3	4.4	—
.64	—	—	—	8.3	5.0	0.57
.68	—	—	—	8.0	5.1	1.44
.70	28	17	—	—	—	—
.72	—	—	—	7.6	5.1	1.96
.76	—	—	—	7.0	5.07	2.14
.80	21	12	—	6.7	4.8	2.24
.84	—	—	—	—	4.6	2.2
.88	—	—	—	—	4.15	2.1
.90	14	8.5	—	—	—	—
1.00	8.7	5.6	—	—	—	—

[7] W. Binks, *Reports on Progress in Physics* (The Physical Society, London, 1936), Vol. III, p. 387.

B. The reflectivity of the crystal

Ulrey states that his crystal was a cleaved surface of calcite, "the best of some twenty pairs." Davis and Stempel[8] have measured the reflectivity of calcite in the range in question, and find that the reflectivity of an "excellent" cleaved surface is practically independent of wave-length.

C. The absorption in the path

The absorption in Ulrey's arrangement is concentrated in the glass wall of the x-ray tube, of unknown thickness. However, by requiring that Ulrey's curve join smoothly with Kirkpatrick's in the region where they overlap (50,000 volts, $0.4<\lambda<0.48$A), this absorption can be determined very accurately. It is equivalent to 0.21 g/cm² (about 1 mm) of Pyrex glass, a very reasonable value.

D. Second-order reflections

This correction is large and cannot be computed. For this reason, the usefulness of Ulrey's curves is limited to the region $\lambda_0<\lambda<2\lambda_0$, where second-order reflections do not occur.

[8] B. Davis and D. Stempel, Phys. Rev. **17**, 608 (1921).

Cathode Spot Initiation on a Mercury Pool by Means of an External Grid

MARK A. TOWNSEND
Lamp Development Laboratory, General Electric Company, Nela Park, Cleveland, Ohio
(Received January 2, 1941)

Experiments relating to mercury-pool stroboscope tubes with external starting bands are described. Of particular interest is the unidirectional current that is found to flow in the plate circuit when grounded and its relationship to the formation of a cathode spot on the mercury cathode. Cathode-ray oscillograms are exhibited showing the periodic nature of this current. The potential of a disconnected electrode is negative with respect to the cathode and has a value of several thousand volts. Curves of the volt-ampere characteristics of an anode are given as a function of tube dimensions, gas pressure and other factors.

INTRODUCTION

THE mercury-pool cathode, although used for many years as a practical and reliable source of electrons, is still only partially understood. Always associated with the use of a mercury-pool cathode is the problem of initiating the cathode spot. Well-known methods of accomplishing this are: (1) separating mercury contacts through which a current is flowing, (2) applying a surge of current to a high resistance rod immersed in the mercury surface (the Ignitron), or, (3) applying a surge of voltage to a conductor near the mercury surface but electrically insulated from it.[1-3]

This third method listed above is found to be satisfactory and convenient for initiating the cathode spot in the mercury-pool stroboscope tube. The stroboscope tube is usually in the form of a glass cylinder from $\frac{3}{4}$" to 2" in diameter and from 4" to 12" in length. A pool of mercury at the lower end serves as the cathode and a nickel or iron plate at the upper end serves as the anode. A conductor, such as a wire screen, is placed around the tube in contact with the outside of the glass

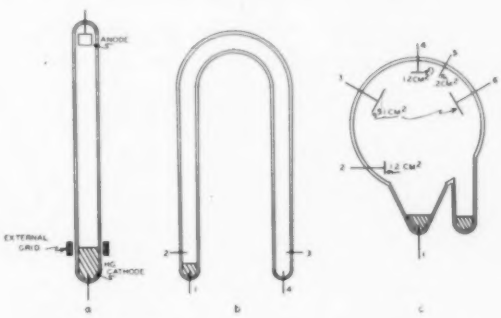

FIG. 1. Experimental types of mercury-pool stroboscope tubes.

[1] K. J. Germeshausen, Phys. Rev. **55**, 228 (1939).
[2] Y. Watanabe, H. Kasahara and Y. Nakamura, Elektrotech. J. **2**, 180 (1938).
[3] L. J. Buttolph and D. W. Dana, Rev. Sci. Inst. **4**, 206 (1933).

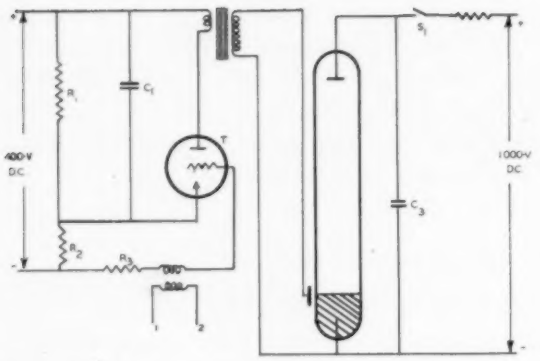

FIG. 2. Control circuit for a mercury-pool stroboscope tube.

opposite the mercury meniscus, forming an external grid. Figure 1(a) shows a typical form of this tube.

It is possible to start a cathode spot capable of carrying a high current discharge through the main body of the tube by supplying in the proper manner a small amount of energy to the external grid. The starting time and duration of the discharge may be controlled to within a few microseconds. The light from this discharge may be used as an accurately timed source of high intensity light for both stroboscopic work and high speed motion pictures.[4] In addition, the accurate control provided by the stroboscope tube makes it useful as a timing element in other circuits.[5, 6]

This paper describes experiments on stroboscope tubes. Under certain conditions a unidirectional current flows in the anode circuit when there is no e.m.f. source therein. A correlation is established between this current and the starting of the tube. The conditions both of the stroboscope tube and of the circuit, under which this unidirectional current is produced, are studied in detail.

Normal tube operation

A control circuit commonly used with the stroboscope tube is shown in Fig. 2. Condenser C_1 is charged to about 350 volts d.c. but is prevented from discharging by the thyratron tube T. Condenser C_3 is charged to about 1000 volts d.c. which is below the steady-state breakdown voltage of the mercury-pool tube. A small tripping voltage applied to terminals 1–2 allows the thyratron to become conducting and discharges condenser C_1 through the primary of the induction coil. This causes a high voltage oscillation in the secondary of the induction coil which is applied to the external grid of the stroboscope tube. The high voltage grid excitation causes the formation of a cathode spot on the mercury pool and the discharge of condenser C_3 through the stroboscope tube. It is this discharge of C_3 which produces the stroboscopic light.

The phenomenon of unidirectional current

In the circuit of Fig. 2, if the anode supply voltage is disconnected by opening switch S_1 and if the grid excitation is continuously applied, an unexpected result is obtained: The condenser C_3 acquires a powerful charge. If this condenser is shunted by a microammeter, a unidirectional current of several microamperes is observed in the anode circuit. The direction of flow is that which would be produced by electrons striking the anode. A faint glow appears along the length of the tube accompanied by streamers of light extending from the mercury meniscus a short distance along the surface of the glass. The mercury surface is greatly agitated. The same effects are produced if a 60-cycle sine wave of the order of magnitude of 5 kv is substituted for the induction coil grid excitation.

A somewhat clearer picture of the nature of this current is given by the oscillograph. In the

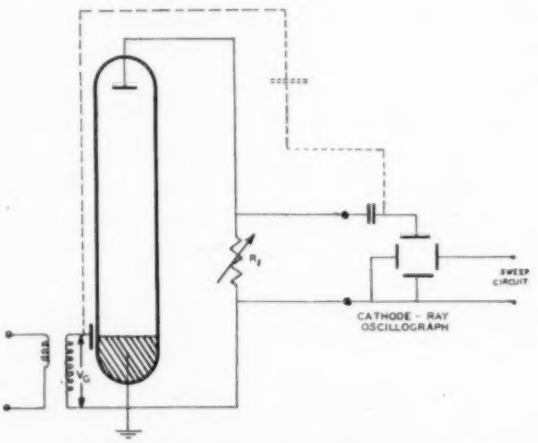

FIG. 3. Circuit for obtaining oscillograms of the unidirectional current.

[4] H. E. Edgerton, Elec. Eng. **54**, 149 (1935).
[5] H. E. Edgerton, K. J. Germeshausen and H. E. Greer, J. App. Phys. **8**, 2 (1937).
[6] T. S. Gray and W. B. Nottingham, Rev. Sci. Inst. **8**, 65 (1937).

circuit of Fig. 3 the voltage drop of the current flowing through resistor R_1 is impressed directly on the vertical deflecting plates of the oscillograph. The wave shape of the grid voltage is superimposed on this by means of an electrostatic pick-up obtained by simply bringing the lead wire close to the high voltage grid. Figure 4(a) shows the form of oscillogram obtained with a 60-cycle grid voltage. Figure 4(b) shows the same thing except that the oscillatory induction coil grid voltage is used. Both figures show that the unidirectional current consists of a series of short, high current discharges occurring at definite portions of the grid voltage wave. These figures represent many superimposed traces on the oscillograph screen. The current varies from cycle to cycle and, although the pattern has the general shape shown here, the details continually change. Notable features of the oscillograms are that the current flow is in the same direction during both half-cycles of the grid voltage wave and that the larger currents flow during the negative half-cycle. Measurements with a calibrated oscillograph indicate that the average height of the current impulses corresponds to 0.06 ampere for a typical condition.

Correlation of the unidirectional current with cathode-spot formation

The multi-anode tube of Fig. 1(c) was connected in such a manner that the unidirectional current due to grid excitation could be studied on one anode (No. 3) while an arc could be established to a second symmetrically placed anode (No. 6). The circuit is shown in Fig. 5. The following observations were made: (1) It was necessary to apply a grid voltage of at least 6.8 kv before an appreciable current could be observed in the circuit of anode 3, with no voltage applied

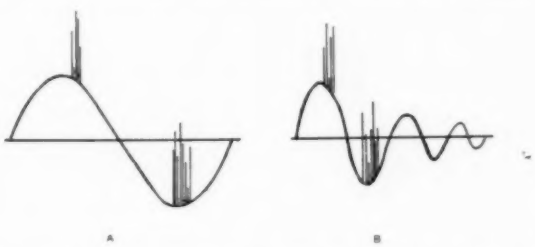

FIG. 4. Oscillograms of unidirectional current. (A) with 60-cycle sine-wave excitation. (B) with oscillatory induction coil excitation.

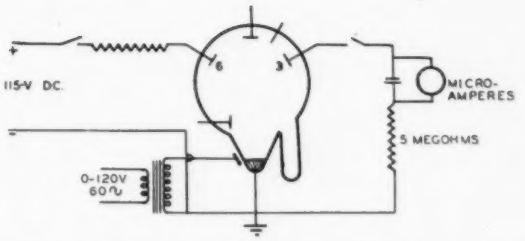

FIG. 5. Circuit for studying the correlation of cathode spot formation with unidirectional current production.

to anode 6. With 6.8 kv grid excitation an arc would form to anode 6 when the line switch was closed. (2) When the grid voltage was reduced slightly below 6.8 kv, no current could be observed in the circuit of anode 3. No arc would form to anode 6 when voltage was applied to it. (3) With an arc to anode 6 and with a grid excitation of 6.8 kv continuously applied, current did not flow in the circuit of anode 3. If the arc to anode 6 was suddenly interrupted, a current began to flow to anode 3 after a time delay of a few seconds. If the arc to anode 6 was interrupted and the circuit immediately reclosed, the same time delay of a few seconds occurred before an arc would restrike.

These observations indicate that the arc will not strike unless conditions are so adjusted that application of the grid voltage produces a unidirectional current to a non-energized anode.

The mechanism involved in the formation of a cathode spot in this tube is probably similar to that of the Cooper Hewitt lamp described by Kenty:[7] "The electrostatic field between the external starting band and the mercury meniscus causes field emission of electrons. The electrons are projected up the tube—causing ionization of the vapor in the tube. As a result of this ionization a self-maintaining discharge becomes established." In the Cooper Hewitt lamp the anode is connected to the starting band and, during starting, the cathode is forced to a high negative potential relative to the anode and starting band. Kenty[7] observed that, even with the anode insulated, electrons were sometimes projected up the tube with high energies. In the case of the stroboscope tube described here the anode is only a few hundred volts positive with respect to the cathode during starting. Nevertheless, experi-

[7] C. Kenty, J. App. Phys. **9**, 705 (1938).

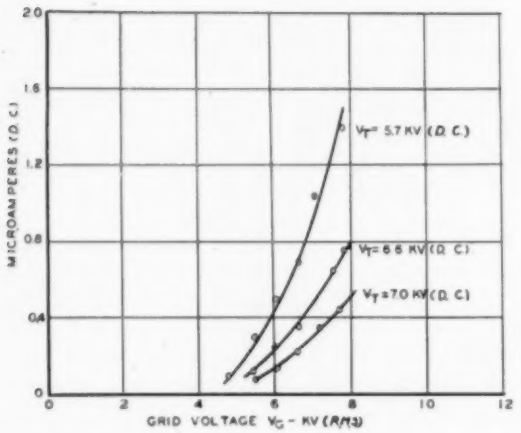

FIG. 6. Unidirectional current as a function of grid voltage for different values of retarding voltage.

ments show that electrons reach the anode with energies corresponding to several thousand volts.

The remaining portion of this paper describes experiments which were performed to determine the factors influencing the flow of the unidirectional current to a non-energized electrode.

Effect of circuit constants on the unidirectional current

The curves of Fig. 6 show the unidirectional current as a function of grid excitation for several fixed values of retarding voltage. The current was measured by means of the circuit of Fig. 7. The microammeter was protected from any large alternating current by the shunt condenser and, with switch S in position 1, the unidirectional current was unopposed. With switch S in position 2, the d.c. power supply was connected in opposition to the flow of current. The magnitude of this d.c. retarding voltage was controlled by varying the voltage input to the rectifier circuit. The 60-cycle grid voltage was controlled by means of a variable transformer connected to the primary of the high voltage grid transformer.

We see from Fig. 6 that as the grid voltage is increased from zero, no current flows until a critical value is reached. Past this point the current increases rapidly with the grid voltage. The current decreases with an increase in retarding voltage. This decrease would be expected to occur since all the electrons going toward the anode will be repelled if their energy is below that consumed by the field between the cathode and anode. The curves of Fig. 8 show this variation of unidirectional current with retarding voltage for several fixed values of grid voltage. These curves represent the energy distribution of the electrons producing the current.

If the anode is left floating when the grid excitation is applied it will acquire a voltage corresponding to the maximum energy of the electrons striking it. This open circuit anode voltage is shown in Fig. 9 as a function of the peak value of grid voltage. It is seen that the anode voltage is always below the peak value of the grid voltage although in some cases this difference is quite small. In making these measurements of anode voltage a null type of electrostatic voltmeter was used.

Of a similar nature to the voltage acquired by the anode is the charge acquired by the tube walls. The presence of the wall charges can be demonstrated by wrapping a conductor around the outside of the tube and connecting it to the ground through a galvanometer. When the grid voltage is applied, a current flows in the galvanometer circuit until the walls become charged.

Effect of gas pressure on the unidirectional current

At normal temperatures a mercury-pool cathode tube always contains mercury vapor at a few microns pressure. In a sealed-off tube there is also usually present a trace of other gases which come from the tube walls and internal parts. In making a study of the effects of gases on the flow of the unidirectional current it would be desirable to use various pure gases for separate experiments.

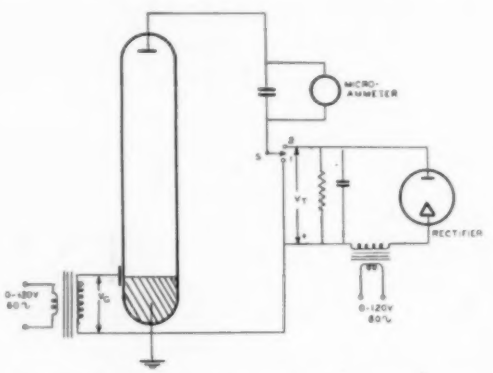

FIG. 7. Circuit for measuring unidirectional current as a function of grid voltage and retarding voltage.

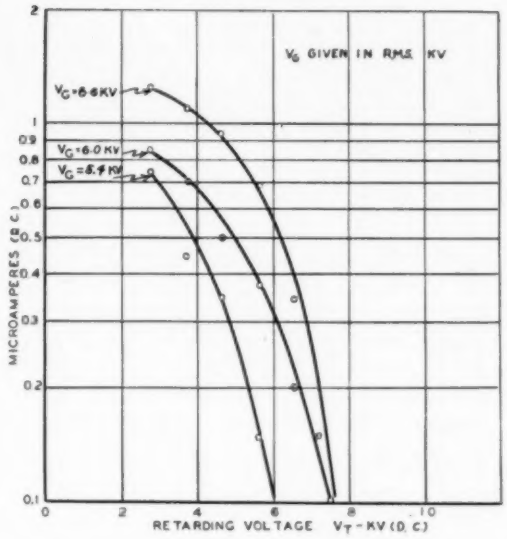

FIG. 8. Unidirectional current as a function of retarding voltage for various values of grid voltage.

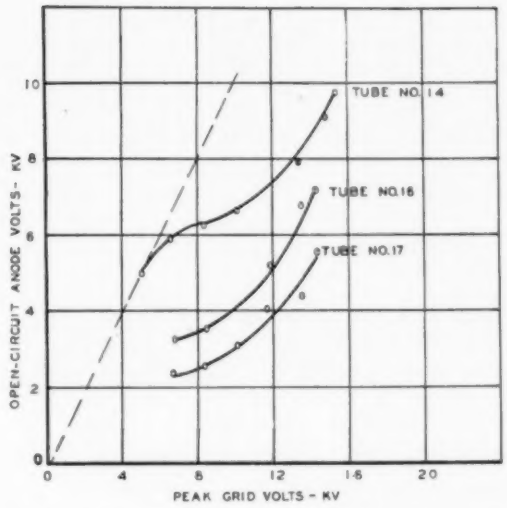

FIG. 9. Open circuit anode voltage as a function of grid voltage for several different stroboscope tubes.

However, in approximating conditions met in practical tubes it is convenient to use air. The method used was to connect the tube under test to a vacuum system and admit air at various pressures, maintaining other conditions as nearly constant as possible.

Some typical curves are given in Fig. 10 showing the current at a fixed value of grid voltage as a function of gas pressure. The circuit of Fig. 7 was used with switch *S* in position 1 and with a 60-cycle sine wave of grid voltage. Although the tubes used to obtain the data of Fig. 10 differed widely in construction, the same general trend is observable in all cases.

In addition to causing the greatly increased currents shown in curves 1, 2 and 3 of Fig. 10, the presence of the gas affected the value of retarding voltage required to stop the flow of current. Curve 4 of Fig. 10 shows this "stopping voltage" as a function of gas pressure. As the gas pressure is increased the stopping voltage decreases until at high pressures the current in some experimental tubes reverses even with no retarding voltage applied. In this range of pressure large currents flow with comparatively few volts applied to the anode and complicated effects are encountered which are not directly connected with the phenomenon of unidirectional current with which this paper is concerned. It is significant, however, that a faint glow was always observable along the entire length of the tube in all experiments where the current was produced.

In order to test the effect of a very low value of mercury vapor pressure, experiments were made using dry ice around the tube. It was found that current could be produced in a standard type of sealed-off stroboscope tube even when the mercury cathode was solidified by placing it in dry ice. However, when the tube was connected to a vacuum system, well evacuated and entirely surrounded by dry ice, no current was produced. In this latter case the permissible grid voltage was limited by the fact that moisture collected on the outside of the tube. When air was admitted to the tube surrounded by dry ice the unidirectional current was again observed. This current increased with the gas pressure as shown by curve 1 of Fig. 11. The fact that currents could be produced with the mercury cathode solidified led to experiments with other types of metallic cathodes. Curve 2 of Fig. 11 was taken with a tube in which the mercury cathode was replaced by a nickel wire screen similar to the external grid except mounted on the inside of the tube. These curves are not strictly comparable since curve 1 is for a grid voltage of 6.0 kv while curve 2 is for a grid voltage of 8.6 kv. In spite of this difference there appears to be considerable similarity between the results with a mercury cathode and with a nickel wire screen cathode, especially at the higher gas pressures.

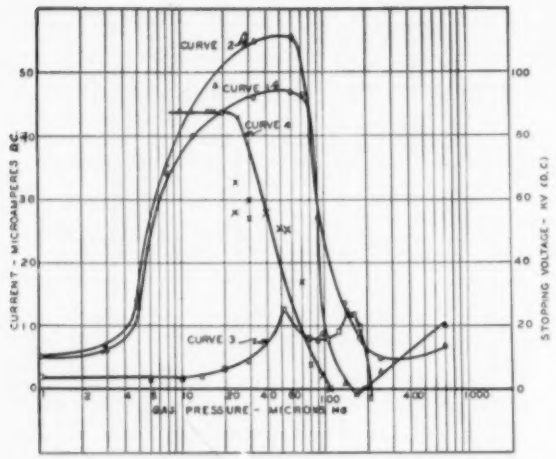

FIG. 10. Unidirectional current and stopping voltage as a function of gas pressure. Curves 1 and 2 show current for anodes 4 and 5 of the tube of Fig. 1(c). Curve 3 shows current for the tube of Fig. 1(a). Curve 4 shows stopping voltage for the tube of Fig. 1(a). The mercury vapor pressure was approximately 1 micron, corresponding to room temperature.

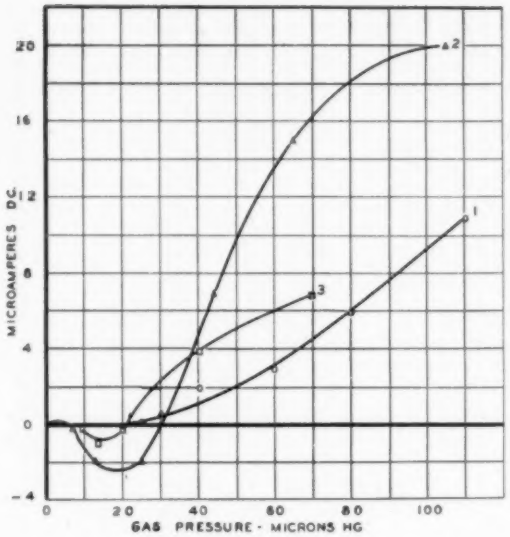

FIG. 11. Unidirectional current as a function of gas pressure. Curve 1 for a frozen mercury-pool cathode. Curves 2 and 3 for a nickel screen cathode; curve 2 with the current unopposed, curve 3 with a 17-megohm resistor in series with the anode. Except for curve 1, the mercury vapor pressure was approximately 1 micron.

Effect of tube geometry on the unidirectional current

The anode area was found to have negligible effect on the magnitude of the current when other conditions were kept constant. One experimental method for testing the effect of anode area was to vary the amount of mercury in the anode end of a "U"-shaped tube (Fig. 1(b)). Changing the area from 0.02 cm² to 3.0 cm² made no appreciable difference in the amount of direct current obtained. Because this U-shaped tube was relatively long and narrow, experiments were made with the tube shown in Fig. 1(c). This tube was designed to reduce the effect of highly charged walls in the neighborhood of the anode and to provide a control of anode area by having several anodes of widely differing area arranged at a constant distance from the cathode. Using this tube with good vacuum conditions, the current was practically independent of the anode area as is shown by Table I.

TABLE I.

CURRENT IN MICROAMPERES	ANODE AREA CM²	ANODE NO.
1.2	0.2	5
1.2	1.26	4
1.2	5.1	3
1.4	5.1	6
1.6	5.3	6+5
1.6	6.76	6+4
1.7	10.2	6+3

It is noticed that the current obtained with two anodes in parallel is increased over that obtained for one alone by about the same amount regardless of the total areas involved. The current differences shown in Table I may be attributed to field effects produced by open circuited anodes near those to which the current is being measured and are slight compared to the range of anode areas covered.

The cathode-anode distance is apparently not an important factor in determining the flow of unidirectional current. Tests made with several different tubes showed only very slight changes in current for changes in anode distance of as much as 25 to 1. Table II shows some data obtained with the tube of Fig. 1(b) using different anode distances and keeping other conditions constant.

Tests made with varying thickness of the tube wall at the mercury meniscus indicate that the current decreases as the glass thickness is increased. Table III shows some data obtained with tubes identical except for the different wall thicknesses at the mercury meniscus.

TABLE II.

CURRENT IN MICROAMPERES	ANODE-CATHODE DISTANCE—CM.
2.6	65
2.6	59
2.1	2.5

TABLE III.

TUBE NO.	1	2	3
WALL THICKNESS, INCHES	0.01	0.046	0.092
GRID VOLTS, KV	CURRENT, MICROAMPERES		
4.8	0.2	—	—
6.0	0.5	0.01	—
7.8	rupture	0.2	—
9.6	of wall	0.4	0.1
10.8		0.6	0.2

In any tube containing a liquid mercury pool, the production of direct current is always accompanied by a strong agitation of the mercury meniscus. Tests were made to determine the effect of different lengths of excited meniscus by varying the length of the external grid so as to surround only a part of the tube circumference. It was found that decreasing the length of the grid by as much as one-half did not appreciably affect the current flowing. Cutting down the length to one-fourth the circumference reduced the current by about one-half. It is necessary that some portion of the external grid be opposite the mercury meniscus. With the grid entirely above or entirely below the mercury edge no direct current is produced. The maximum current is produced when the center of the external grid is placed opposite the mercury meniscus.

This work was done at the Massachusetts Institute of Technology in 1937 in partial fulfillment of the requirements for a Master's degree. Earlier work on the starting of stroboscope tubes was done in 1936 by Mr. Charles Mueller. Work subsequent to that reported here was done in 1939 by Mr. Frederick Gemmill and Mr. Louis Hutchins. All these theses are on file in the library at the Massachusetts Institute of Technology. The author wishes to acknowledge gratefully the help and encouragement of Professor H. E. Edgerton who suggested the thesis and made many valuable contributions.

The Effect of X-Rays on the Breakdown Strength and Flashover Voltage of Certain Dielectrics

ERIC A. WALKER*
Hooper Laboratories, Tufts College, Massachusetts
(Received April 17, 1940)

Qualitative measurements are made on the reduction of breakdown strength of certain solid, liquid, and gaseous insulations. The observed reduction in breakdown strength is influenced by the gap length as well as the quantity of the x-rays. Exposing a solid to air boundary to x-rays increases the flashover voltage. A theory for this effect is offered.

OBJECT

IT is a well-known fact that x-rays will reduce the breakdown strength of insulation although little or no data have been presented to show the magnitude of this reduction.[1] It is believed that electrical breakdown of insulation is caused by three different mechanisms. First, there is the well-known "ionization by collision" phenomena as explained by Townsend,[2] and extended by others.[3] The second method of electrical breakdown is the pyro-electric phenomenon as offered by Wagner and Steinmetz.[4] This theory states that local heating reduces the resistance of a

* Now at the University of Connecticut, Storrs, Connecticut.

[1] F. W. Peek, *High Voltage Engineering* (McGraw-Hill, New York, 1929).

[2] J. S. Townsend, *Electricity in Gases* (Oxford University Press, 1914).

[3] J. Slepian and R. C. Mason, "Electric Discharges in Gases," Elec. Eng. **53**, 511 (1934).

[4] K. W. Wagner, "Physical nature of electrical breakdown in solid dielectrics," Trans. A.I.E.E. **41**, 288 (1922).

small region in a heterogeneous solid which in turn increases the heat generated. Thus a cycle is originated which progresses until the resistance approaches zero and failure is complete. The third cause of insulation failure is found in chemical changes which are caused by weathering, oxidation or ionic bombardment. The times required for these three effects to produce breakdown differ widely. The collision mechanism produces electrical failure in a small fraction of a second, the thermal mechanism takes several minutes because of the thermal capacity of the insulations. The last cause of failure, however, takes hours and sometimes years to produce a noticeable result. Furthermore, if an agent which tends to lower the breakdown strength by ionization is used, the insulation will rapidly recover its original properties as soon as the agent is removed because the ions will rapidly recombine. If local heating is the cause of breakdown it, too, will allow the recovery of the original dielectric strength unless the insulation has been chemically changed. On the other hand, any chemical change has caused an irreparable impairment of dielectric strength.

It is believed that the illumination by x-rays contributes to lowering the breakdown strength only because of the copious supply of free ions which are produced in the insulation under electrical stress. Certainly no permanent lowering of the breakdown strength was produced, for the reduction was only noticeable if the x-rays and breakdown voltage were applied simultaneously. The heat generated in the insulation by the

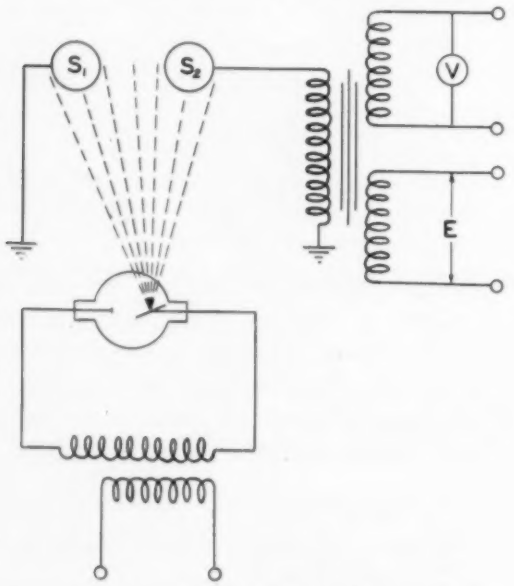

FIG. 1. Diagram of circuit used for tests.

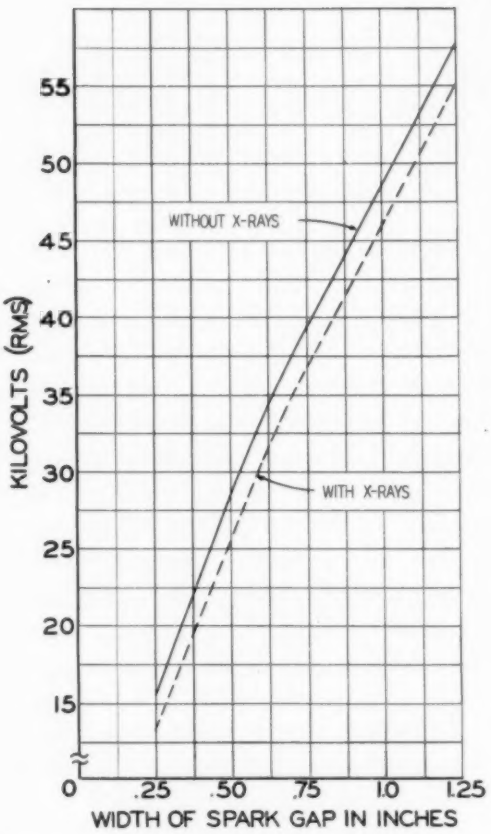

FIG. 2. Breakdown of air in the presence of x-rays.

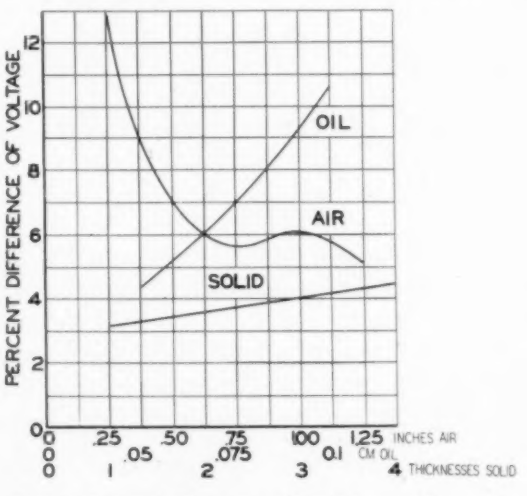

FIG. 3. Percent difference of breakdown voltage in presence of x-rays.

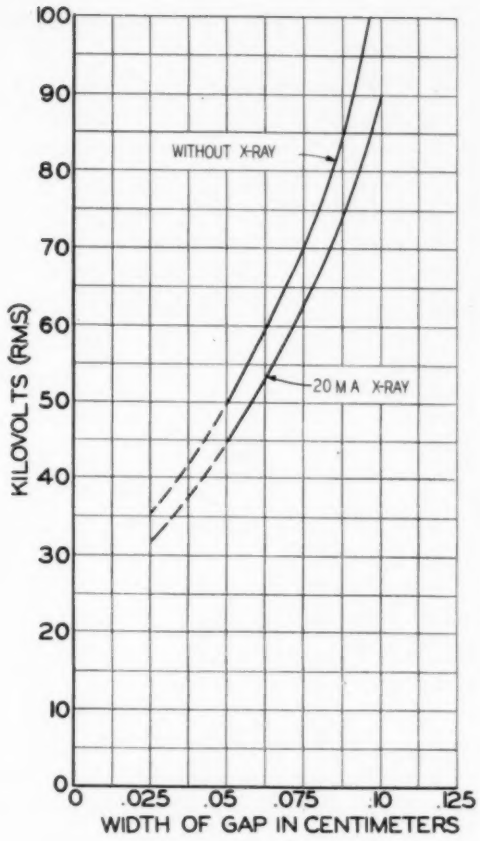

FIG. 4. Breakdown of oil.

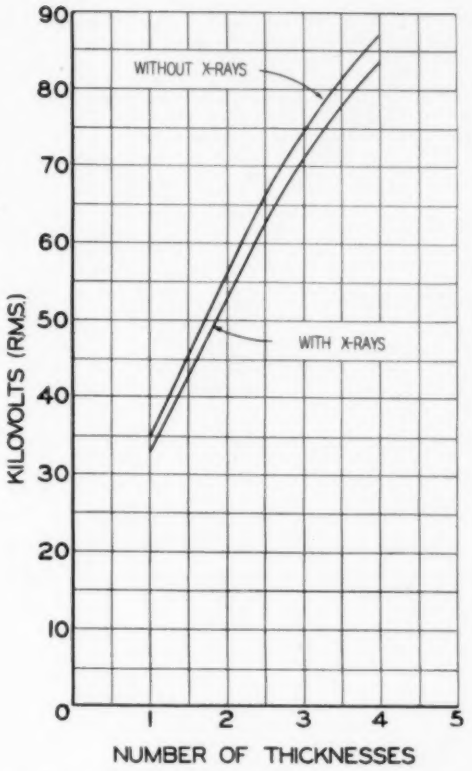

FIG. 5. Breakdown of solid dielectric (yellow varnished cambric).

x-rays is negligible. Therefore, it is reasonable to suppose that the effects to be described are caused exclusively by ionization phenomena.

METHOD

Figure 1 shows the arrangement used for most tests. The transformer voltage was determined by reading the peak voltage on the tertiary winding. Such procedure is preferable to reading the r.m.s. voltage because it eliminates the error caused by a nonsinusoidal wave shape.

The gaps S_1 and S_2 may be changed for different tests, and for tests on oil they may be immersed in a suitable tank of oil.

The x-ray tube was placed about 3 feet from the sphere gap and the distance was kept constant throughout the investigation. The x-ray tube was the conventional Coolidge type for 30 ma current. The x-ray transformer will supply 80,000 volts peak and the testing transformer is rated at 200 kv r.m.s. Usually five readings of each point were taken both with and without the application of x-rays.

RESULTS: BREAKDOWN TESTS

Figure 2 shows the breakdown voltage between two 6.25-centimeter spheres as a function of the separation of the gap with and without x-rays. It will be noticed that the reduction in breakdown voltage is relatively constant. This means the percentage reduction becomes less marked as the separation of the gaps is made larger. Such a result is probably to be expected because, as the gap separation becomes larger, there is a greater quantity of air and, therefore, more free ions in the electric field which are available to initiate further ionization. Curve *A*, Fig. 3, shows the percentage decrease in breakdown strength of air for this gap as a function of the separation between the spheres.

Figure 4 shows the effect of x-rays on the breakdown strength of insulating oil between two 6.25-centimeter spheres. In this case the differ-

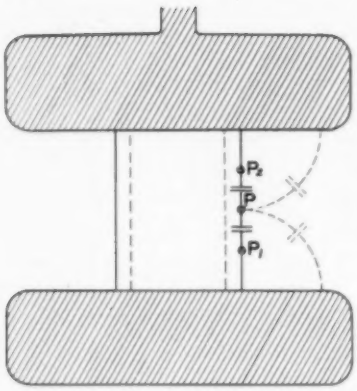

FIG. 6. Cylindrical insulator showing stray capacitance to both electrodes.

ence between the voltage necessary to cause electrical breakdown in the presence of x-rays and the voltage when they are not present increases as the gap is lengthened. In fact, the percentage change also increases as is shown by curve *B* of Fig. 3.

Figure 5 shows the results obtained on yellow varnished cambric, a material used extensively for transformer insulation. Again there is a decrease in breakdown strength but the decrease is approximately proportional to the breakdown voltage so that the percentage decrease is approximately constant as is shown in Fig. 3, curve *C*.

FLASHOVER TESTS

The electrode arrangement for flashover tests is shown in Fig. 6. Various diameters *d* and height *h* were used. The results differed somewhat but the results shown in Table I for a glass tube $1\frac{3}{4}$ inches high with a diameter of $1\frac{1}{4}$ inches is typical.

This shows a percentage *increase* of 7.5 percent in flashover voltage when the surface is illuminated with x-rays. The explanation of this phenomenon is not difficult. Consider a point *P* as shown on the surface of the glass cylinder in Fig. 6. This point is a point on an impedance which extends from the upper to the lower electrode. This impedance is composed of conductance caused by dust and moisture on the surface of the glass and also capacitance coupling such as between the point *P* and P_2 just above, or P_1 just below. Now if the conductance and capacitance are the only impedances and if they are evenly distributed, it is evident that the voltage gradient along the surface will be uniform. However, they are not the only impedances. Point *P* has capacitance coupling through the air and glass to both the upper and lower electrodes as is indicated in Fig. 6. It has been shown that the voltage curve for such an arrangement is nonuniform.[5] A typical distribution curve is shown in Fig. 7.

TABLE I.

WITHOUT X-RAY	WITH X-RAY
36.5	38.7
36.8	38.4
36.6	40.1
36.4	40.5
36.4	40.3
Average 36.5	39.6

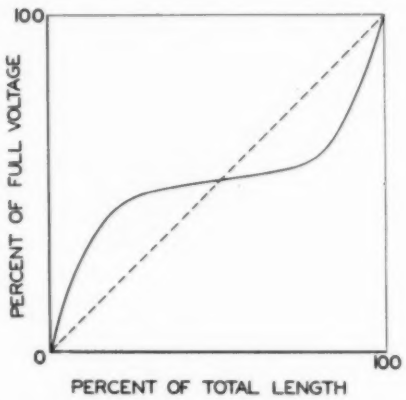

FIG. 7. Voltage distribution on insulator with stray capacitance to both electrodes.

The gradient is obviously not uniform. However, it can also be shown that any decrease in the resistance along the surface will cause the curve to approach more nearly the ideal voltage distribution shown in Fig. 7. If the flashover gradient is fixed this effect will increase flashover voltage. Such a mechanism is thought to be the reason an increase was noted in the table.

ACKNOWLEDGMENT

The author wishes to acknowledge the assistance of Mr. L. F. Kilham, who performed all of the laboratory tests.

[5] Eric A. Walker, "Electric circuits with double linkages," Phil. Mag. (in press) (1941).

Electromagnetic Waves in Transformer Coils Treated by Maxwell's Equations

REINHOLD RÜDENBERG
Graduate School of Engineering, Harvard University, Cambridge, Massachusetts
(Received November 4, 1940)

A rigorous solution of Maxwell's equations is derived for waves in a thin single-layer coil, a concentric ground electrode being at a short distance from the coil. Simple transformer coils resemble such an ideal to a considerable degree. Any electromagnetic state of the coil propagates slowly in axial direction with such a velocity that the phase velocity along the helical conductor equals the velocity of light. The surge impedance of the coil is constant for low frequency, but decreases with higher frequency, the boundary wave-length being determined by the insulating distances.

1. INTRODUCTION

THE behavior of electric waves and oscillations in tightly wound coils is a problem which has been discussed for a long time in the field of communication circuits[1] as well as in the field of power transmission.[2–4] The investigators agree on the character and on the quantitative effect caused by the internal capacitance between adjacent elements. There are various opinions, however, as to the complete influence of neighboring turns on one another. The mutual capacitive and inductive interaction of each and every turn in a compact coil is still an open question and merits further consideration.

Particularly for transformer windings, the various conceptions concerning this interaction have led to very different conclusions as to the frequency of the natural oscillations of the winding and the traveling velocity of surge waves. Some authors believe that the core flux in the steel sheets common to all turns plays a major part.[5,6] Others think that the transverse flux between the elements of the winding is of primary importance.[7,8] Still others feel that the main agent is the axial flux between the primary and secondary coils.[9,10]

With regard to this situation, it may be interesting to show that a rigorous solution of such a problem is possible by using Maxwell's equations. We have only to stipulate certain assumptions which enable us to find suitable boundary conditions, assumptions, however, which are fulfilled to a considerable degree in many actual transformers.

2. SPATIAL ASSUMPTIONS AND SYMMETRY CONDITIONS

Figure 1 shows the cross section of a usual transformer with concentric primary and secondary windings, the resistances of which may be neglected. We concentrate our attention on the primary high voltage winding which is exposed to traveling waves impinging from the incoming line.

We assume first that the secondary winding of the transformer can be considered as short-circuited and grounded throughout. This assumption is valid to a good approximation for the rapid oscillations here considered when the transformer is in actual operation, since its secondary low voltage external network then

[1] W. Lenz, "Berechnung der Eigenschwingungen einlagiger Spulen," Ann. d. Physik **43**, 749 (1914).
[2] R. Rüdenberg, "Entstehung und Verlauf elektrischer Sprungwellen," Elektrotech. u. Maschinenbau **32**, 729 (1914); *Elektrische Schaltvorgänge* (Berlin, 1923/33), p. 528 ff.
[3] K. W. Wagner, "Das Eindringen einer elektromagnetischen Welle in eine Spule mit Windungskapazität," Elektrotech. u. Maschinenbau **33**, 89 (1915).
[4] O. Böhm, "Rechnerische und experimentelle Untersuchung der Einwirkung von Wanderwellen-Schwingungen auf Transformatoren-Wicklungen," Archiv f. Elektrotechnik **5**, 383 (1917).
[5] G. Frühauf, "Phénomènes transitoires dans les enroulements de transformateurs abordés par des ondes mobiles," Comptes rendus du Congrès International d'Électricité **5**, 939 (1932).
[6] J. Pirenne, "Théorie générale des phénomènes oscillatoires dans les enroulements des transformateurs," Revue Générale de l'Électricité **47**, 19 (1940).
[7] L. F. Blume and A. Boyajian, "Abnormal voltages within transformers," Trans. A.I.E.E. **38**, 577 (1919).
[8] L. V. Bewley, *Travelling Waves on Transmission Systems*" (New York, 1933), p. 207 ff.
[9] W. Steidinger, "Das elektromagnetische Verhalten der einlagigen Zylinderspule," Archiv f. Elektrotechnik **13**, 237 (1924).
[10] R. Rüdenberg, "Performance of travelling waves in coils and windings," Trans. A.I.E.E. **59**, 1031 (1940).

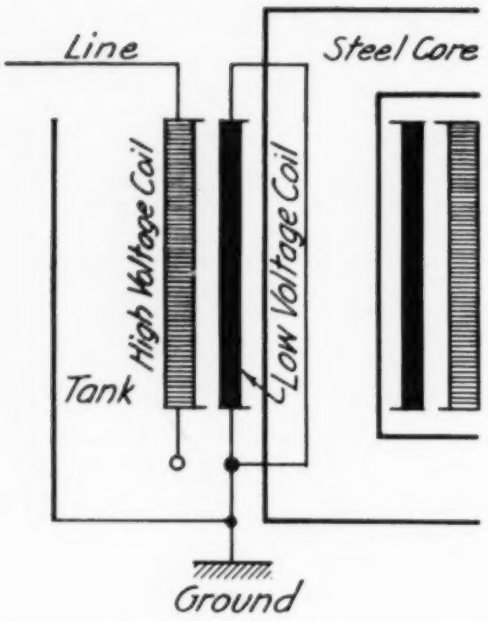

FIG. 1. Spatial position of windings in a transformer.

forms a very low impedance. The low voltage winding thus acts as a screening grounded metallic surface with respect to any waves within the high voltage coils and therefore no core flux can be produced within the iron.

Second, we assume that the radial thickness of the uniformly wound primary coil and, also, the insulating distance between primary and secondary coils are small in comparison with the diameter of the coils. If the interspace is relatively small, which is true in most actual designs, the problem is reduced from a cylindrical to a plane problem. If the primary coil is very thin, any considerable internal capacitance between adjacent turns within the primary winding is excluded.

Third, we consider the primary coil as axially long compared with the insulating distance to the secondary. For most transformer windings of the concentric tube type, this condition is closely approximated. For shorter coils, as in shell-type transformers, the influence of the finite ends may be considered separately, in accordance with well-known methods.

With this idealization we have removed from the problem the influence of any direct turn-to-turn capacitance, the effect of which is well known, while all other mutual interactions of the turns, capacitive as well as inductive, about which investigators are in disagreement, are retained in a pure form.

Two further properties of the coils which are present in every actual transformer will be taken into consideration: the winding has a helical structure, as shown in Fig. 2(a), and it is surrounded by an exterior electrode represented in Fig. 2(a) as a grounded, concentric cylinder. With an oil transformer this outer electrode consists actually of the metallic tank; with an open air-insulated design it consists of the remote surface of the earth. In accordance with well-known rules, even an irregular cylindrical exterior electrode can be reduced to a circular one and we shall see, moreover, that its influence for the most part is slight.

In accordance with our second assumption, a coil with a large winding diameter may be cut along an axial line and unrolled from a circular form to a plane, as indicated in Fig. 2(b), without introducing any considerable error. Fig. 2(c) then shows the insulating or dielectric spaces transverse to the winding in which we now must find the components of the electromagnetic field expressed in rectangular coordinates.

We measure the x coordinate in the direction of the former circumference of the coil, y in the direction of the axis, and z perpendicular to the thin layer of current, which now flows in a system of parallel wires having an axial separation s equal to the pitch of the helical coil.

Since the electromagnetic state is equal at both edges of the circumference u along the

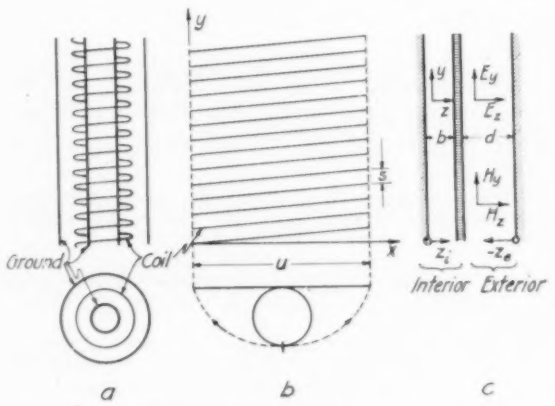

FIG. 2. (a) High voltage coil between core and tank. (b) Coil, cut open and unrolled to a plane lattice. (c) Plane lattice between ground electrodes.

entire length of the coil, as in Fig. 2(b), we may repeat the representation of the unrolled coil periodically in the $+x$ and $-x$ directions, as in Fig. 3. By this we cover the entire $x-y$ plane with a lattice of closely spaced conductors, represented by the inclined lines, and we can now solve our problem mathematically by a statement valid for any value of x and y within the infinite plane.

If we draw in Fig. 3 along the helical wire of the coil a wave with any change in space represented by + and − signs, we can repeat this wave at the left-hand and right-hand repetitions of the conductors. Instead of pursuing the course of such a wave over the real helical wire, we can follow the wave over one turn only of the real coil but, in addition, over the left-hand and right-hand continuations of this turn in the repeated systems of Fig. 3, which are represented by dotted lines. If we concentrate now on these conductors and look over the entire $x-y$ plane, we see that the electromagnetic state at the wires is independent of x but depends only on the axial coordinate y. This axial symmetry of the actual electromagnetic field of the coil, as shown in Fig. 3 along the chain-dotted line, will greatly simplify our considerations.

In the interspace between the inclined conductors there may be, of course, some change of the electromagnetic state in the x direction, but certainly only a small one. We see this immediately if we either think of our conductors as being wide enough to fill the whole space of the $x-y$ plane, or if we think of the space between the thin wires as being filled up by interleaved wires, composing a multiple thread helical winding in reality.

Thus for our mathematical development we will consider a coil which consists of a thin layer, conducting perfectly in the direction of the wires and insulating perfectly perpendicular to the wires. With this idealization, we can solve rigorously the problem of electric oscillations in such a coil. We neglect hereby only the change of the electromagnetic field within the immediate neighborhood of every single wire, which is identical with neglecting the capacitive interaction of adjacent turns. However, by our assumption of constancy in the x direction, we

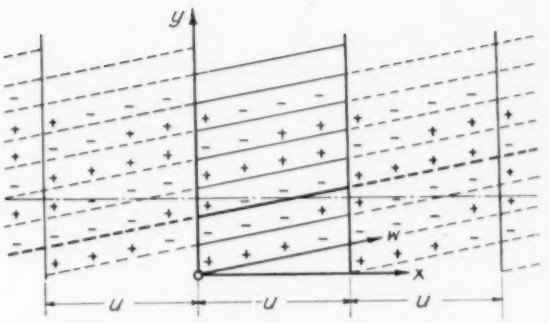

FIG. 3. Development of waves on an inclined lattice, repeated on both sides periodically and covering the infinite plane.

do not restrict any variation of the electromagnetic field in the y direction, and therefore also in the direction of the inclined wires. Hence we include by our statement even those oscillations which may be shorter in space than a turn length.

3. FUNDAMENTAL EQUATIONS

If at the wires the electromagnetic field varies to a negligible extent in the x direction, it is justifiable the more to assume that it remains constant at some distance from the lattice of wires. With the condition, therefore, that

$$\partial/\partial x = 0 \tag{1}$$

for every field component within the entire space, we have the following Maxwellian equations in rectangular components corresponding to Figs. 2 and 3 and expressed in electromagnetic units. The variation of the electric intensity E with time t is

$$\frac{\epsilon}{v_0^2}\frac{\partial E}{\partial t} = \text{curl } H \tag{2a}$$

or

$$\left.\begin{aligned} \frac{\epsilon}{v_0^2}\frac{\partial E_x}{\partial t} &= \frac{\partial H_z}{\partial y} - \frac{\partial H_y}{\partial z} \\ \frac{\epsilon}{v_0^2}\frac{\partial E_y}{\partial t} &= \frac{\partial H_x}{\partial z} \\ \frac{\epsilon}{v_0^2}\frac{\partial E_z}{\partial t} &= -\frac{\partial H_x}{\partial y}, \end{aligned}\right\} \tag{2}$$

while the time variation of the magnetic intensity

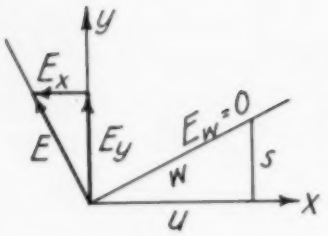

FIG. 4. Vector E of electrical intensity, perpendicular to the wire direction w.

H is

$$-\mu\frac{\partial H}{\partial t}=\text{curl } E \tag{3a}$$

or

$$\left.\begin{aligned}-\mu\frac{\partial H_x}{\partial t}&=\frac{\partial E_z}{\partial y}-\frac{\partial E_y}{\partial z}\\ -\mu\frac{\partial H_y}{\partial t}&=\frac{\partial E_x}{\partial z}\\ -\mu\frac{\partial H_z}{\partial t}&=-\frac{\partial E_x}{\partial y}.\end{aligned}\right\} \tag{3}$$

ϵ and μ denote dielectric constant and magnetic permeability within the space considered, and v_0 the velocity of light in vacuum. Furthermore, the spatial variation of the magnetic intensity is

$$\text{div } H=0 \quad \text{or} \quad \frac{\partial H_y}{\partial y}+\frac{\partial H_z}{\partial z}=0, \tag{4}$$

and that of the electric intensity is

$$\text{div } E=0 \quad \text{or} \quad \frac{\partial E_y}{\partial y}+\frac{\partial E_z}{\partial z}=0. \tag{5}$$

These relations are valid within the dielectric spaces of Fig. 2(c). At the surfaces of the unidirectionally conducting coil layer, however, the electric intensity must be zero in the conductive direction. From Fig. 4 we see that the electric intensity E_w in the direction of the turn length w, which is given by circumference u and pitch s as

$$w=(u^2+s^2)^{\frac{1}{2}}, \tag{6}$$

disappears only if the components in the x and y directions are in the proportion

$$E_z/E_y=-s/u. \tag{7}$$

Furthermore, since all currents in Fig. 3 are flowing in the w direction, they cannot produce a magnetic intensity in that direction. Therefore, we have, by the same geometric consideration as in Fig. 4, likewise

$$H_z/H_y=-s/u. \tag{8}$$

We assume these relations as valid within the entire space.

Equations (1), (7) and (8) state the structural conditions of the electromagnetic field of the coil and they alone determine one important part of the Maxwellian solution. The boundary conditions at the entire surfaces of the dielectric spaces determine another part and will be considered later.

If we eliminate by Eqs. (7) and (8) the x components of the electric and magnetic intensities in Eqs. (2) and (3), we obtain from the first group

$$\left.\begin{aligned}-\frac{s}{u}\frac{\epsilon}{v_0^2}\frac{\partial E_y}{\partial t}&=\frac{\partial H_z}{\partial y}-\frac{\partial H_y}{\partial z}\\ \frac{\epsilon}{v_0^2}\frac{\partial E_y}{\partial t}&=-\frac{s}{u}\frac{\partial H_y}{\partial z}\\ \frac{\epsilon}{v_0^2}\frac{\partial E_z}{\partial t}&=\frac{s}{u}\frac{\partial H_y}{\partial y}\end{aligned}\right\} \tag{9}$$

and from the second group

$$\left.\begin{aligned}-\frac{s}{u}\mu\frac{\partial H_y}{\partial t}&=\frac{\partial E_z}{\partial y}-\frac{\partial E_y}{\partial z}\\ -\mu\frac{\partial H_y}{\partial t}&=-\frac{s}{u}\frac{\partial E_y}{\partial z}\\ -\mu\frac{\partial H_z}{\partial t}&=-\frac{s}{u}\frac{\partial E_y}{\partial y}.\end{aligned}\right\} \tag{10}$$

Before proceeding further, we realize from Eqs. (7) and (8) that the x components, corre-

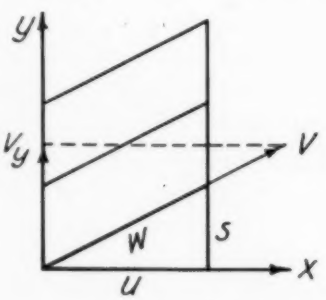

FIG. 5. Correlation of wire velocity v with axial velocity v_y of traveling waves.

sponding to the field in the circumferential direction of the coil, are very weak if the pitch s is only a small fraction of the circumference u, as is true for most actual windings. Furthermore, the second and the third lines in Eqs. (9) and (10) show that the time variations of the electric as well as the magnetic field in the y and z directions are very small as compared with the variation of the field components in space, determined by the factor s/u. This means that the field in the y and z directions is almost static, although rapid time variations in the x direction may occur. The smaller the pitch, or the greater the number of turns per cm coil length, the more closely the field approaches the static state.

4. Solution for the Field Components

We eliminate now $\partial/\partial z$ from the first two lines in Eqs. (9) and (10) and obtain

$$\left.\begin{aligned} \frac{\epsilon}{v_0^2}\left(\frac{u}{s}+\frac{s}{u}\right)\frac{\partial E_y}{\partial t} &= -\frac{\partial H_z}{\partial y} \\ \frac{\epsilon}{v_0^2}\left(\frac{u}{s}+\frac{s}{u}\right)\frac{\partial H_y}{\partial t} &= \frac{\partial E_z}{\partial y}. \end{aligned}\right\} \tag{11}$$

If we combine the first Eq. (11) with the last Eq. (10) we obtain

$$\frac{\epsilon\mu}{v_0^2}\left(1+\frac{u^2}{s^2}\right)\frac{\partial^2 E_y}{\partial t^2}=\frac{\partial^2 E_y}{\partial y^2} \tag{12}$$

and exactly the same relation follows for H_z. If we combine the second Eq. (11) with the last Eq. (9), there results for E_z and H_y the same relation as (12).

This well-known wave equation (12) can be solved by an arbitrary function of the form

$$E_y,\ E_z,\ H_y,\ H_z=f(y\pm v_y t), \tag{13}$$

which shows that the entire electromagnetic field is propagated undistorted in the direction y of the axis of the coil with a velocity given by the constant coefficient on the left-hand side of Eq. (12) as

$$v_y=\frac{v_0}{(\epsilon\mu(1+u^2/s^2))^{\frac{1}{2}}}=\frac{s}{w}\frac{v_0}{(\epsilon\mu)^{\frac{1}{2}}}. \tag{14}$$

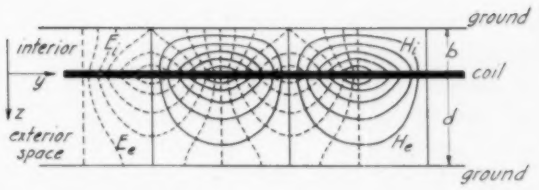

Fig. 6. Flow of the electric and magnetic lines of force in radial and in axial direction of the coil.

Since this axial velocity depends only on the fundamental electromagnetic velocity $v_0/(\epsilon\mu)^{\frac{1}{2}}$ and on the relative pitch or slope of the turns, s/w we see that it is a natural velocity inherent in every coil given only by the slope but independent of all other dimensions of the coil. It is a small fraction of the velocity of light, confirming the fact that the change of the phenomena in the axial direction is nearly static. The velocity is independent of the variation of the field in time, or of the exciting frequency. Any shape of the waves, sinusoidal as well as irregular, or impact waves of any steep front, travel with the same axial velocity. The front of every wave is propagated throughout in the axial direction of the coil. For coils of small pitch the velocity may be very low; however, if the pitch s approaches the wire length w of a turn, the velocity approaches the velocity of light. For stranded cables, with finite pitch, forming the limiting case of a multiconductor coil, the velocity is still somewhat less than that of light; the velocity of light is attained only with solid wires.

Furthermore, we can determine the phase-velocity of the waves along the wires. Figure 5 shows immediately that this is larger in the ratio of w/s, and is therefore

$$v=(w/s)v_y=v_0/(\epsilon\mu)^{\frac{1}{2}}. \tag{15}$$

Hence we see that every electromagnetic excitation travels along the wire of a transformer coil with the universal velocity of light, as adapted to the dielectric and magnetic constants of the surrounding material. According to the structure of the Maxwellian equations this result is caused by the fact that the electric and magnetic intensities vanish in the direction of the wires and that the lines of force are therefore perpendicular to the wire direction. Since the magneto-dielectric constant for oil transformers with imbedded solid insulation is of the order of 4,

the wave velocity is about half the velocity of light in vacuum. Hence the natural frequencies, fundamental as well as higher harmonic, can be determined easily for any given length of wire of the winding.

After having expressed the dependence of the field on the x, y and t coordinates in a form of general validity, the variation in the z direction remains to be determined. We eliminate the time variation $\partial/\partial t$ from the first two Eqs. (9) and (10) and obtain

$$\left.\begin{aligned}(1+s^2/u^2)\partial H_y/\partial z-\partial H_z/\partial y=0\\(1+s^2/u^2)\partial E_y/\partial z-\partial E_z/\partial y=0.\end{aligned}\right\} \quad (16)$$

If we combine these relations with the second lines in Eqs. (4) and (5), we obtain for the variation of one of the components in z and y

$$(w/u)^2\partial^2 H_y/\partial z^2+\partial^2 H_y/\partial y^2=0, \quad (17)$$

and exactly the same equation for each of the other three field components, H_z, E_y and E_z.

This relation (17) is similar to the well-known potential equation and therefore we can use any suitable solution given by the potential theory, except that in comparison with the potential problem the z dimension in our problem is extended by the ratio of the turn length w to the circumference u of the coil. For tightly wound coils this ratio is very nearly equal to 1; for loosely wound coils it is considerably larger and increases to infinity, when approaching the limiting case of a straight conductor.

A simple solution of Eq. (17) can be obtained for waves which vary sinusoidally in the y direction along the axis of the coil. This variation enforces an exponential distribution in the z axis perpendicular to the coil surface. We see immediately that the magnetic intensities

$$\left.\begin{aligned}H_y=H_1\cdot\cosh\beta z\cdot\sin\alpha(y\pm v_y t)\\H_z=H_2\cdot\sinh\beta z\cdot\cos\alpha(y\pm v_y t)\end{aligned}\right\} \quad (18)$$

and the electric intensities

$$\left.\begin{aligned}E_y=E_1\cdot\sinh\beta z\cdot\cos\alpha(y\pm v_y t)\\E_z=E_2\cdot\cosh\beta z\cdot\sin\alpha(y\pm v_y t)\end{aligned}\right\} \quad (19)$$

satisfy the differential equation (17). One such entire group of field components is valid within the internal dielectric space of the coil, and another one within the external space. Both may be distinguished by subscripts i and e where necessary, as in Fig. 2(c).

We have expressed Eqs. (18) and (19) in terms of hyperbolic functions, rather than exponential functions, in order to make the equations symmetrical in $+z$ and $-z$. Moreover, in this manner we can satisfy immediately the boundary conditions $H_z=E_y=0$ at the perfectly conducting ground electrodes in Fig. 2(c), if we fix the two origins $z=0$ for the internal and the external spaces at the respective positions of these electrodes.

By inserting the field components (18) and (19) in Eq. (17), we obtain a conditional equation between attenuation constant β in the z direction and wave density α in the y direction as

$$\beta=(u/w)\alpha, \quad (20)$$

valid for both the internal and external spaces.

The field intensities of Eqs. (18) and (19) vary in time with an angular frequency given by the coefficient of t namely

$$\omega=\alpha v_y. \quad (21)$$

If we excite the coil with this frequency ω, the wave density in the y direction becomes, with the use of Eqs. (14) and (15),

$$\alpha=\omega/v_y=\omega(w/s)[(\epsilon\mu)^{\frac{1}{2}}/v_0]=(w/s)(\omega/v). \quad (22)$$

From this we can easily determine the wave-length of the field intensities along the y axis as

$$\lambda=2\pi/\alpha=(2\pi/\omega)(s/w)v. \quad (23)$$

Along the coil wires the wave-length is w/s times greater; namely,

$$\Lambda=(2\pi/\omega)v. \quad (24)$$

These wave-lengths are given, as usual, by the quotient of velocity and frequency.

The spatial attenuation of Eq. (20) transverse to the wires now becomes, using Eqs. (22) and (23),

$$\beta=(u/s)(\omega/v)=(u/w)(2\pi/\lambda). \quad (25)$$

Thus we see that the extension of the field in the z direction, given by $1/\beta$, is directly proportional to the relative pitch s/u of the coil, and inversely proportional to the exciting frequency ω. Hence for high frequency and small slope of the turns, the electromagnetic field concentrates

more and more in the neighborhood of the coil layer. If, for example, as in many power transformers, the slope of the winding is $s/u = 1/1000$ and the velocity of the waves is $v = 1.5 \cdot 10^{10}$ cm/sec., the attenuation space constant, with an exciting frequency 10^4 c.p.s., is

$$\frac{1}{\beta} = \frac{1}{1000} \frac{1.5 \cdot 10^{10}}{2\pi \cdot 10^4} = 240 \text{ cm}.$$

With 10^5 c.p.s. this constant reduces to 24 cm and with 10^6 c.p.s. to merely 2.4 cm.

Figure 6 shows the general picture of the electric and magnetic lines of force, according to Eqs. (18) and (19). In addition to these components in the y and z directions, there exist also circumferential components in the x direction, given by Eqs. (7) and (8), which are, however, negligible as long as the pitch s is only a small fraction of the circumference u.

For determining the constants H and E in Eqs. (18) and (19), we insert the field intensities in Eq. (16). Then we obtain for the magnetic amplitudes, using Eqs. (6) and (20),

$$H_2 = -(w/u)H_1 \tag{26}$$

and for the electric amplitudes

$$E_2 = (w/u)E_1. \tag{27}$$

Furthermore, an interdependence of the magnetic and electric amplitudes can be derived by inserting the field components in Eqs. (9) or (10). If we take E_z from Eq. (19) and H_y from Eq. (18) and introduce them into the last Eq. (9), we obtain

$$(\epsilon/v_0^2)v_y E_2 = (s/u)H_1 \tag{28}$$

and if then we use Eq. (15), this simplifies to

$$H_1 = (1/v_0)(u/w)(\epsilon/\mu)^{\frac{1}{2}} E_2. \tag{29}$$

All these relations refer to the internal as well as to the external insulating space.

5. Boundary Conditions with Respect to Voltage and Current

In order to coordinate all the field amplitudes with voltage and current in the winding, we have to consider the boundary conditions at the surface of the coil. The line integral of the electric field between coil and ground electrodes in Fig. 2(c) gives the voltage E at the point considered. Thus we have over a distance b, using the last field component of Eq. (19), and confining ourselves to the amplitude of the spatial sine wave

$$E = \int_0^b E_z dz = (E_2/\beta) \sinh \beta b. \tag{30}$$

This is valid for the internal dielectric distance b. Since a similar expression yields the voltage E for the external distance d, only with opposite sign, the amplitudes in both spaces are determined by

$$\left.\begin{aligned} E_{2i} &= (\beta/\sinh \beta b)E \\ E_{2e} &= -(\beta/\sinh \beta d)E. \end{aligned}\right\} \tag{31}$$

These maximum electric intensities thus can be computed easily by β, Eq. (25), if the exciting voltage is given by amplitude E and frequency ω.

The magnetic intensities at the interior and at the exterior surfaces of the coil layer are interlinked by the conditions that the components H_z perpendicular to the layer must be equal, while the difference of the axial components H_y is determined by the current within the layer. From the first condition we have for $z_i = b$ and $-z_e = d$, using the last Eq. (18),

$$H_{2i} \sinh \beta b = -H_{2e} \sinh \beta d = H_0, \tag{32}$$

where H_0 is merely an abbreviation for these maximum values. From the second condition there follows, using the first Eq. (18)

$$H_{1i} \cosh \beta b - H_{1e} \cosh \beta d = 4\pi A_x. \tag{33}$$

Herein we denote by A_x the amplitude of the linear current density in the circumferential direction of the coil, measured perpendicular to the field intensities H_y. Since the real current I within the turns flows at an angle to the x direction, we see from Fig. 7 that the x component of the linear current density A is

$$A_x = (u/w)A = (u/w)(NI/k) = NI/h, \tag{34}$$

where N is the number of turns in a coil of the axial length h, while k is the projection of this length perpendicular to the wires.

Considering Eq. (32), we can express both amplitudes H_2 by the maximum value H_0 of

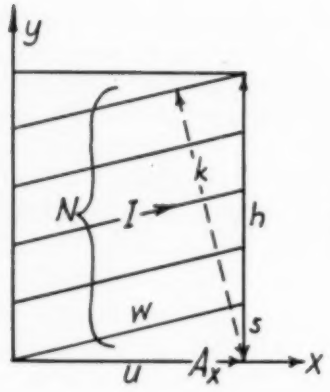

FIG. 7. Linear current density A_x developed by the wire current I.

the transverse magnetic field through the coil layer, and using Eq. (26) we obtain the components H_1 as

$$\left.\begin{aligned} H_{1i} &= -(u/w)(H_0/\sinh \beta b) \\ H_{1e} &= (u/w)(H_0/\sinh \beta d). \end{aligned}\right\} \quad (35)$$

If we introduce these values into the left-hand side of Eq. (33) and the value of Eq. (34) into its right-hand side, there results

$$4\pi NI/h = -(uH_0/w)(\operatorname{ctnh} \beta b + \operatorname{ctnh} \beta d), \quad (36)$$

from which H_0 can be computed if the current is given by amplitude I and frequency ω.

We consider now the interdependence of magnetic intensity H and electric intensity E, given by Eq. (29), and insert in (29) the values of Eqs. (31) and (35). The internal as well as the external fields give the same relation

$$-H_0 = (\beta/v_0)(\epsilon/\mu)^{\frac{1}{2}}E \quad (37)$$

between the maximum magnetic intensity H_0 and the maximum coil voltage E, both in the z direction and thus perpendicular to the wire layer. Inserting Eq. (37) in (36) in order to eliminate H_0, we obtain a definite interdependence between current I in the turns and voltage E to ground at any point of the coil. The surge impedance Z of the coil as ratio of voltage and current is determined therefore by

$$Z = E/I = 4\pi v_0(\mu/\epsilon)^{\frac{1}{2}} \frac{w}{u} \frac{N}{h} \frac{1/\beta}{\operatorname{ctnh} \beta b + \operatorname{ctnh} \beta d} \quad (\times 10^{-9} \text{ in } \Omega). \quad (38)$$

In order to transfer the electromagnetic units of Z into the practical unit ohm we have to multiply by 10^{-9}, as indicated in parentheses.

6. Surge Impedance of Transformer Coils

In a discussion of the surge impedance, as given by Eq. (38), the first group of factors on the right-hand side and the last fraction term can be considered separately. The group contains merely a numerical term 4π, the universal velocity of light v_0, the quotient μ/ϵ of the insulating space, and a few winding data of the coil. These are: the ratio w/u of turn length to circumference, which for transformers is always equal 1, and the number of turns N per length h of the coil which is a characteristic value of the winding, varying from 100 to 1 turns/cm for small-size to large-size power transformers. Thus into this group of factors there enter only very few data of the transformer; namely, the electromagnetic constants of the insulating space and the number of turns per axial unit length.

The second part of Eq. (38), given by the fraction

$$g = \frac{1/\beta}{\operatorname{ctnh} \beta b + \operatorname{ctnh} \beta d} \quad (39)$$

determines the equivalent ground distance of the winding. We see this immediately if at first small values of the arguments βb and βd are specified, which means either relatively slow oscillations, see β in Eq. (25), or small distances to ground. Then the ctnh's are equal to the reciprocals of their arguments and hence

$$g_0 = \frac{1/\beta}{1/\beta b + 1/\beta d} = \frac{1}{1/b + 1/d}. \quad (40)$$

In this case the equivalent ground distance g_0 is given by the actual interior and exterior ground distances in parallel connection, and thus the surge impedance for low frequency or narrow insulating spaces becomes

$$Z_0 = 4\pi v_0(\mu/\epsilon)^{\frac{1}{2}} \frac{N}{h} \frac{b}{1+b/d} \quad (\times 10^{-9} \text{ in } \Omega). \quad (41)$$

We see that this value is determined by only two more numerical data of the transformer than those just mentioned, namely the insulating distances b and d, and that in the range of

small βb and βd, the surge impedance is independent of the frequency and of the many other design data of a transformer.

If only one insulating distance, perhaps the interior one b, is small and the exterior one d is large, measured in terms of βb and βd as mentioned above, the ctnh of βd approaches the value 1 and therefore the equivalent ground distance becomes

$$g=\frac{1/\beta}{1/\beta b+1}=\frac{b}{1+\beta b}\leqq b. \qquad (42)$$

Thus the influence of one remote ground electrode disappears, as already indicated by Eq. (40).

A few experiments may confirm the validity of formula (41). A coil consisting of a single-layer winding of flat copper wire 1.2×7 mm in cross section and 59 m long was wound on an insulating tube of 36.3 cm diameter with $N=52$ turns over an axial length of $h=65$ cm. Concentrically in the interior was a closed cylindrical steel sheet representing a core or a secondary winding at a distance from coil to core $b=5.4$ cm. All this was imbedded in oil and there was no external metal tank. From the shape of the switching-on voltage curves, measured with a cathode-ray oscillograph, in comparison with those of a known smooth line, the traveling velocity along the winding could be determined as $v=155$ m/μsec., and the surge impedance as $Z=920$ ohms, approximately.

With an average dielectric constant $\epsilon=3.5$ and a permeability $\mu=1$, our formulae (15) and (41) give

$$v=300/(3.5)^{\frac{1}{2}}=160 \text{ m}/\mu\text{sec.}$$
$$Z=120\pi(1/3.5)^{\frac{1}{2}}(52/65)5.4=870 \text{ ohms,}$$

which is in good agreement with the measurements.

Another coil, also with a single-layer winding, but with air insulation, consisting of $N=4144$ turns of round wire of 0.254 mm diameter and 3380 m length, was wound on an insulating cylinder of 26.0 cm diameter and $h=116.5$ cm length, surrounding a closed copper tube of 24.38 cm diameter at an interior distance $b=0.81$ cm. The resultant dielectric constant was measured as $\epsilon=1.34$ and the permeability was $\mu=1$. The natural oscillations of the coil, with open as well as with closed ends, were measured by cathode-ray oscillograms which yielded a wave velocity $v=260$ m/μsec. Variation of an ohmic resistance, connected between the distant end and ground, until no wave reflection occurred on the cathode-ray oscillogram, yielded a surge impedance $Z=9020$ ohms. Our formulae (15) and (41) give

$$v=300/(1.34)^{\frac{1}{2}}=259 \text{ m}/\mu\text{sec.}$$
$$Z=120\pi(1/1.34)^{\frac{1}{2}}(4144/116.5)0.81=9350 \text{ ohms,}$$

again in close agreement with the experiments.

Hence we see that for coils of different sizes with a small as well as with a large number of turns per cm length, our theoretical derivations are verified experimentally.

For relatively high frequency and large value of β, or for large distances b and d, the values of the ctnh's in Eq. (39) approach 1 and thus we obtain as equivalent ground distance the asymptotic value

$$g_\infty=1/2\beta=(s/u)(v/2\omega). \qquad (43)$$

In this range the surge impedance with use of Eq. (15) and noting that $s=h/N$, is therefore,

$$Z_\infty=(2\pi/\omega)(v_0^2/\epsilon)(w/u^2). \qquad (44)$$

It varies inversely as the frequency and in addition to this and to universal constants is determined for tightly wound coils by the dielectric constant and the circumference of the coil.

If we draw a curve for the equivalent ground distance g, dependent on β, we obtain a shape as in Fig. 8, which also shows the dependence of the surge impedance Z on frequency ω. The lower and the upper asymptotic ranges are separated by a boundary frequency ω' which is determined by the intersection of the asymptotes of the two ranges just mentioned. The boundary frequency, therefore, according to Eqs. (40) and (43), is

$$\omega'=(s/u)(v/2)(1/b+1/d). \qquad (45)$$

For a power transformer of average size let us take $v=150$ m/μsec., $s/u=1/1000$, $b=2$ cm and $d=20$ cm. Then we obtain

$$\omega'=\frac{1}{1000}\,\frac{1.5\cdot10^{10}}{2}\left(\frac{1}{2}+\frac{1}{20}\right)=4.12\cdot10^5 \text{ c.p.s.}$$

This is much higher than the fundamental natural frequency of such a transformer, which is of the order of 10^4 c.p.s. The surge impedance of transformers of usual design remains constant therefore for frequencies of the order of the natural frequency up to a first group of higher harmonics and decreases only for frequencies of the order of very high harmonics.

Another way of expressing the boundary between the two ranges in Fig. 8 is to compute the corresponding wave-length. By Eq. (23) this boundary wave-length is

$$\lambda' = (4\pi u/w)[b/(1+b/d)]. \qquad (46)$$

Thus we see, that only for waves which are in the axial direction shorter than 4π times the resultant insulating distance does the surge impedance decrease with frequency. For $b=2$ cm and $d=20$ cm

$$\lambda' = 4\pi \cdot 1 \cdot 2/1.1 = 22.8 \text{ cm},$$

which is small as compared with a coil length of about $h=100$ cm for such a transformer, forming natural oscillations of $\lambda=200$ or 400 cm axial length dependent on the end conditions. In this example the boundary between the two ranges of constant and hyperbolically decreasing surge impedance is near the 9th or the 17th harmonic oscillation. For most transformers, with coils which are long as compared with the insulating distance, the use of the lower range Eq. (41) for the surge impedance is therefore sufficiently accurate.

However, if we remove the ground electrodes on both sides of the coil to greater distances, the boundary frequency decreases and therefore the upper approximation of the surge impedance in Eq. (44) extends to lower frequencies. The reason for the variation of surge impedance with frequency now occurring is, as seen in Fig. 6, that not all the electric lines of force end at the ground electrodes, but that many of them pass directly between the plus and minus sections of voltage and current along the coil. Thus we have solved here rigorously the problem of the mutual influence of neighboring parts of the coil in the case of harmonic waves of voltage and current. We realize that this effect has no influence on the velocity of traveling waves, which, according

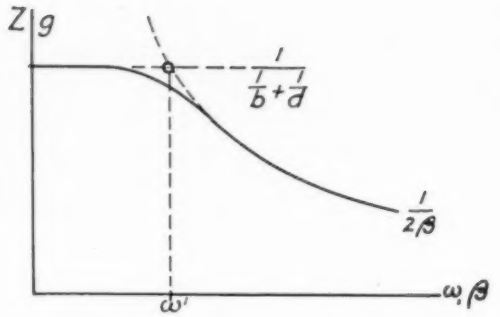

FIG. 8. Dependence of the equivalent ground distance, and of the surge impedance of a coil on the frequency of exciting oscillations.

to Eqs. (14) and (15), is independent of the frequency.

There still remains a discussion of the factor w/u in the surge impedance, Eq. (38), which is the ratio of turn length to circumference. For tightly-wound coils w/u is always 1, but for loosely wound coils we can express it, combined with the turn density N/h, and using Eq. (6), as

$$wN/uh = w/su = (1/u^2+1/s^2)^{\frac{1}{2}}. \qquad (47)$$

Thus both pitch and circumference of the coil influence the surge impedance. The deviation from the tight-coil formula becomes greatest when we consider a stranded concentric cable in which the wires are wound in spirals. Since such cables always have lengths which are very large as compared with the insulating distances, the boundary wave-length λ' is comparatively very small, and so the surge impedance becomes, with Eq. (40) for the lower range of frequencies,

$$Z = 4\pi v_0(\mu/\epsilon)^{\frac{1}{2}} \frac{(1/u^2+1/s^2)^{\frac{1}{2}}}{(1/b+1/d)} \quad (\times 10^{-9} \text{ in } \Omega). \qquad (48)$$

This expression agrees with the usual relation for cables with small insulating distances, except for the influence of the twist of the conductors, which is accurately considered here.

If we draw out axially a helical winding so that it finally becomes a straight conductor, the ratio of turn length w to circumference u gradually increases towards ∞. Since Eq. (17) has shown that the z dimension of any potential solution must then be lengthened increasingly up to ∞, we see from Fig. 6 that the lines of force straighten out radially more and more

until for a linear conductor they become straight lines perpendicular to the axis. This gives the transition to the well-known picture of lines of force for waves on smooth wires, where the electric and magnetic forces lie strictly in radial planes.

For many applications it is useful to derive rigorous expressions for self-inductance l and ground capacitance c of the coil. Since wave velocity and surge impedance are determined by these magnitudes as

$$v=1/(lc)^{\frac{1}{2}}, \quad Z=(l/c)^{\frac{1}{2}}, \tag{49}$$

we obtain the self-inductance

$$l=Z/v=4\pi\mu(w/u)(N/h)g \tag{50}$$

and the ground capacitance

$$c=1/Zv=(\epsilon/4\pi v_0^2)(u/w)(h/N)/g, \tag{51}$$

both per cm wire length of the coil. For low frequencies and constant equivalent ground distance g_0, as in Eq. (40), these last equations coincide with expressions which can easily be derived from the dimensions of transformer coils by elementary considerations.

For very high frequencies, however, by use of Eq. (43), we obtain

$$\left.\begin{aligned} l&=(2\pi/\omega)\mu v w/u^2 \\ c&=(\omega/2\pi)u^2/\mu v^3 w. \end{aligned}\right\} \tag{52}$$

The self-inductance now decreases with frequency, caused by the rapid spatial attenuation of the magnetic field perpendicular to the winding area, as shown by Eq. (25). The capacitance increases with frequency, caused by the diminishing distances between the plus- and minus-sections of voltage along the coil. Hereby more and more electric lines of force close themselves directly to the neighboring parts of the coil without touching the ground electrodes as represented in the exterior space of Fig. 6. Finally, for very high frequencies or for remote ground electrodes, far above the criterion (45), the ground does not play any part whatever. Thus we have found in Eq. (52) the electromagnetic characteristics for a long single coil, not too small in diameter, situated in empty space without ground.

7. Conclusions

We realize from all the preceding considerations that, according to the rigorous Maxwellian equations, the wire velocity of waves in windings under the conditions stated always is identical with the fundamental velocity of light in the insulating space.

Under conditions prevailing for the most part in actual transformers the surge impedance of the winding is, under the conditions stated, independent of the frequency of oscillations and dependent on only three characteristic data of the winding, namely turn-density, insulating distances and magneto-dielectric ratio of the insulating space. For extremely high frequencies or for very large insulating spaces on both sides of the coil, the surge impedance decreases gradually with frequency. Furthermore, the relative pitch of the turns, if large, enters the result and determines in every case the attenuation of the electromagnetic field perpendicular to the axis of the coil.

As an important result of the rigorous theory we have found that, under the stated conditions, tightly wound coils perform, up to a boundary frequency, along their wires with respect to traveling waves exactly like smooth lines. In the direction of their axis, however, they perform nearly statically. Perpendicular to this axis the spatial field of harmonic oscillations appears, above that boundary frequency as exponentially attenuated.

Special Symbols

b = internal insulating distance
d = external insulating distance
g = equivalent ground distance
h = axial length of the coil
s = pitch of the helical coil
u = circumference of the coil
v = velocity of waves
w = wire length of a turn.
A = linear current density
N = number of turns of the winding
Z = surge impedance
α = wave density in space
β = attenuation constant
λ = wave-length in axial direction
ω = angular frequency.

Steady-State Solutions of Electromagnetic Field Problems

I. Forced Oscillations of a Cylindrical Conductor

J. A. Stratton and L. J. Chu
Massachusetts Institute of Technology, Cambridge, Massachusetts
(Received December 9, 1940)

The object of this investigation is a study of the current distribution in or on the surface of a conductor and its associated field under the influence of a localized e.m.f. Steady-state solutions of the field equations are found for conductors of simple geometric form. The results clarify many electromagnetic problems involving localized sources, especially in the *u-h-f* region, for which ordinary circuit theory fails to give a satisfactory quantitative explanation. Part I treats the problem of a straight cylindrical conductor and shows the relation of the principal and complementary waves to the nature of the exciting field. A driving point impedance is calculated for the case of an external field applied over a vanishingly short section of conductor. The driving point impedance is infinite for a conductor of infinite length and perfect conductivity. Likewise the case of a conductor of finite length bounded at either end by an infinite, perfectly conducting plane is discussed. This problem bears a direct relation to that of a hollow pipe excited by a linear antenna.

THE object of this investigation is a study of the current distribution in or on the surface of a conductor and its associated field under the influence of a localized e.m.f. Solutions of electromagnetic field problems are ordinarily constructed from wave functions satisfying a *homogeneous* set of equations, which in rationalized m.k.s. units can be written

$$\nabla\times\mathbf{E}+i\omega\mu\mathbf{H}=0, \qquad \text{(I)}$$

$$\nabla\times\mathbf{H}-(\sigma+i\omega\epsilon)\mathbf{E}=0. \qquad \text{(II)}$$

It is assumed here that all quantities contain the time in the form of a factor $\exp(i\omega t)$. The field intensity $\mathbf{E}$ is measured in volts/meter, $\mathbf{H}$ in ampere-turns/meter, and conductivity σ in mhos/meter. In free space $\mu_0=4\pi\times10^{-7}$ henry/meter, $\epsilon_0=10^{-9}/36\pi$ farad/meter. When the usual boundary conditions are applied in an appropriate coordinate system, (I) and (II) reduce to a set of homogeneous algebraic equations whose determinant must vanish. The complex roots of this determinantal equation fix the frequencies and damping of the allowed or free modes of oscillation. The amplitudes, however, are completely arbitrary and will be determined by the nature of the exciting source, to which (I) and (II) give no clue.

Exact steady-state solutions of electromagnetic problems have been found in a number of simple cases, such as that of a plane wave incident upon a cylinder or sphere. The equations relating the coefficients of the various particular solutions are now *inhomogeneous;* hence the amplitudes of the excited modes are uniquely determined and the system oscillates with the frequency of the impressed field. In such problems the diffracting body is entirely enveloped in the incident wave. Quite as numerous as these problems of purely optical interest are those in which the impressed field is applied as a local e.m.f., confined essentially to a small domain of the conductor. The applied field intensity will be designated by the vector $\mathbf{E}'$ measured in volts/meter. $\mathbf{E}'$ is a specified function of position and time but is not necessarily analytic. It represents the intensity of any external force, of whatever origin, acting on the free charges of the conductor. It may be introduced by a mechanical or chemical agency, by the motion of an external magnet, or by a shielded transmission line. In the latter case, which is the common and practical one, it is obvious that the entire problem is modified to some extent by the presence of the line. It is reasonable to assume, however, that in most cases the effect of the leads on the current distribution in the principal conductor or upon the field at a distance is small and that the perturbation can be taken into account by a second approximation.

It will be assumed in the following that a

conducting body is embedded in a homogeneous dielectric medium and that the external e.m.f. is applied within or on the surface of the conductor only. The grounds for the latter assumption are, perhaps, open to some question, since an applied field at the surface of a conductor must inevitably extend into the neighboring dielectric and thereby effect its polarization; but the effect on the total field of such additional dielectric displacement currents is small relative to that of the conduction current, and its neglect seems entirely warranted. Hence the field within the dielectric is governed by Eqs. (I) and (II). If the conductor is metallic the displacement current term is negligible, and since the current density $\mathbf{J}$ is proportional to the resultant field intensity, $\mathbf{J}=\sigma(\mathbf{E}+\mathbf{E}')$, we have to satisfy in this domain the inhomogeneous system

$$\nabla\times\mathbf{E}+i\omega\mu\mathbf{H}=0, \qquad \text{(I)}$$

$$\nabla\times\mathbf{H}-\sigma\mathbf{E}=\sigma\mathbf{E}'. \qquad \text{(II-a)}$$

Analytic continuation of the solutions from one domain to the other is insured by the boundary conditions which call for a continuous transition of the tangential components of $\mathbf{E}$ and $\mathbf{H}$. Note, however, that the transition of $\mathbf{E}'$ across a boundary is arbitrary and in general discontinuous.

$$\mathbf{n}\times(\mathbf{E}_2-\mathbf{E}_1)=0, \quad \mathbf{n}\times(\mathbf{H}_2-\mathbf{H}_1)=0, \qquad \text{(III)}$$

where $\mathbf{n}$ is a unit normal vector drawn from medium (1) to medium (2). The normal will always be drawn outward from a metallic surface into the dielectric.

There is, of course, nothing new in these equations and they are discussed in most of the older texts on electromagnetic theory.[1] The purpose of the present work is to show that in many cases they are easily integrated and that the solutions can be of greater practical interest than those giving simply the transient oscillations. As a first example we consider the propagation of waves along a single, infinite conductor of circular cross section. The classical treatments of this problem are due to Rayleigh and to Sommerfeld. It was shown by Sommerfeld that the system admitted a principal wave propagated with negligible damping and a velocity approaching that of light, together with an infinite series of complementary waves associated with damping factors so great as to result in immediate extinction. In dielectric wires or hollow pipes, on the other hand, no principal mode occurs and for sufficiently high frequencies the complementary waves are propagated with relatively little attenuation. These are free modes of oscillation whose amplitudes are determined by the initial conditions and which are responsible for resonance phenomena. A "surface impedance" was also defined by Rayleigh and used as a basis for the discussion of the alternating-current resistance of linear conductors. It differs from the driving-point impedance to be observed at the point of application of an external e.m.f.

We shall assume that $\mathbf{E}'$ is parallel to the axis of the conductor and is uniform over the cross section. In Fig. 1 the axis of the conductor is shown coinciding with the z axis of the coordinate system and the impressed e.m.f. is introduced in the neighborhood of $z=0$. Particular solutions of (I) and (II) in cylindrical coordinates r, ϕ, z appropriate for the dielectric domain $r>a$ can be taken directly from Sommerfeld's discussion.[2]

Thus for $r>a$

$$\left.\begin{aligned} E_z &= AH_0^{(2)}(p_2r) \\ E_r &= (iu/p_2)AH_1^{(2)}(p_2r) \\ H_\phi &= (i\omega\epsilon_2/p_2)AH_1^{(2)}(p_2r) \end{aligned}\right\} e^{i\omega t-iuz}, \qquad (1)$$

$$p_2=(k_2^2-u^2)^{\frac{1}{2}}, \quad k_2^2=\omega^2\epsilon_2\mu_2, \qquad (2)$$

where $H_n^{(2)}(p_2r)$ is a Hankel function of the second kind insuring proper behavior of the field at infinity.

Inside the conductor

$$E_x'=E_y'=0, \quad E_z'=E'(z), \qquad (3)$$

where E' is a prescribed function of z and t.

[1] M. Abraham, *Theorie der Elektrizität* (Teubner, seventh edition, 1923); O. Heaviside, *Electrical Papers* (Macmillan, 1892).

[2] A. Sommerfeld, Ann. d. Physik **67**, 233 (1899); also in Riemann-Weber, *Differentialgleichungen der Physik*, Vol. 2, (Vieweg, 1935) eighth edition.

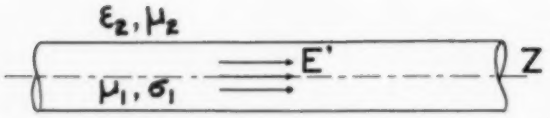

FIG. 1. Section of infinite conductor of circular cross section a embedded in dielectric medium ϵ_2, μ_2.

Equations (I) and (II-a) now reduce to

$$\frac{\partial E_r}{\partial z}-\frac{\partial E_z}{\partial r}+i\omega\mu_1 H_\phi=0,$$

$$\frac{\partial H_\phi}{\partial z}+\sigma_1 E_r=0, \tag{4}$$

$$\frac{1}{r}\frac{\partial}{\partial r}(rH_\phi)-\sigma_1 E_z=\sigma_1 E'.$$

Eliminating E_r and H_ϕ one obtains

$$\frac{1}{r}\frac{\partial}{\partial r}\left(r\frac{\partial E_z}{\partial r}\right)+\frac{\partial^2 E_z}{\partial z^2}-i\omega\mu_1\sigma_1 E_z = i\omega\mu_1\sigma_1 E'-\frac{\partial^2 E'}{\partial z^2}. \tag{5}$$

If now we place

$$F=E_z+E' \tag{6}$$

and note that the field is finite on the axis, it is apparent that for $r<a$ particular solutions of (5) must be constructed from the functions

$$F=BJ_0(p_1 r)e^{i\omega t-iuz}, \tag{7}$$

$$p_1=(k_1^2-u^2)^{\frac{1}{2}}, \quad k_1^2=-i\omega\mu_1\sigma_1, \tag{8}$$

where $J_0(p_1 r)$ is a Bessel function of the first kind.

The impressed field E' is a prescribed function of z. For the moment we shall assume only that $E'(z)$ and its first derivative are piecewise continuous and that the integral

$$\int_{-\infty}^{\infty}|E'|\,dz$$

exists. Under these circumstances the impressed field can be represented by the Fourier integral

$$E'=G(z)e^{i\omega t} =(e^{i\omega t}/2\pi)\int_{-\infty}^{\infty}du\int_{-\infty}^{\infty}d\alpha\, G(\alpha)e^{iu(\alpha-z)}. \tag{9}$$

The coefficients A and B of the particular solutions (1) and (7) are now considered to be functions of a parameter α. Upon integrating with respect to u and α the field at any point is represented as a superposition of cylindrical waves. Thus for $r>a$

$$E_z=\frac{e^{i\omega t}}{2\pi}\int_{-\infty}^{\infty}du\int_{-\infty}^{\infty}d\alpha\, A(\alpha)H_0^{(2)}(\lambda_2 r)\,e^{iu(\alpha-z)}.$$

$$H_\phi=i\omega\epsilon_2\frac{e^{i\omega t}}{2\pi}\int_{-\infty}^{\infty}du\int_{-\infty}^{\infty}d\alpha\,\frac{A(\alpha)}{p_2}H_1^{(2)}(p_2 r)\,e^{iu(\alpha-z)}, \tag{10}$$

while for $r<a$

$$E_z=\frac{e^{i\omega t}}{2\pi}\int_{-\infty}^{\infty}du\int_{-\infty}^{\infty} \times d\alpha[B(\alpha)\,J_0(p_1 r)-G(\alpha)]e^{iu(\alpha-z)},$$

$$H_\phi=\sigma_1\frac{e^{i\omega t}}{2\pi}\int_{-\infty}^{\infty}du\int_{-\infty}^{\infty}d\alpha\,\frac{B(\alpha)}{p_1}J_1(p_1 r)e^{iu(\alpha-z)}. \tag{11}$$

These equations are next subjected to the boundary conditions (III) at the surface $r=a$. There results the algebraic system

$$B\,J_0(p_1 a)-A\,H_0^{(2)}(p_2 a)=G(\alpha),$$

$$\frac{\sigma_1}{p_1}B\,J_1(p_1 a)-\frac{i\omega\epsilon_2}{p_2}A\,H_1^{(2)}(p_2 a)=0 \tag{12}$$

from which we obtain

$$B=\frac{x}{\sigma_1 a}\frac{G(\alpha)}{J_1(x)}\frac{1}{Z(u)},$$

$$Z(u)=\frac{x}{\sigma_1 a}\frac{J_0(x)}{J_1(x)}-\frac{y}{i\omega\epsilon_2 a}\frac{H_0^{(2)}(y)}{H_1^{(2)}(y)}, \tag{13}$$

$$x=p_1 a, \quad y=p_2 a.$$

In the absence of a driving force G, the natural modes of propagation are given by the roots of $Z(u)=0$, exactly the condition found by Sommerfeld. This condition has an interesting physical interpretation. By definition the wave impedance of a cylindrical wave in the radial direction is $-E_z/H_\phi$. The rule for the algebraic sign is that of the Poynting vector. The ratio is positive when the components of **E** and **H** follow in cylindrical order.[3] It is clear that apart from a sign the first term of $Z(u)$ is the radial impedance of the cylindrical field within the conductor, while the second term expresses this impedance in the external medium. $Z(u)$ is the difference of the two impedances at the boundary. The free oscillations

[3] S. A. Schelkunoff, Bell Sys. Tech. J. **17**, 17–48 (1938).

of any system of bodies embedded in a homogeneous medium follow from the condition of equality, or "matching," of the normal components of wave impedance across the bounding surfaces, expressed in the present instance by the vanishing of $Z(u)$.

Let us now calculate the current passing any cross section of the conductor. Since $J_z=\sigma_1(E_z+E')$, we find for the current I at any point z

$$I=ae^{i\omega t}(2\pi)^{\frac{1}{2}}\int_{-\infty}^{\infty}\frac{g(u)}{Z(u)}e^{-iuz}du, \qquad (14)$$

where

$$g(u)=(1/(2\pi)^{\frac{1}{2}})\int_{-\infty}^{\infty}G(u)e^{iu\alpha}d\alpha \qquad (15)$$

is the Fourier transform of the applied field $G(z)$.

The zeros of the impedance function $Z(u)$ occur at the values of u corresponding to the propagation constants of the principal and complementary natural modes, and all are complex provided σ_1 is finite. $Z(u)$ is symmetric in u and the roots lie in the first and third quadrants, with none falling on the real axis. It follows, moreover, from the asymptotic behavior of the Bessel and Hankel functions that as $u\to\infty$, $Z(u)\to\infty$ as $(1/\sigma_1+1/i\omega\epsilon_2)u$. Hence the path of integration along the real axis may be closed by a semicircle of very large radius in the upper or lower half-plane according as z is greater or less than zero. This is illustrated in Figs. 2(a) and 2(b), the dots indicating schematically the location of the zeros.

We assume the transform $g(u)$ to be analytic everywhere within the closed contour and properly bounded at infinity. Let u_n designate the roots of $Z(u)=0$. Then

$$I=\pm a(2\pi)^{\frac{1}{2}}e^{i\omega t}2\pi i\sum_n b_n, \qquad (16)$$

where b_n is the residue at the pole u_n and the plus or minus sign holds as z is less or greater than zero.

To determine the residues we need only the first term in the Taylor expansions of $Z(u)$ about the poles.

$$Z(u)=(u-u_n)\left(\frac{dZ}{du}\right)_{u=u_n}+\cdots, \qquad (17)$$

and hence

$$I=a(2\pi)^{\frac{1}{2}}e^{i\omega t}2\pi i\sum_n\frac{g(u_n)e^{-iu_n}}{(dZ/du)_{u=u_n}}. \qquad (18)$$

Thus the source excites all modes and these travel along the line with the propagation factors determined by Sommerfeld's analysis. The amplitudes are uniquely determined by the form of the exciting function $g(u)$. It will be recalled that if the radius of the conductor and its conductivity are not too small, the propagation factor of the principal wave is given approximately by

$$u_1\backsimeq k_2=\omega(\epsilon_2\mu_2)^{\frac{1}{2}}=2\pi/\lambda. \qquad (19)$$

The effect of a finite conductivity is to introduce a very small imaginary part and a corresponding attenuation. The attenuation of the complementary modes, on the other hand, is exceedingly large and so for all practical purposes (18) reduces to

$$I=a(2\pi)^{\frac{1}{2}}2\pi i\frac{g(k_2)}{(dZ/du)_{u\simeq k_2}}e^{i\omega t-ik_2z}. \qquad (20)$$

To calculate the denominator in (20) note that

$$p_2\backsimeq 0, \quad |k_1|\gg k_2, \quad x\backsimeq k_1a\gg 1. \qquad (21)$$

If we write $k_1=\alpha_1-i\beta_1$, it follows from the asymptotic representations of the Bessel functions that

$$\lim_{\beta_1\to\infty}\frac{J_0(x)}{J_1(x)}=\lim_{\beta_1\to\infty}\cot\left[a(\alpha_1-i\beta_1-\pi/4a)\right]=i, \qquad (22)$$

while from the first term of the series expansions of the Hankel functions in the neighborhood of $y=0$ it is easily shown that

$$H_0^{(2)}(y)/H_1^{(2)}(y)\to y\ln(\gamma yi/2) \quad \text{as } y\to 0, \qquad (23)$$

where $\gamma=1.781$. From this it follows that

$$dZ/du\to 2ia(\mu_2/\epsilon_2)^{\frac{1}{2}}\ln(\gamma yi/2) \quad \text{as } u\to k_2, \qquad (24)$$

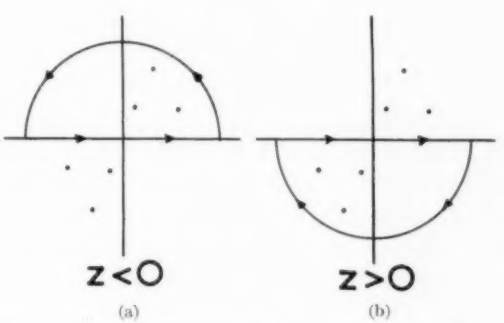

FIG. 2. Closed contours of integration in u plane.

and the current at any point on the line is

$$I=2\pi(\pi\epsilon_2/2\mu_2)^{\frac{1}{2}}\frac{g(k_2)}{\ln(\gamma yi/2)}e^{i\omega t-ik_2z}. \quad (25)$$

In case the external dielectric is air, the first factor reduces to $2\pi(\epsilon_0/\mu_0)^{\frac{1}{2}}=1/60$.

For the sake of example consider the case of an applied field whose form is represented by the "impulse function."

$$G(z)=\frac{E_0}{(2\pi)^{\frac{1}{2}}}\frac{e^{-z^2/2d^2}}{d} \quad (26)$$

with the property

$$\int_{-\infty}^{\infty}G(z)dz=E_0, \quad (27)$$

where E_0 is a constant and d a parameter. Its Fourier transform is

$$g(k_2)=\frac{E_0}{(2\pi)^{\frac{1}{2}}}e^{-d^2k_2^2/2}. \quad (28)$$

By definition the applied voltage is

$$V=\int_{-\infty}^{\infty}E'dz=E_0e^{i\omega t}. \quad (29)$$

The ratio of this voltage to the current at the point $z=0$ depends in general on the parameter d, which measures effectively the length of the segment to which the driving force is actually applied. In the present instance

$$V/I(0)=120\,e^{d^2k_2^2/2}\ln(\gamma yi/2). \quad (30)$$

In the limit as $d\to 0$ the region of application reduces to a point and the ratio represents the true driving-point impedance of the line.

$$Z_i=\lim_{d\to 0}V/I(0)=120\ln(\gamma yi/2)\text{ ohms}, \quad (31)$$

assuming the external medium to be air. Practically, it is only necessary that the region of applied field be small relative to the wave-length to justify the concept of a voltage V applied at a definite driving point $z=0$. In this limit the impedance is independent of the exact functional form of the applied field. This is easily verified for the case of a "rectangular" distribution defined by

$$\begin{aligned} G(z)&=E_0 \quad \text{when} \quad |z|<d,\\ G(z)&=0 \quad \text{when} \quad |z|>d. \end{aligned} \quad (32)$$

The ratio of V to the current at the midpoint is now

$$V/I(0)=120\,(dk_2/\sin dk_2)\ln(\gamma yi/2), \quad (33)$$

which reduces to (31) in the limit $d=0$.

One will note that u is exactly equal to k_2 and y equals zero only in the case of a perfectly conducting wire. In these circumstances the driving-point impedance of the system is infinite, a result entirely comprehensible from the fact that the wire is of infinite length. Sommerfeld's solution has shown how currents, established in an unspecified manner, are propagated. We now see how these currents are related to the source and it appears that a finite current in a perfect conductor of infinite length cannot be established by a finite voltage. If the conductivity of the wire is finite, the input impedance is large but bounded. A current enters the wire and the inflowing energy is eventually dissipated in heat.

It is of some interest to consider the case of a wire of finite length, although it has no direct bearing on the free antenna problem to be discussed later. The procedure followed above will give us, by a slight modification, the driving-point impedance at the center of a linear, vertical antenna bounded at either end by horizontal, perfectly conducting planes. The problem is thus related indirectly to the establishment of waves in hollow pipes.

The applied field is now represented by a Fourier series in place of an integral. Let the transverse, perfectly conducting planes be located at $z=l$ and $z=-l$. The tangential component E_r must vanish over these surfaces and hence in place of (1) when $r>a$ we construct a solution of the form

$$\begin{aligned} E_r&=e^{i\omega t}\sum_{n=0}^{\infty}\frac{n\pi}{2lp_2}A_n H_1^{(2)}(p_2r)\sin\frac{n\pi}{2l}(z+l),\\ E_z&=e^{i\omega t}\sum_{n=0}^{\infty}A_n H_0^{(2)}(p_2r)\cos\frac{n\pi}{2l}(z+l),\\ H_\phi&=i\omega\epsilon_2e^{i\omega t}\sum_{n=0}^{\infty}\frac{A_n}{p_2}H_1^{(2)}(p_2r)\cos\frac{n\pi}{2l}(z+l),\\ p_2&=\left(\frac{4\pi^2}{\lambda^2}-\frac{n^2\pi^2}{4l^2}\right)^{\frac{1}{2}}=\frac{2\pi}{\lambda}\left(1-\left(\frac{n\lambda}{4l}\right)^2\right)^{\frac{1}{2}}, \end{aligned} \quad (34)$$

where λ is the wave-length in the dielectric. The

applied field is expanded in the series

$$E' = e^{i\omega t} \sum_{n=0}^{\infty} C_n \cos \frac{n\pi}{2l}(z+l), \tag{35}$$

so that the field within the wire is represented by

$$E_z = e^{i\omega t} \sum_{n=0}^{\infty} [B_n J_0(p_1 r) - C_n] \cos \frac{n\pi}{2l}(z+l),$$

$$H_\phi = \sigma_1 e^{i\omega t} \sum_{n=0}^{\infty} \frac{B_n}{p_1} J_1(p_1 r) \cos \frac{n\pi}{2l}(z+l). \tag{36}$$

The boundary conditions at $r=a$ lead to

$$B_n = \frac{x}{\sigma_1 a} \frac{C_n}{J_1(x)} \frac{1}{Z_n} \tag{37}$$

in which Z_n is formally identical with (13) but with u restricted to the discrete set of values $n\pi/2l$. The current at any point on the line is now

$$I = 2\pi a e^{i\omega t} \sum_{n=0}^{\infty} \frac{C_n}{Z_n} \cos \frac{n\pi}{2l}(z+l). \tag{38}$$

Assume next the rectangular distribution of applied field defined in (33). E' is then a symmetric function of z, so that all odd coefficients of (36) are zero, while for the even coefficients one obtains

$$C_0 = \frac{d}{l} E_0, \quad C_{2n} = \frac{2(-1)^n}{n\pi} E_0 \sin \frac{n\pi d}{l}, \quad (n = 1, 2, \cdots). \tag{39}$$

The input impedance at the central point of the wire is again found by taking the ratio of the applied voltage to the current at $z=0$ and passing to the limit as $z \to 0$.

$$Z_i = \frac{l}{\pi a} 1 \Big/ \left[\frac{1}{Z_0} + 2 \sum_{n=1}^{\infty} \frac{1}{Z_{2n}} \right], \tag{40}$$

or for the admittance

$$Y_i = \frac{\pi a}{l} \left(Y_0 + 2 \sum_{n=1}^{\infty} Y_{2n} \right), \tag{41}$$

where $Y_n = 1/Z_n$. Let us assume for the moment that the conductivity of the radiating cylinder is infinite. Then Y_n reduces to

$$Y_{2n} = -\frac{i}{(1-\beta_n^2)^{\frac{1}{2}}} (\epsilon_2/\mu_2)^{\frac{1}{2}} \times \frac{H_1^{(2)}[(2\pi a/\lambda)(1-\beta_n^2)^{\frac{1}{2}}]}{H_0^{(2)}[(2\pi a/\lambda)(1-\beta_n^2)^{\frac{1}{2}}]}, \tag{42}$$

where $\beta_n = n\lambda/2l$. If $\beta_n > 1$, the ratio of Hankel functions is a pure imaginary. Hence if $\lambda > 2l$, all admittance terms with the exceptions of Y_0 have susceptance components but no conductance. The complex power associated with these terms is purely reactive. If now λ is decreased, a critical wave-length is reached at which Y_2 assumes a nonvanishing conductance. Further decrease of λ introduces successively in step-wise fashion the conductances of higher modes, and with each entry there is a corresponding increase in real power input representing outward radiation of a higher order wave. It will be noted in passing that the sum of these terms fails, in the present instance, to approach a limit, due to the assumption of a voltage concentrated at a mathematical point rather than over a small but finite segment of the cylinder. This matter will be referred to later.

The term Y_0 has a nonvanishing conductance at all wave-lengths and represents the principal wave. Its field is strictly two dimensional, there being no variation along the z axis. The component E_r is zero everywhere and energy flows radially outward from the cylinder. Such a mode is possible because of the absence of any further boundaries transverse to the conducting planes. It will be recalled that the principal wave is completely suppressed in hollow wave guides of finite cross section.

In case the conductivity of the cylinder is finite the term $xJ_0(x)/J_1(x)$ in (13) contributes a small conductance to each admittance component at all wave-lengths, accounting for the dissipation of a certain amount of energy in heat.

Steady-State Solutions of Electromagnetic Field Problems

II. Forced Oscillations of a Conducting Sphere

J. A. Stratton and L. J. Chu
Massachusetts Institute of Technology, Cambridge, Massachusetts

(Received December 9, 1940)

The method discussed in Part I for the determination of steady-state solutions of electromagnetic problems is applied to a finitely conducting sphere as the simplest illustration involving a body of finite dimensions. The external e.m.f. is applied across an infinitesimal strip at the equator. The induced field appears as the sum of an infinite number of partials or modes. As the frequency is increased these modes become successively dominant. There are a series of resonance points. The real part of the driving-point admittance rises step-wise with increasing frequency and the behavior of the system is notably different from that of a normal circuit. Expressions are given for the power dissipated in heat and in radiation and it is shown that the complex power input at the driving point is equal to the integral of the complex Poynting vector over the surface of the sphere.

THE preceding paper[1] has dealt with the forced oscillations of a cylindrical conductor under the influence of a local applied e.m.f. In the case of a cylinder of infinite length there is no radiation loss and the real part of the driving-point impedance is due solely to the finite conductivity of the material. In the case of a vertical cylindrical conductor bounded at either end by horizontal, perfectly conducting planes of infinite dimensions, the radiation is mainly two dimensional. In both cases the conductors extend to infinity and the significance of the results is in some respects obscure. In this present paper, we consider certain forced oscillations of a metallic body of simple geometric form and finite dimensions—a sphere—and discuss in more detail the resonance phenomena, the radiation impedance to be measured at the driving point, and the relations between radiation power, conduction loss and power input. The foundations are laid for a discussion of the generalized case of a prolate spheroid of arbitrary eccentricity.[2]

If $\mathbf{E}'$ is the intensity of the applied field, one has at any point in a homogeneous medium

$$\nabla\times\mathbf{E}+i\omega\mu\mathbf{H}=0, \tag{1}$$

$$\nabla\times\mathbf{H}-(\sigma+i\omega\epsilon)\mathbf{E}=\sigma\mathbf{E}'. \tag{2}$$

Any influence of $\mathbf{E}'$ upon the polarization of dielectric material has been neglected, since it is understood that the external field is to be applied directly to conductors, with the result that polarization currents will be masked by neighboring conduction currents. From (1) and (2) it follows that $\mathbf{E}$ and $\mathbf{H}$ satisfy

$$-\nabla\times\nabla\times\mathbf{E}+k^2\mathbf{E}=i\omega\mu\sigma\mathbf{E}', \tag{3}$$

$$-\nabla\times\nabla\times\mathbf{H}+k^2\mathbf{H}=-\sigma\nabla\times\mathbf{E}', \tag{4}$$

where $k^2=\omega^2\epsilon\mu-i\omega\mu\sigma$.

Consider a metallic sphere of finite conductivity embedded in a dielectric of zero conductivity, with $\sigma_1\gg\omega\epsilon_2$. It will be assumed that $\mathbf{E}'$ is applied uniformly over the equatorial plane and in a direction normal to this plane. This corresponds to the assumption made in I. Strictly, such a field does not exist, since it is irrotational. Due to the high conductivity of the metal, however, the *total* field, which is the resultant of the applied and induced fields, is confined to a thin layer near the surface, and the resultant current distribution is governed essentially by the value of $\mathbf{E}'$ within this layer alone. Its thickness is small relative to the wavelength, so that $\mathbf{E}'$ may be assumed uniform over the layer cross section and consequently $\nabla\times\mathbf{E}'=0$. To this approximation the field equations are homogeneous in the dependent variables $\mathbf{H}$ and $\mathbf{E}+\mathbf{E}'$, within the conductor as well as within the external dielectric. Assuming, therefore, that $\mathbf{E}'$ is applied in the z direction and is

[1] J. A. Stratton and L. J. Chu, J. App. Phys. **12**, 230 (1941).
[2] L. J. Chu and J. A. Stratton, J. App. Phys. **12**, 241 (1941).

symmetrical about the z axis, one finds for the spherical components of the induced field:

In the dielectric, medium 2, $R>a$,

$$H_\phi = e^{i\omega t}\sum_{n=1}^{\infty} A_n h_n^{(2)}(k_2R)\, P_n^1(\cos\theta),$$

$$E_R = \frac{-e^{i\omega t}}{i\omega\epsilon_2 R\sin\theta}\sum_{n=1}^{\infty} A_n n\, h_n^{(2)}(k_2R) \times[\cos\theta\, P_n^1(\cos\theta) - P_{n+1}^1(\cos\theta)], \tag{5}$$

$$E_\theta = i(\mu_2/\epsilon_2)^{\frac{1}{2}} e^{i\omega t}\sum_{n=1}^{\infty} A_n[h_{n-1}^{(2)}(k_2R) - (n/k_2R)h_n^{(2)}(k_2R)]P_n^1(\cos\theta),$$

while in the metal sphere, medium 1, $R<a$,

$$H_\phi = e^{i\omega t}\sum_{n=1}^{\infty} B_n j_n(k_1R)\, P_n^1(\cos\theta),$$

$$E_R = \frac{-e^{i\omega t}}{\sigma_1 R\sin\theta}\sum_{n=1}^{\infty} B_n n\, j_n(k_1R) \times[\cos\theta\, P_n^1 - P_{n+1}^1] - E_R', \tag{6}$$

$$E_\theta = (\omega\mu_1/i\sigma_1)^{\frac{1}{2}} e^{i\omega t}\sum_{n=1}^{\infty} B_n[j_{n-1}(k_1R) - (n/k_1R)j_n(k_1R)]P_n^1 - E_\theta',$$

where

$$k_1 = (-i\omega\mu_1\sigma_1)^{\frac{1}{2}}, \quad k_2 = \omega(\epsilon_2\mu_2)^{\frac{1}{2}},$$
$$h_n^{(2)}(k_2R) = (\pi/2k_2R)^{\frac{1}{2}} H_{n+1}^{(2)}(k_2R),$$
$$j_n(k_1R) = (\pi/2k_1R)^{\frac{1}{2}} J_{n+1}(k_1R),$$
$$P_n^1(\cos\theta) = -(d/d\theta)P_n(\cos\theta).$$

The applied field $\mathbf{E}'$ is expanded in a series of spherical harmonics as

$$E_\theta' = (\omega\mu_1/i\sigma_1)^{\frac{1}{2}} e^{i\omega t}\sum_n C_n(R)\, P_n^1(\cos\theta). \tag{7}$$

the coefficients $C_n(R)$ being functions of R alone. The conditions on the continuity of the tangential components of $\mathbf{E}$ and $\mathbf{H}$ at the boundary $R=a$ then lead to

$$B_n = -\left(\frac{\omega\mu_1}{i\sigma_1}\right)^{\frac{1}{2}} \frac{C_n(a)}{j_n(k_1a)\, Z_n}, \quad A_n = \frac{j_n(k_1a)}{h_n^{(2)}(k_2a)} B_n, \tag{8}$$

$$Z_n = \frac{i\omega\mu_2}{k_2}\left[\frac{h_{n-1}^{(2)}(k_2a)}{h_n^{(2)}(k_2a)} - \frac{n}{k_2a}\right] - \frac{i\omega\mu_1}{k_1}\left[\frac{j_{n-1}(k_1a)}{j_n(k_1a)} - \frac{n}{k_1a}\right]. \tag{9}$$

The quantity Z_n expresses the difference between the radial wave impedances E_θ/H_ϕ inside and outside the sphere, and free oscillation of the sphere occurs when these impedances are matched, or $Z_n=0$, an equation whose roots determine the characteristic frequencies of the natural modes.[3] Because of the extremely large value of σ in metals one has, even for very small values of radius a, the condition $|k_1a|\gg 1$, so that

$$(i\omega\mu_1/k_1)[j_{n-1}(k_1a)/j_n(k_2a) - n/k_1a] \cong -(i\omega\mu_1/\sigma_1)^{\frac{1}{2}},$$

a very small quantity, and hence

$$Z_n \cong i(\mu_2/\epsilon_2)^{\frac{1}{2}}[h_{n-1}^{(2)}(k_2a)/h_n^{(2)}(k_2a) - n/k_2a] + (i\omega\mu_1/\sigma_1)^{\frac{1}{2}}. \tag{10}$$

Now $k_2a = 2\pi a/\lambda$, where λ is the wave-length measured in the dielectric. It is therefore a measure of the curvature of the sphere. When $k_2a\to\infty$, the terms within the square brackets approach $-i$, and Z_n reduces to

$$(\mu_2/\epsilon_2)^{\frac{1}{2}} + (i\omega\mu_1/\sigma_1)^{\frac{1}{2}},$$

the difference between the intrinsic impedances of dielectric and conductor. One will recall that the wave in the dielectric propagates away from the center of the sphere while that in the conductor supplying the conduction loss travels toward the center. Looking outward from the center, the intrinsic impedance of the conductor is $-(i\omega\mu_1/\sigma_1)^{\frac{1}{2}}$. When $k_2a<n$, the terms within the square brackets are essentially real, and

$$Z_n \cong i\left(\frac{\mu_2}{\epsilon_2}\right)^{\frac{1}{2}}\left[-\frac{n}{k_2a} + \frac{k_2a}{2n-1} + \frac{(k_2a)^3}{(2n-1)^2(2n-3)} + \frac{2(k_2a)^5}{(2n-1)^3(2n-3)(2n-5)} + \cdots\right] + \left(\frac{i\omega\mu_1}{\sigma_1}\right)^{\frac{1}{2}}. \tag{11}$$

The θ component of current density in the metal is according to (2).

$$J_\theta = \sigma(E_\theta + E_\theta') = \frac{1}{R}\frac{\partial}{\partial R}(RH_\phi), \tag{12}$$

[3] P. Debye, Ann. d. Physik **30**, 57 (1909).

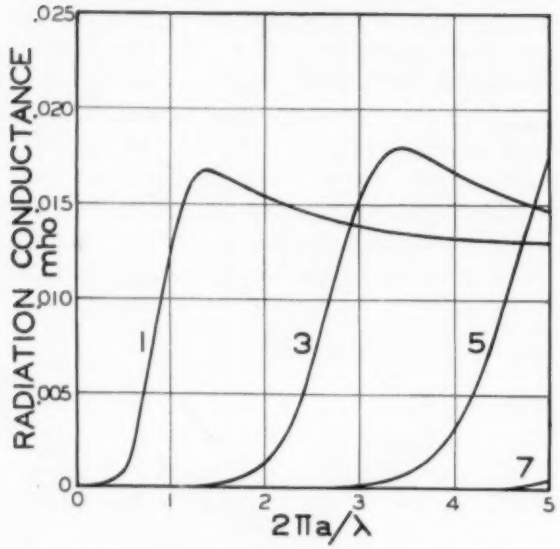

FIG. 1. Radiation conductance of first few modes as functions of $2\pi a/\lambda$.

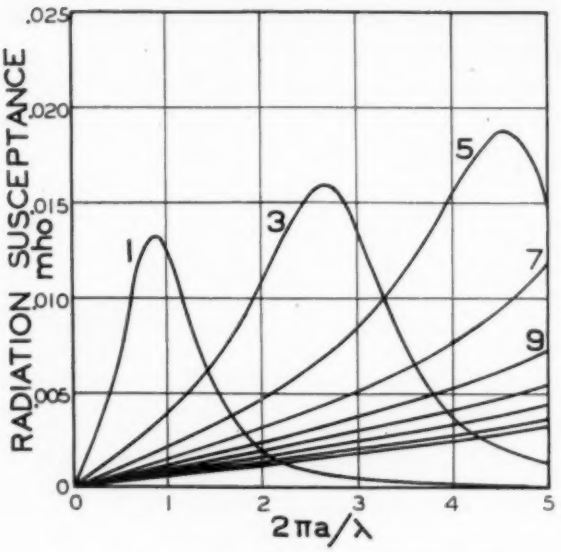

FIG. 2. Radiation susceptance of first few modes as functions of $2\pi a/\lambda$.

and hence the total current crossing the surface θ=constant is

$$I_\theta=\int_0^{2\pi}\int_0^a J_\theta R\sin\theta\,dR\,d\phi = 2\pi a\sin\theta\,H_\phi|_{R=a}. \quad (13)$$

This determines the current distribution on the sphere. In particular, the current crossing the equatorial plane $\theta=90°$ is

$$I_0=-2\pi a\,e^{i\omega t}(\omega\mu_1/i\sigma_1)^{\frac{1}{2}}\sum_{n=1}^{\infty}\frac{C_n(a)}{Z_n}P_n^1(0). \quad (14)$$

In passing, one sees that whatever the value of $\mathbf{E}'$ in the interior of the sphere, the resultant field $\mathbf{E}+\mathbf{E}'$, and therefore also the current density, vanish everywhere due to the high conductivity except within a thin layer at the surface. This skin effect is governed by the spherical Bessel functions of complex argument. Thus the assumption that $\nabla\times\mathbf{E}'=0$ is justified so long as $\mathbf{E}'$ is effective only within the thin layer at the surface.

In virtue of the assumption that $\mathbf{E}'$ is irrotational, one may write

$$\mathbf{E}'=-\nabla V, \quad (15)$$

where V is the potential, or voltage with respect to some reference plane. Consequently

$$E_\theta'=-(1/R)(\partial V/\partial\theta),\quad E_R'=-\partial V/\partial R. \quad (16)$$

This voltage is applied at the equator across a small strip or band of width $a\Delta\theta$ on the surface. On the surface of the sphere $E_R'=0$ and hence

$$E_\theta'=-\frac{V}{a\Delta\theta}\ \text{for}\ \frac{\pi-\Delta\theta}{2}<\theta<\frac{\pi+\Delta\theta}{2},$$
$$E_\theta'=0\qquad\text{for}\ \theta<\frac{\pi-\Delta\theta}{2}\ \text{or}\ \theta>\frac{\pi+\Delta\theta}{2}. \quad (17)$$

In virtue of the orthogonal properties of the $P_n^1(\cos\theta)$ the coefficients $C_n(a)$ are found to be

$$C_n(a)=-\left(\frac{i\sigma_1}{\omega\mu_1}\right)^{\frac{1}{2}}\frac{(2n+1)}{2a\,n(n+1)}P_n^1(0)\,Ve^{-i\omega t}, \quad (18)$$

where

$$P_n^1(0)=i^{n-1}2^{1-n}n!\Big/\left[\left(\frac{n-1}{2}\right)!\right]^2,$$

when n is odd, and $P_n^1(0)=0$ when n is even. Upon introducing this into (14) one is led to

$$I_0=\pi V\sum_n\frac{2n+1}{n(n+1)}\frac{[P_n^1(0)]^2}{Z_n} \quad (19)$$

while for the input admittance at $\theta=90°$ one obtains

$$Y_i=\frac{I_0}{V}=\pi\sum_n\frac{2n+1}{n(n+1)}\frac{[P_n^1(0)]^2}{Z_n}. \quad (20)$$

The input impedance Z_i is the reciprocal of Y_i. The summations are over odd values of n.

This expression for the input admittance obviously suggests for the equivalent circuit of the sphere an infinite system of parallel, resonating networks, the admittance Y_n of each branch being represented by one of the modes of the sphere, or

$$Y_n = \pi \frac{2n+1}{n(n+1)} \frac{[P_n^1(0)]^2}{Z_n}. \qquad (21)$$

The real and imaginary parts are respectively conductance g_n and susceptance b_n. If one assumes the conductivity of the sphere to be infinite, the admittance Y_n reduces to a pure conductance as $k_2 a \to \infty$, and contains only susceptance when $k_2 a < n$. For intermediate values of $k_2 a$ the admittance is complex.

In Figs. 1 and 2 the real and imaginary parts of the admittance Y_n are plotted as functions of $2\pi a/\lambda$. The conductivity of the sphere is assumed infinite. Since there is then no loss in the metal, the ordinates represent radiation conductance and radiation susceptance. The conductance associated with each mode or harmonic term rises to a peak at resonance, then drops off gradually to a constant value. The total conductance rises step-wise with increasing a/λ as shown in Fig. 4. Thus as the applied frequency is increased the harmonic terms add their contributions successively, each new term giving rise to a corresponding increase in the radiation. Inversely, for a fixed wave-length an increase in the radius of the sphere increases its effectiveness as a radiator.

From Fig. 2 it appears that the radiation susceptance of each successive harmonic rises to a maximum near resonance and then falls rapidly to zero as the wave-length decreases. The susceptance is always positive, showing that the admittance is capacitive. It is evident from the figure that the sum of the susceptances fails to approach a limit. The ratio Y_n/Y_{n-2} in fact approaches unity as $n \to \infty$. This is a consequence of our assumption that the impressed voltage is applied across a surface of discontinuity at $\theta = \pi/2$, a singularity implying an infinite value of field intensity. Actually the voltage will be applied across a strip or gap of small but finite width, with a corresponding decrease in the magnitudes of the higher order harmonics. The general form of the conductance and susceptance curves will not be materially altered, but their sum then converges, as it obviously must on physical grounds. In this case the susceptance of each harmonic is small except in the neighborhood of its own resonance point. The total input susceptance will vary only slightly with the ratio a/λ as compared with the total input conductance. Since the susceptance of each harmonic term is always positive, under no condition will the input admittance, or the input impedance become a real quantity.

It is apparent that the resonance phenomena associated with a radiating sphere differ fundamentally from those encountered in conventional circuit theory. In this connection it will prove interesting in a following paper to observe the transition of resonance curves from the case of a linear oscillator represented by a prolate spheroid of unit eccentricity to that of a sphere of zero eccentricity.

Figure 3 illustrates the amplitudes, or absolute values, of the first few admittances.

The power input into the system is equal to one-half the product of the applied voltage and the conjugate of the current at the driving point.

$$P_i = \frac{1}{2} V I_0^* = \frac{\pi}{2} |V|^2 \sum_n \frac{2n+1}{n(n+1)} \frac{[P_n^1(0)]^2}{Z_n^*}. \qquad (22)$$

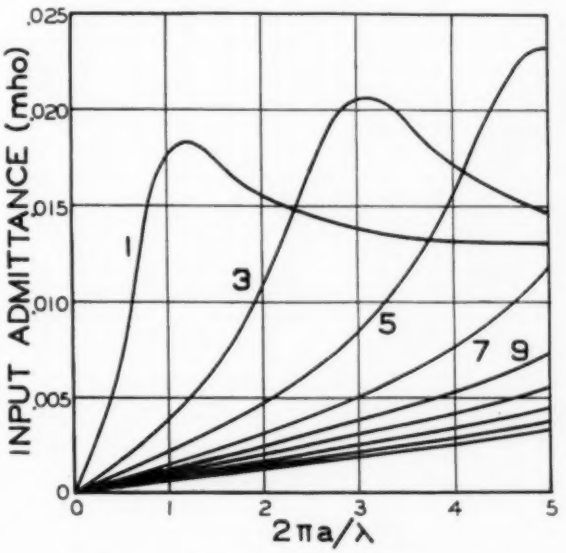

FIG. 3. Input admittance of first few modes as functions of $2\pi a/\lambda$.

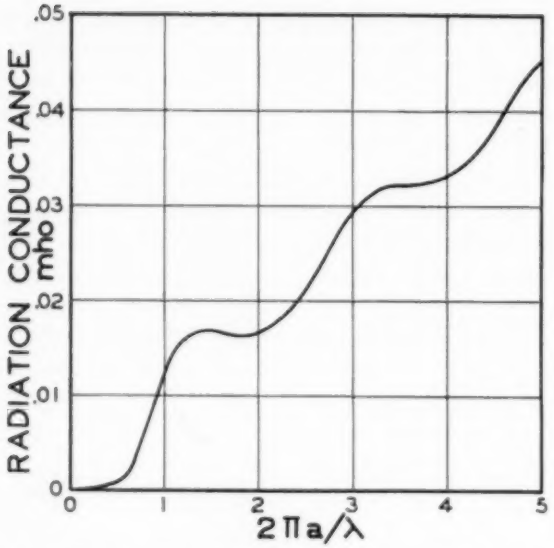

FIG. 4. Total radiation conductance as function of $2\pi a/\lambda$.

Upon rationalizing Z_n^* in the denominator one obtains

$$P_i=\frac{\pi}{2}|V|^2\sum_n\frac{2n+1}{n(n+1)}\frac{[P_n^1(0)]^2}{|Z_n|^2}\times\left\{i\left(\frac{\mu_2}{\epsilon_2}\right)^{\frac{1}{2}}\left[\frac{h_{n-1}^{(2)}(k_2a)}{h_n^{(2)}(k_2a)}-\frac{n}{k_2a}\right]+\left(\frac{i\omega\mu_1}{\sigma_1}\right)^{\frac{1}{2}}\right\}. \quad (23)$$

The real part of P_i must equal the sum of the power radiated from the system and that dissipated in the conductor. The radiated power P_r is given by the integral of the radial component of the Poynting vector over a sphere of radius greater than a and concentric with the conductor.

$$P_r=\tfrac{1}{2}\int_0^{2\pi}d\phi\int_0^{\pi}E_\theta H_\phi^* R^2\sin\theta\,d\theta$$

$$=i\left(\frac{\mu_2}{\epsilon_2}\right)^{\frac{1}{2}}\frac{\pi R^2}{2a^2}|V|^2\sum_n\frac{2n+1}{n(n+1)}\frac{[P_n^1(0)]^2}{|h_n^{(2)}(k_2a)Z_n|^2}\times h_n^{(1)}(k_2R)\left[h_{n-1}^{(2)}(k_2R)-\frac{n}{k_2R}h_n^{(2)}(k_2R)\right]. \quad (24)$$

Since

$$|h_n^{(2)}(k_2a)|^2=h_n^{(1)}(k_2a)\,h_n^{(2)}(k_2a)$$

on the surface of the sphere ($R=a$), we have

$$P_r=i\frac{\pi}{2}\left(\frac{\mu_2}{\epsilon_2}\right)^{\frac{1}{2}}|V|^2\sum_n\frac{2n+1}{n(n+1)}\frac{[P_n^1(0)]^2}{|Z_n|^2}\times\left[\frac{h_{n-1}^{(2)}(k_2a)}{h_n^{(2)}(k_2a)}-\frac{n}{k_2a}\right]. \quad (25)$$

The power dissipated as heat in the metallic conductor is evidently

$$P_d=P_i-P_r=(1+i)\frac{\pi}{2}(\omega\mu_1/2\sigma_1)^{\frac{1}{2}}|V|^2\times\sum_n\frac{2n+1}{n(n+1)}\frac{[P_n^1(0)]^2}{|Z_n|^2}. \quad (26)$$

One will note that as the conductivity becomes infinite, not only does the real part of the input power P_i equal that of the radiated power P_r, but also the imaginary parts are equal to each other, the wattless component of P_r being measured at the surface of the conductor. The real part of P_r, from which one finds immediately the radiation resistance is

$$Re[P_r]=\frac{\pi}{2}(\epsilon_2/\mu_2)^{\frac{1}{2}}|V|^2\times\sum_n\frac{2n+1}{n(n+1)}\frac{[P_n^1(0)]^2}{|[k_2a\,h_n^{(2)}(k_2a)]'|^2}\text{ watts}, \quad (27)$$

the prime in the denominator indicating differentiation with respect to the argument k_2a. It can be shown that

$$Y_i^*=2P_i/V^2. \quad (28)$$

That is, when a unit r.m.s. voltage is applied to the system, the power input is equal to the conjugate of the input admittance, as illustrated in Figs. 1, 2, and 4.

Steady-State Solutions of Electromagnetic Field Problems

III. Forced Oscillations of a Prolate Spheroid

L. J. Chu and J. A. Stratton
Massachusetts Institute of Technology, Cambridge, Massachusetts
(Received December 9, 1940)

The method discussed in Parts I and II for the determination of steady-state solutions of electromagnetic problems is applied to a prolate conducting spheroid. An external e.m.f. is applied across the central section of the spheroid and the resultant field is represented as an infinite sum of wave modes expressed in terms of spheroidal functions. To each mode there corresponds a definite resonant frequency. As the applied frequency passes through the resonance point of a given mode, the corresponding term in the driving-point admittance changes from capacitive through a pure conductance to inductive. The sharpness of resonance increases with the eccentricity. Curves are drawn showing the behavior of the real and imaginary parts of the admittance for several values of eccentricity. The solution goes over, in the limit of zero eccentricity, to that discussed in II. When the eccentricity approaches unity one obtains a linear antenna of finite length and the driving-point impedance at the resonance frequency of the first mode is shown to be about 72 ohms.

IN Part I of this investigation[1] we have discussed the generation of waves in an infinite straight conductor, while Part II[2] dealt with the forced oscillations of a sphere and the relation of radiation conductance and susceptance to the nature of the applied e.m.f. Although these examples give a clear insight into the general problem of forced oscillations, they are otherwise of no great technical importance. By the same method, however, we shall treat now the forced oscillations of a prolate spheroid, a problem of somewhat greater mathematical complexity but having a direct bearing on the operation of linear antennas, since a prolate spheroid reduces to a line of finite length as the eccentricity approaches unity. Furthermore, since the case of the sphere is obtained by allowing the eccentricity to become zero, one may follow the transition from the linear to a spherical configuration and the effect of increasing the central cross section on the radiation impedance.

The free oscillations of a prolate spheroid were first studied in detail by Maclaurin[3] and by Abraham,[4] and much work has been reported since then on the orthogonal solutions of the wave equation in spheroidal coordinates. Several spheroidal functions have recently been investigated by Stratton[5] in an effort to establish relations between the angular and radial functions defined as series of Gegenbauer and Bessel functions, respectively. This work has been extended by the present authors and the results reduced to a form suitable for practical application.[6] The formulas obtained are the basis of the present paper. The free oscillations of a spheroid have lately been discussed by Page and Adams,[7] who consider also a problem of forced oscillations. The driving field in their case is a homogeneous plane wave of length very much greater than the smaller dimension of the spheroid. A closer approach to the problem considered here has been made by Ryder,[8] based on the work of Page and Adams. The primary advantage of the functions which we shall employ in the following lies in the fact that they have been appropriately defined for every part of the domain of the independent variable and all analytic connections are specified. Convergence difficulties are thus largely circumvented and the

[1] J. A. Stratton and L. J. Chu, J. App. Phys. **12**, 230 (1941).
[2] J. A. Stratton and L. J. Chu, J. App. Phys. **12**, 236 (1941).
[3] R. C. Maclaurin, Camb. Phil. Trans. **17**, 33 (1898).
[4] M. Abraham, Ann. d. Physik **66**, 435 (1898); **2**, 32 (1900).
[5] J. A. Stratton, Proc. Nat. Acad. Sci. **21**, 51–56 (1935); **21**, 317–321 (1935).
[6] L. J. Chu and J. A. Stratton, J. Math. Phys. To be published.
[7] L. Page and N. I. Adams, Phys. Rev. **53**, 819 (1938).
[8] R. M. Ryder, thesis, Yale University (1940).

numerical discussion need not be confined to eccentricities near unity or zero.

Let the foci of a family of confocal spheroids be located on the z axis at the points $\pm f$. A right-hand system of spheroidal coordinates ξ, η, ϕ is defined in terms of the cylindrical system r, ϕ, z by

$$r=f[(\xi^2-1)(1-\eta^2)]^{\frac{1}{2}}, \quad \phi=\phi, \quad z=f\xi\eta, \quad (1)$$

where $\xi\geqq 1$, $-1\leqq\eta\leqq 1$, $0\leqq\phi\leqq 2\pi$. They are related also to the spherical coordinates R, $\cos\theta$, ϕ by

$$R=f(\xi^2+\eta^2-1)^{\frac{1}{2}},$$
$$\cos\theta=\xi\eta/(\xi^2+\eta^2-1)^{\frac{1}{2}}, \quad \phi=\phi. \quad (2)$$

As $\xi\to\infty$ the spheroid goes over to a sphere such that

$$R\to f\xi, \quad \cos\theta\to\eta. \quad (3)$$

Therefore ξ is often called the radial, and η the angular variable. If $\mathbf{i}_\xi$, $\mathbf{i}_\eta$, $\mathbf{i}_\phi$ are unit vectors in the direction of ξ, η, ϕ, respectively, then

$$\nabla\xi=\mathbf{i}_\xi/h_\xi, \quad \nabla\eta=\mathbf{i}_\eta/h_\eta, \quad \nabla\phi=\mathbf{i}_\phi/h_\phi, \quad (4)$$

and the metrical coefficients are

$$h_\xi=f\left(\frac{\xi^2-\eta^2}{\xi^2-1}\right)^{\frac{1}{2}}, \quad h_\eta=f\left(\frac{\xi^2-\eta^2}{1-\eta^2}\right)^{\frac{1}{2}},$$
$$h_\phi=f[(\xi^2-1)(1-\eta^2)]^{\frac{1}{2}}. \quad (5)$$

We shall consider a prolate spheroid of infinite conductivity embedded in a homogeneous perfect dielectric medium. It will be assumed that the applied electric field intensity is circularly symmetric about the major axis and linearly polarized in a direction parallel to this axis. All components of the field vary with the time as $\exp(i\omega t)$. Then the Maxwell equations for the field in the external dielectric (ϵ_2, μ_2; $\sigma_2=0$) are

$$i\omega\epsilon_2 E_\xi=\frac{1}{h_\eta h_\phi}\frac{\partial}{\partial\eta}(h_\phi H_\phi),$$
$$i\omega\epsilon_2 E_\eta=\frac{-1}{h_\phi h_\xi}\frac{\partial}{\partial\xi}(h_\phi H_\phi), \quad (6)$$
$$i\omega\mu_2 H_\phi=\frac{1}{h_\xi h_\eta}\left[\frac{\partial(h_\xi E_\xi)}{\partial\eta}-\frac{\partial(h_\eta E_\eta)}{\partial\xi}\right].$$

Upon eliminating E_ξ and E_η one obtains for H_ϕ the equation

$$(\xi^2-1)\frac{\partial^2}{\partial\xi^2}\left(\frac{H_\phi}{h_\phi}\right)+(1-\eta^2)\frac{\partial^2}{\partial\eta^2}\left(\frac{H_\phi}{h_\phi}\right)$$
$$+4\xi\frac{\partial}{\partial\xi}\left(\frac{H_\phi}{h_\phi}\right)-4\eta\frac{\partial}{\partial\eta}\left(\frac{H_\phi}{h_\phi}\right)$$
$$+f^2k_2^2(\xi^2-\eta^2)\frac{H_\phi}{h_\phi}=0, \quad (7)$$

where $k_2=\omega(\epsilon_2\mu_2)^{\frac{1}{2}}$. Let

$$H_\phi=h_\phi U(\xi)V(\eta)e^{i\omega t}. \quad (8)$$

Equation (7) is separable and leads to

$$(1-\xi^2)U''-4\xi U'+(b_l-f^2k^2\xi^2)U=0 \quad (9)$$

and an identical equation for $V(\eta)$, where b_l is one of a set of separation constants chosen such that H_ϕ remains finite at the poles $\eta=\pm 1$. It appears that both U and V satisfy the general equation

$$(1-z^2)W''-2(a+1)zW'+(b-c^2z^2)W=0 \quad (10)$$

for the special case $a=1$, $c=fk_2$. The angular function $V(\eta)$ will be represented by the spheroidal function of the first kind $Se^1_{1,l}(fk_2,\eta)$ defined as

$$Se^1_{1,l}(fk_2,\eta)=(\eta^2-1)^{-1}\sum_n{}' a_n i^{n-l}T^{-1}_{n+2}(\eta), \quad (11)$$

where

$$T^{-1}_{n+2}(\eta)=(\eta^2-1)^{\frac{1}{2}}\frac{n!}{(n+2)!}P^1_{n+1}(\eta), \quad (12)$$

the P^1_{n+1} are associated Legendre functions as defined by Hobson.[9] and the prime over the summation sign indicates that n has the values $n=0, 2, 4, \cdots$ if l is an even integer, and $n=1, 3, 5\cdots$ if l is odd. The function

$$Se^1_{1,l}\to(\eta^2-1)^{-\frac{1}{2}}P^1_{l+1}(\eta)$$

as $fk_2\to 0$, i.e., as the spheroid degenerates into a sphere. At large distances from the center the field must reduce to a wave traveling radially outward. To insure the proper behavior as $\xi\to\infty$, we choose for $U(\xi)$ the radial spheroidal function of the fourth kind.

$$Re^4_{1,l}(fk_2,\xi)$$
$$=\frac{1}{fk_2\xi\sum_n{}' a_n i^{n-l}}\sum_n{}' a_n h^{(2)}_{n+1}(fk_2\xi), \quad (13)$$

[9] E. W. Hobson, *Theory of Spherical and Ellipsoidal Harmonics* (Cambridge University Press, 1931).

where $h^{(2)}_{n+1}$ is the spherical Hankel function defined by

$$h^{(2)}_{n+1}(fk_2\xi)=(\pi/2fk_2\xi)^{\frac{1}{2}}H^{(2)}_{n+3/2}(fk_2\xi), \quad (14)$$

and $H^{(2)}_{n+3/2}$ is the ordinary, or cylindrical, Hankel function of half-order. This construction of the angular and radial functions $Se^{1}_{1,l}$ and $Re^{4}_{1,l}$ employs the same set of coefficients a_n and simplifies the computation accordingly. As $fk_2\xi\to\infty$ we find that

$$Re^{4}_{1,l}(fk_2,\xi)\to-\frac{1}{(fk_2\xi)^2}e^{-i(fk_2\xi-l\pi/2)},$$

while at the singular points $\xi=\pm1$ the function has poles of the first order. Thus the series representation (13) of the function $Re^{4}_{1,l}$ diverges on and within a circle in the ξ plane of unit radius about the origin. However $Re^{4}_{1,l}$ may be replaced by $Se^{4}_{1,l}$, a different representation of one and the same function which converges in the neighborhood of $\xi=\pm1$. The function $Se^{4}_{1,l}$ is a linear combination of the two independent solutions $Se^{1}_{1,l}$ and $Se^{2}_{1,l}$, where $Se^{2}_{1,l}$ is obtained by replacing the P^{1}_{n+1} in $Se^{1}_{1,l}$ by the associated Legendre functions Q^{1}_{n+1} of the second kind.[6] But, Q^{1}_{n+1} contains a factor that becomes infinite when n is a negative integer <-2. Consequently the series does not break off on the lower side at $n=0$ or $n=1$ as in the case of $Se^{1}_{1,l}$: *the summation of the $Se^{2}_{1,l}$ series extends from negative infinity to positive infinity, over all even or all odd values of n as l is even or odd.*

The complete steady-state solution is, therefore,

$$H_\phi=\sum_l A_l h_\phi U(\xi)V(\eta)e^{i\omega t}$$
$$=f[(\xi^2-1)(1-\eta^2)]^{\frac{1}{2}}e^{i\omega t}\times\sum_{l=0}^{\infty}A_l Re_l^{4}(\xi)Se_l^{1}(\eta), \quad (15)$$

$$E_\xi=\frac{1}{i\omega\epsilon_2}\left(\frac{\xi^2-1}{\xi^2-\eta^2}\right)^{\frac{1}{2}}e^{i\omega t}\times\sum_{l=0}^{\infty}A_l Re_l^{4}(\xi)\frac{d}{d\eta}[(1-\eta^2)Se_l^{1}(\eta)], \quad (16)$$

$$E_\eta=-\frac{1}{i\omega\epsilon_2}\left(\frac{1-\eta^2}{\xi^2-\eta^2}\right)^{\frac{1}{2}}e^{i\omega t}\times\sum_{l=0}^{\infty}A_l Se_l^{1}(\eta)\frac{d}{d\xi}[(\xi^2-1)Re_l^{4}(\xi)], \quad (17)$$

where $Re^{4}_{1,l}(fk_2,\xi)$ and $Se^{1}_{1,l}(fk_2,\eta)$ have been abbreviated to $Re_l^{4}(\xi)$ and $Se_l^{1}(\eta)$, respectively. The coefficients A_l are to be determined by the distribution of applied e.m.f.

We now apply to a perfectly conducting spheroid of eccentricity $1/\xi_0$ an electric field $\mathbf{E}'$ that is independent of ϕ. The nature of this field need not be otherwise restricted. It may be the radiation field of a distant source whose wave-length is large relative to the dimensions of the spheroid. In such a case (15)–(17) above constitute the reflected wave.[7] It may also be the field appearing near the terminals of a transmission line. In this case, a small section of the metallic spheroid is to be replaced by dielectric and the inner terminal faces of the metal are connected to the line as shown in Fig. 1. It is clear that the current from one terminal of the split spheroid will pass into one conductor of the transmission line, through the oscillator, and back to the other terminal of the spheroid. If the system is electrically balanced the current passing out of the one terminal must equal that entering the other, and the voltage or potential difference across the gap must equal that across the terminals of the line. The transmission line, therefore, serves the purpose of providing a metallic link to the split spheroid and applying a voltage across the gap. Neglecting distortion of the field caused by the presence of the line, we replace the line and source by a conductor short-circuiting the gap to insure continuity of current, and assume that a voltage equaling that across the terminals of the transmission line is applied over this short-circuiting link. The altered or equivalent system thus contains a complete spheroid with an external field intensity applied symmetrically over the surface of a short segment. The relation between current and voltage across this inserted segment is identical with that at the terminals of the line. This argument applies equally well to the case of a cylindrical conductor and that of a sphere, although in the latter case the cross-sectional dimensions are of the order of the wave-length

and the line must be designed such as to produce a circularly symmetric field.

Since the conductivity has been assumed infinite the current within the spheroid must vanish. This implies that the sum of the applied field $\mathbf{E}'$ and the induced field $\mathbf{E}$ is zero. Since the transition of tangential components of $\mathbf{E}$ across a boundary is continuous, it follows that

$$E_\eta + E_\eta' = 0 \text{ at } \xi = \xi_0, \tag{18}$$

where E_η is the field in the dielectric and given by (17). Let the applied field on the surface of the spheroid be expanded in the series

$$E_\eta' = -\frac{1}{i\omega\epsilon_2}\left[\frac{1-\eta^2}{\xi_0^2-\eta^2}\right]^{\frac{1}{2}} \sum_l B_l Se_l^1(\eta). \tag{19}$$

From the boundary condition (18) one obtains

$$A_l = -\frac{B_l}{(d/d\xi_0)[(\xi_0^2-1)Re_l^4(\xi_0)]}. \tag{20}$$

To give a numerical illustration we shall assume a concentrated voltage V applied across an infinitesimal segment of length $h_\eta \Delta\eta$ at the equator $\eta = 0$. Then

$$\begin{aligned} E_\eta' &= -V/h_\eta\Delta\eta \text{ when } |\eta| < \Delta\eta/2, \\ E_\eta' &= 0 \qquad\quad \text{when } |\eta| > \Delta\eta/2. \end{aligned} \tag{21}$$

From (19) and (20), and the orthogonal properties of the $Se_l^1(\eta)$, we find

$$B_l = (i\omega\epsilon_2 V/f)(Se_l^1(0)/N_l), \tag{22}$$

$$A_l = \frac{-i\omega\epsilon_2 V}{f} \frac{Se_l^1(0)}{N_l(d/d\xi_0)[(\xi_0^2-1)Re_l^4(\xi_0)]}, \tag{23}$$

where the normalizing factor is

$$\begin{aligned} N_l &= \int_{-1}^{+1} (1-\eta^2)[Se_l^1(\eta)]^2 d\eta \\ &= 2\sum_n' \frac{a_n^2}{(n+1)(n+2)(2n+3)}. \end{aligned} \tag{24}$$

B_l and A_l are zero for odd values of l since $Se_l^1(0) = 0$ if l is odd.

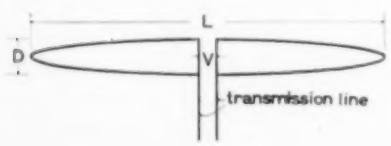

FIG. 1. Spheroidal antenna.

The field in the dielectric is now completely determined. At large distances from the spheroid the asymptotic expression for $Re_l^4(\xi)$ leads to

$$H_\phi \backsimeq (\epsilon_2/\mu_2)^{\frac{1}{2}} E_\eta \backsimeq -(1/f\xi k_2^2) e^{i(\omega t - k_2 f\xi)} \times \sum_l i^l A_l Se_l^1(\eta), \tag{25}$$

in which $l = 0, 2, 4 \cdots$. The distance from the center to the point of observation approaches $f\xi$. The radiation pattern is determined by the sum of angular functions.

It is of greater interest to learn how the power input of the system is distributed among the various "space harmonics," or modes, characterized by the index l, and the relation between the applied voltage and the current of the system. The surface current density J_η on the spheroid is equal in magnitude to H_ϕ at the surface, or $J_\eta = H_\phi|_{\xi=\xi_0}$. The total current crossing a parallel of latitude on the spheroid in the η direction, i.e., from south to north, is

$$\begin{aligned} I_\eta &= \int_0^{2\pi} J_\eta h_\phi d\phi = 2\pi f[(\xi_0^2-1)(1-\eta^2)]^{\frac{1}{2}} H_\phi|_{\xi=\xi_0} \\ &= 2\pi f^2(\xi_0^2-1)(1-\eta^2) \sum_l A_l Re_l^4(\xi_0) Se_l^1(\eta). \end{aligned} \tag{26}$$

Across the equator, where the voltage is applied, the current is

$$I_0 = -\frac{ik_2 f}{60} V \times \sum_{l=0}' \frac{(\xi_0^2-1)Re_l^4(\xi_0)[Se_l^1(0)]^2}{(d/d\xi_0)[(\xi_0^2-1)Re_l^4(\xi_0)]N_l} \text{ amperes}, \tag{27}$$

since $2\pi\omega\epsilon_2 = 2\pi(\epsilon_2/\mu_2)^{\frac{1}{2}}\omega(\epsilon_2\mu_2)^{\frac{1}{2}} = k_2/60$ in rationalized m.k.s. units. If one assumes the current uniform over the strip $h_\eta\Delta\eta$ at the equator the input admittance is

$$Y_i = \frac{I_0}{V} = \frac{-ik_2 f}{60} \times \sum_{l=0}' \frac{(\xi_0^2-1)Re_l^4(\xi_0)[Se_l^1(0)]^2}{(d/d\xi_0)[(\xi_0^2-1)Re_l^4(\xi_0)]N_l} \text{ mho}. \tag{28}$$

The reciprocal of this quantity is the input admittance $Z_i = 1/Y_i$.

The expression for Y_i suggests at once, as in the case of the sphere, an equivalent system composed of an infinite number of circuits con-

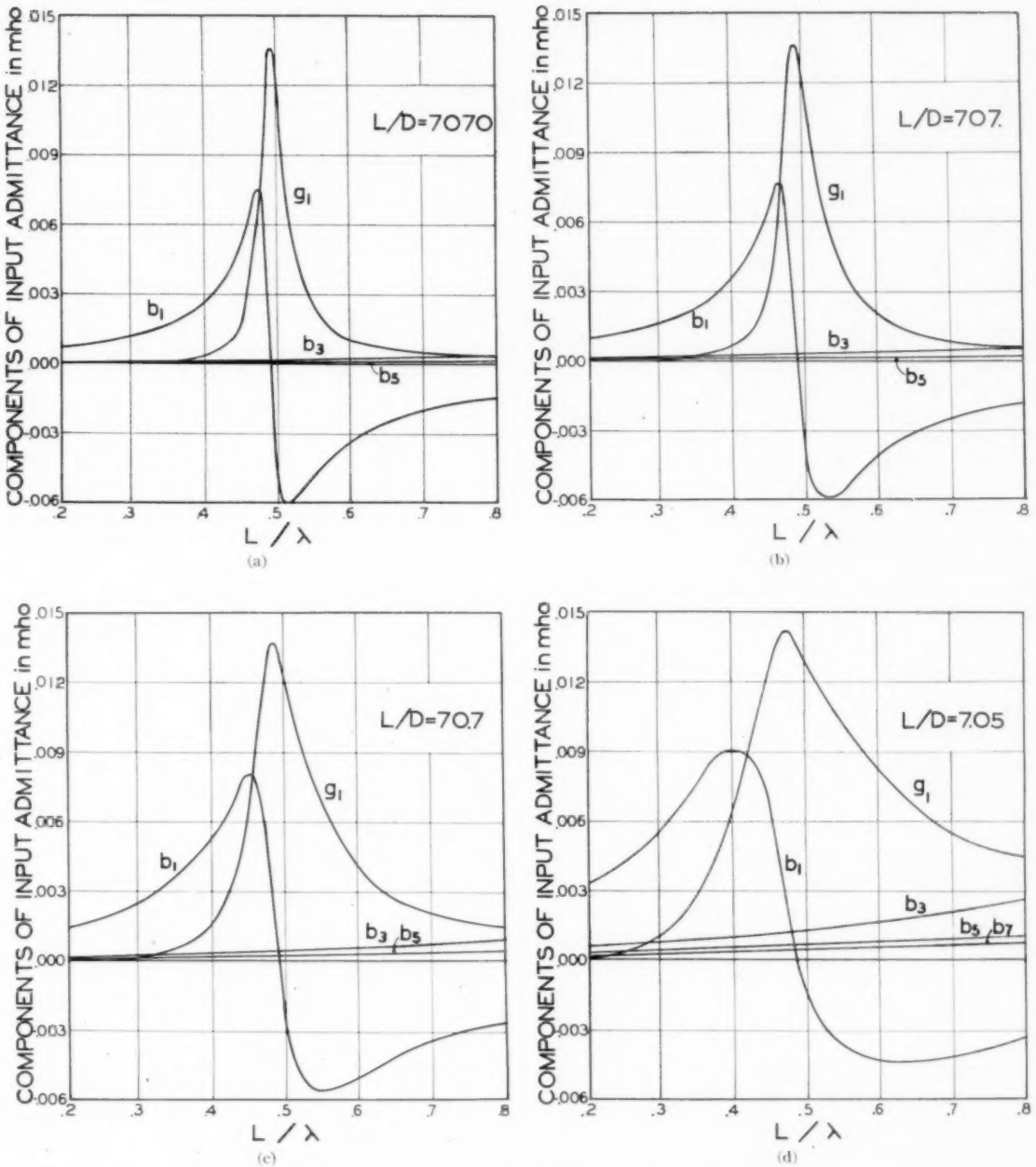

FIG. 2. Components of input admittance as functions of L/λ.

nected in parallel to whose common terminals the voltage V is applied. Each component circuit represents one of the infinite sequence of wave modes. Consistent with the spherical case we shall define the admittance of the $(l+1)$th mode as

$$Y_{l+1}=-\frac{ik_2 f}{60}\frac{(\xi_0^2-1)Re_l^4(\xi_0)[Se_l^1(0)]^2}{(d/d\xi_0)[(\xi_0^2-1)Re_l^4(\xi_0)]N_l}. \quad (29)$$

The total input admittance Y_i is obtained by summing the Y_{l+1} over even values of l. The real part of an admittance component Y_{l+1} is the conductance g_{l+1}, while the imaginary part is the susceptance b_{l+1}.

In Fig. 2 the components of input admittance are plotted *versus* L/λ for a series of values of the ratio L/D, where L is the length of the major

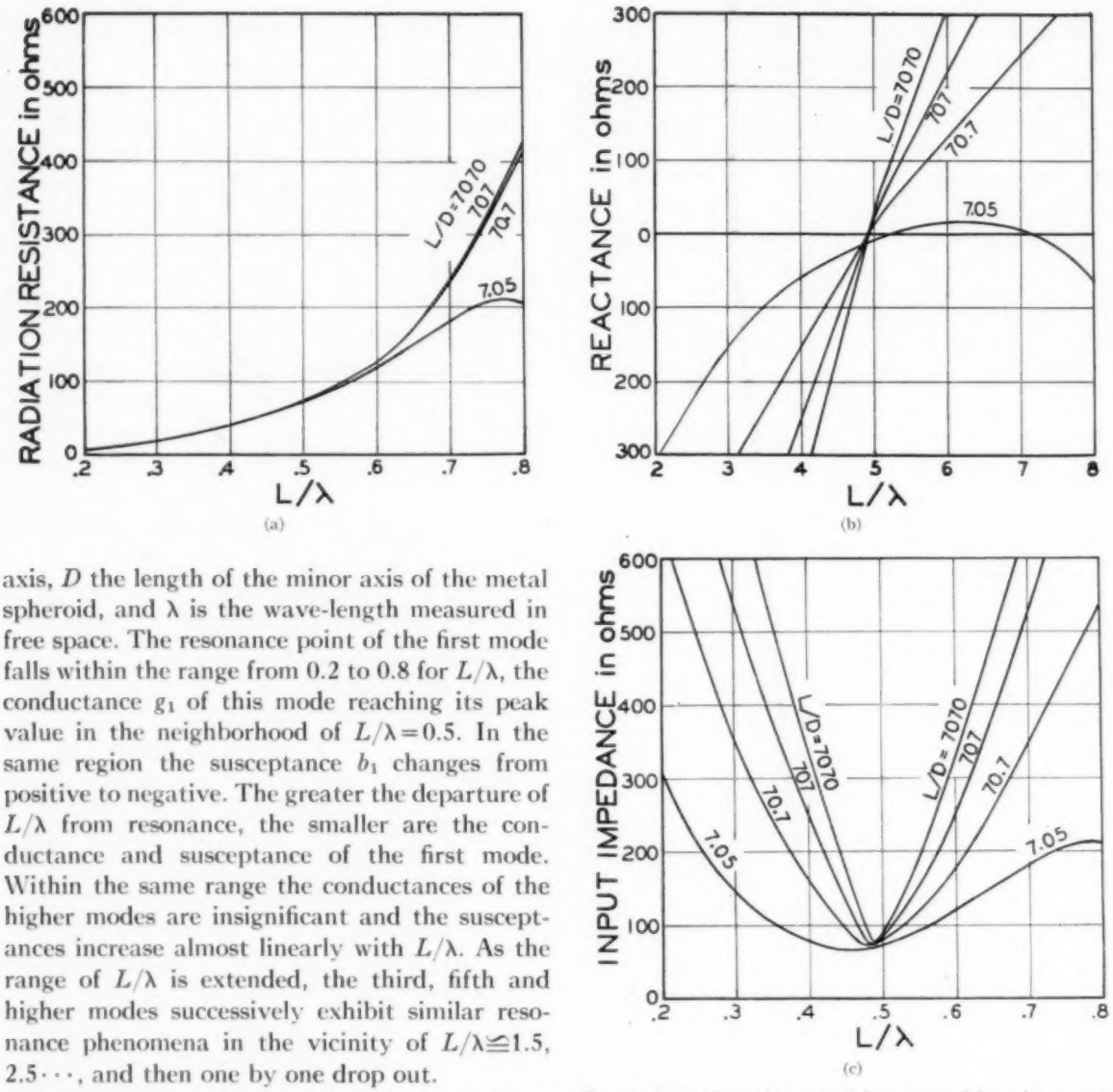

FIG. 3. Input impedance and its real and imaginary parts as functions of L/λ.

axis, D the length of the minor axis of the metal spheroid, and λ is the wave-length measured in free space. The resonance point of the first mode falls within the range from 0.2 to 0.8 for L/λ, the conductance g_1 of this mode reaching its peak value in the neighborhood of $L/\lambda=0.5$. In the same region the susceptance b_1 changes from positive to negative. The greater the departure of L/λ from resonance, the smaller are the conductance and susceptance of the first mode. Within the same range the conductances of the higher modes are insignificant and the susceptances increase almost linearly with L/λ. As the range of L/λ is extended, the third, fifth and higher modes successively exhibit similar resonance phenomena in the vicinity of $L/\lambda \leqq 1.5, 2.5\cdots$, and then one by one drop out.

A decrease in the eccentricity from unity to zero changes the shape of the spheroid from that of a thin wire of finite length to that of a sphere. Numerically the ratio L/D is equal to $\xi_0/(\xi_0^2-1)^{\frac{1}{2}}$, where ξ_0 is the reciprocal of the eccentricity. At large eccentricities, say for $L/D=7070$ (Fig. 2(a)), the conductance g_1 and susceptance b_1 of the first mode are sharply resonant. As the ratio L/D is diminished, the curves broaden at the peak while at the same time the susceptances of higher modes are augmented in magnitude. When $L/D=7.05$, (Fig. 2(d)), the conductance g_1 tends asymptotically to a limiting value comparable in magnitude with the resonance value as L/λ increases. This step-like increase in conductance is most striking in the limiting case of a sphere, $L/D=1$, discussed in II. Summarizing briefly, it appears that for a thin wire each wave mode dominates only at or near its resonant frequency, while for a sphere the equivalent parallel branch circuit corresponding to each mode acts essentially as a capacitance when the frequency is below the resonant value and as a resistance when the frequency is above this value.

It should be remarked here that the present example is not wholly satisfactory, since the

series of input admittance terms fails to converge. For large values of l the ratio of consecutive terms Y_{l+1}/Y_{l-1} is always less than one but approaches unity as a limit as $l \to \infty$. The same situation was encountered in the spherical case. This difficulty is no fault of the mathematical formulation of the problem but results from our assumption that the voltage is applied across a segment of vanishing length, implying in turn an infinite field intensity and infinite current density at the point of application. Actually there is always a finite separation between the terminals, and the length of this segment evidently bears an important relationship to the performance of the spheroid. A review of the properties of the angular spheroidal functions and the process of computing the A_l shows that an increase in the length of the segment across which V is applied will result in a considerable decrease in the magnitude of the coefficients A_l for large values of l, and an inappreciable change for the lower modes. Thus the curves plotted in Fig. 2 are not far wrong if we ignore the contributions of higher modes. On this basis the real and imaginary parts and absolute magnitude of the input impedance have been plotted in Fig. 3. The real part, or radiation resistance, is zero at $L/\lambda=0$ and reaches the value 72 ohms when L/λ is slightly less than one-half. This is in accord with the result obtained by calculating the radiation from the retarded potentials, assuming a sinusoidal current distribution. The fact that this value occurs at a point slightly below $L/\lambda=0.5$ shows the effect of a finite thickness of wire and of a current distribution that deviates slightly from the sinusoidal.

The radiation resistance attains a maximum somewhat below $L/\lambda=1$, and passes through subsequent minima near $L/\lambda=1.5$, 2.5, etc., the resonance points of the third, fifth and higher modes. The behavior of the reactance curves is illustrated by Fig. 3(b), showing that they pass through zero near resonance, and again at higher values of L/λ, as one sees for the case $L/D=7.05$. The recurrence of zero reactance points is to be expected, for as the third mode starts to resonate at $L/\lambda=1.5$, the reactance has to pass from negative value to positive. As shown in the curve, the spheroid of $L/D=7$ has a very small reactance over a rather large range of L/λ. For large values of L/D there will be a sudden drop of reactance from large positive values to large negative values somewhere beyond the range of L/λ shown in Fig. 3(b). The input impedance curves (Fig. 3(c)) indicate that sharp resonance is associated with thin spheroids, and that the impedance at resonance is almost independent of the ratio L/D unless L/D is near unity.

Figure 4 shows the current distributions along a very thin spheroid. In this case the magnitudes of the third and higher modes are insignificant as demonstrated by Fig. 2(a) and 2(b). The abscissa η is directly proportional to the distance along the spheroid. At resonance $L/\lambda \leqq 0.5$ the distribution is sinusoidal, and the curve is sharper or flatter as L/λ is less or larger than one-half.

The power input into the spheroid, assuming that the voltage is applied across a very small distance, is one-half the product of the applied voltage and the conjugate of the current in the region where the voltage is applied. Thus

$$P_i = \tfrac{1}{2} V I_0^* = i \frac{k_2 f}{120} |V|^2 \times \sum_{l=0}^{\infty}{}' \frac{[Se_l^1(0)]^2(\xi_0^2-1)Re_l^3(\xi_0)}{N_l(d/d\xi_0)[(\xi_0^2-1)Re_l^3(\xi_0)]}, \quad (30)$$

where P_i is the input power, I_0^* indicates the conjugate of the quantity I_0 and $Re_l^3(\xi_0)$ is the radial spheroidal function of the third kind, which is the conjugate of $Re_l^4(\xi_0)$. Obviously

$$P_i = \tfrac{1}{2} |V|^2 Y_i^*, \quad (31)$$

and needs no further comment. The real part of P_i should equal the sum of the power dissipated in the metal and that radiated into space. There is no dissipation since the metal is assumed to

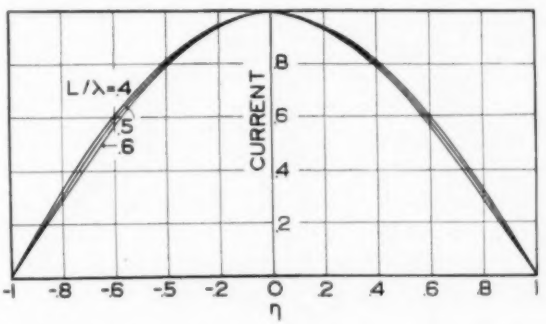

FIG. 4. Current distribution as function of η for thin spheroidal antenna.

have infinite conductivity. The power radiated into space is equal to the integral of the Poynting vector over a closed surface containing the metallic spheroid. If we choose for this surface a confocal spheroid of eccentricity $1/\xi$ then the radiated power P_r is

$$P_r = \tfrac{1}{2}\int_0^{2\pi} d\phi \int_{-1}^{1} d\eta\, h_\phi h_\eta E_\eta H_\phi^* = i\frac{k_2 f}{120}|V|^2 \sum_l{}' \frac{[Se_l'(0)]^2}{N_l} \times \frac{(\xi^2-1)Re_l^3(\xi)(d/d\xi)(\xi^2-1)Re_l^1(\xi)}{|(d/d\xi_0)[(\xi_0^2-1)Re_l^4(\xi_0)]|^2}. \quad (32)$$

It can be shown that the real part of P_r is equal to that of P_i by rationalizing the denominator of P_i and evaluating the Wronskian of

$$(\xi^2-1)Re_l^3(\xi)\frac{\partial}{\partial\xi}[(\xi^2-1)Re_l^4(\xi)].$$

Particularly at the surface of the conductor, $\xi=\xi_0$ and

$$P_r = P_i. \quad (33)$$

Thus we establish the theorem that the complex power input into the spheroid is equal to the complex radiated power at the surface of the spheroid.

We shall discuss later in another place the relation of these results to engineering formulas in current use for practical antenna design.

Relaxation of Metals at High Temperatures

W. E. Trumpler, Jr.
Westinghouse Electric and Manufacturing Company, South Philadelphia Works, Philadelphia, Pennsylvania

(Received November 25, 1940)

Much experimental work has been done on the creep of metals and the long-time creep test is the standard means of rating resistance to slow deformation of metals under tensile stress. In engineering practice, frequently, cases are found in which the total strain and not the stress remains constant. In what has become known as relaxation, an initially pure elastic strain gradually is transformed into a permanent strain while the length of the bar remains unchanged. Several years ago some new apparatus was designed and built primarily to duplicate the above conditions in connection with the study of bolt materials for steam turbines. The unusual accuracy and exceptionally good test results obtained from the automatic relaxation machine during more than two years of operation indicate that the type of test may well become a means of comparison as standard as a creep test and at a great reduction of testing time.

I. Introduction

INDUSTRY has become considerably interested, during the last fifteen years, in what happens to metals under stress at high temperatures. The effective limits to the increase in efficiency of steam turbines are partially set by the temperature at which the steels may be stressed without their "creeping" beyond the allowable amount for a period of years. Creep is the term used to describe the slow plastic deformation taking place in a material due to applied stress. This phenomenon is hardly noticeable in steels at room temperatures but becomes of serious magnitude in most of even the best alloy steels at the maximum operating temperatures of steam turbines (near 500°C). The creep test, which measures the deflection at constant stress, has become the standard method of rating resistance to slow deformations of metals under tensile stress. It is, however, a long-time test because the time normally required for accomplishing one is from three to six months.

In high temperature apparatus, frequently, parts are not subjected to constant load but to constant total strain; bolts are the most important example of this. Attempts to use creep data in estimating the relaxation which occurs have so far been unsuccessful. The relaxation machine was therefore built to supply this urgently needed information. The machine has

proved itself more than successful since it filled the direct need for design purposes, and now it can be shown that the results have further significance. The relaxation test is a short-time test since it normally requires only one week. From the large number of test results now available we conclude that one can obtain qualitative information in terms of creep—and possibly even quantitative information. More tests will be required before we can ascertain how accurately it will be possible to estimate the creep curve.

The relaxation phenomenon is exhibited when a material is stretched to, and subsequently held at, a given elongation. Creep then acts to elongate the bar and the release of load causing elastic shortening balances this effect. The total strain remains constant.

$$\epsilon' + \epsilon'' = \epsilon = \sigma_1 / E \tag{1}$$

$$\epsilon' = \sigma / E \text{ (Hooke's law)}$$

$$\frac{1}{E}\frac{d\sigma}{dt} + \frac{d\epsilon''}{dt} = 0. \tag{2}$$

ϵ'' = plastic strain, ϵ' = elastic strain, ϵ = total strain, σ = stress, σ_1 = initial stress, E = modulus of elasticity. The plastic elongation can be measured by the decrease in stress which is of a magnitude that can conveniently be observed.

In our own laboratory we previously experimented with a smaller relaxation machine which

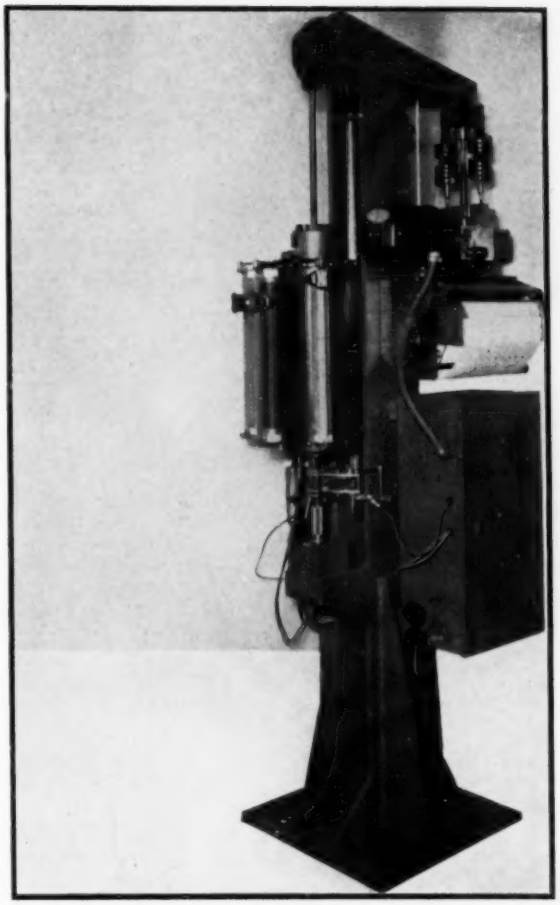

FIG. 2. Automatic relaxation machine.

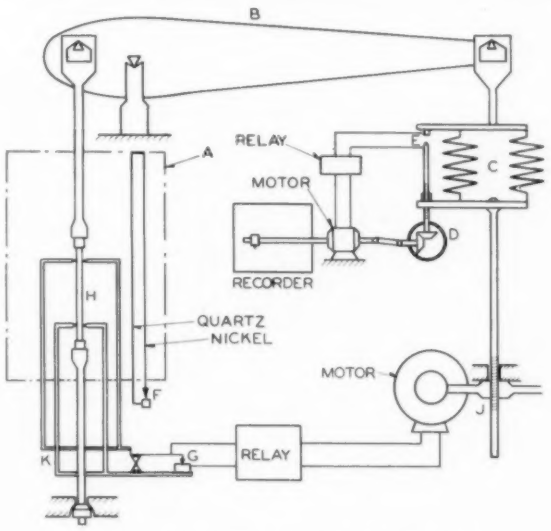

FIG. 1. Diagrammatic sketch of automatic relaxation machine.

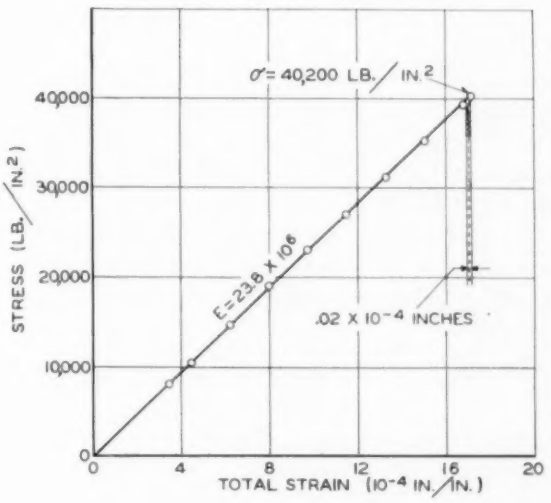

FIG. 3. Stress-strain diagram of relaxation test.

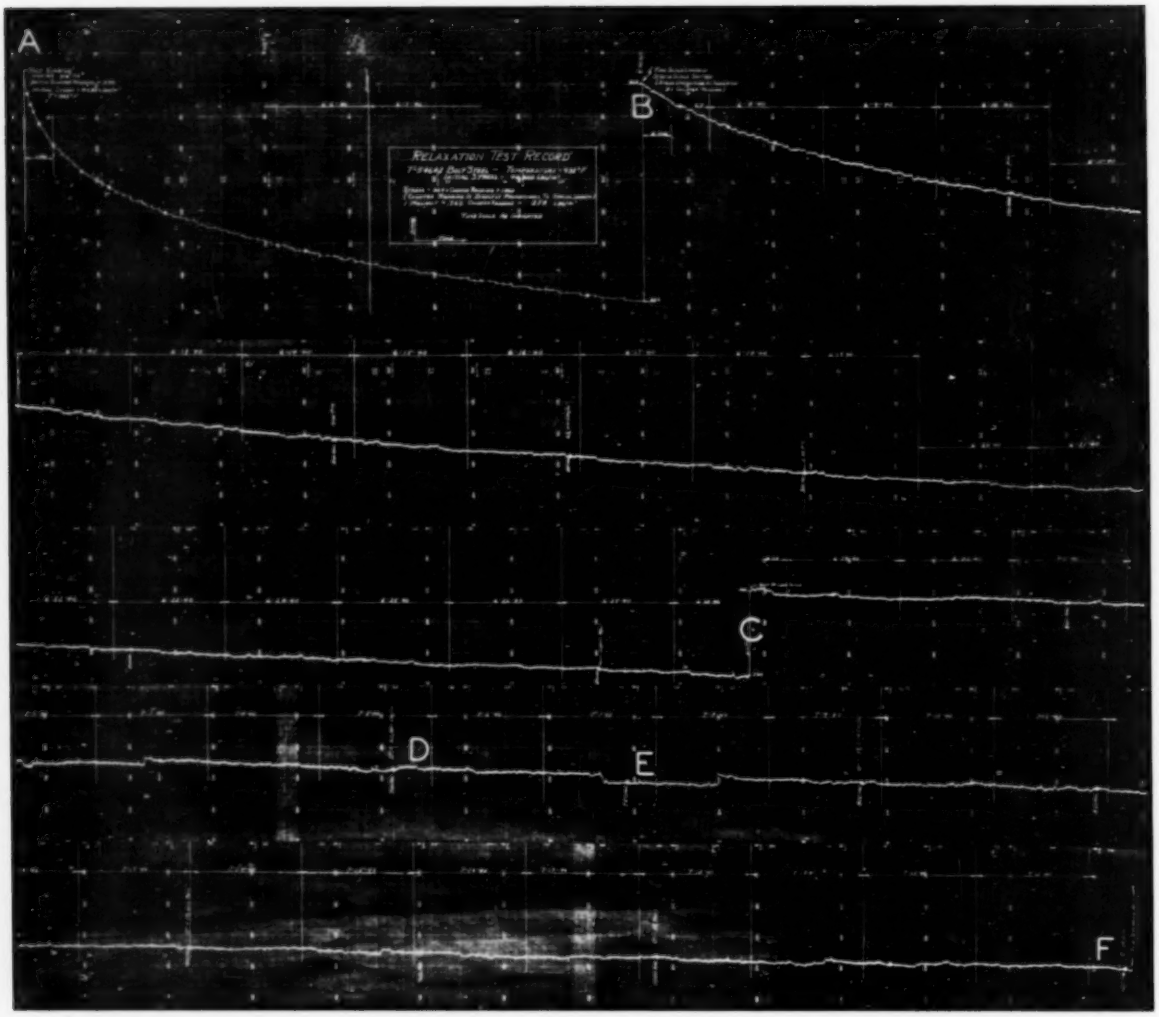

FIG. 4. Relaxation record of steel at 500°C.

gave good results for copper at low temperatures.[1] In recent years relaxation tests have been used by W. Barr and W. E. Bardgett,[2] N. L. Mochel,[3] E. L. Robinson,[4] and C. C. Davenport,[5] but the number of test results available is comparatively small. Our present automatic relaxation machine was developed and built at the Westinghouse Research Laboratories.[6]

[1] J. Boyd, Proc. A.S.T.M. **37**, Part II (1937).
[2] W. Barr and W. E. Bardgett, Proc. Inst. Mech. Eng. **122**, 285 (1932).
[3] N. L. Mochel, Trans. A.S.M.E. **59**, 453 (1937).
[4] E. L. Robinson, Trans. A.S.M.E. **59**, 451 (1937).
[5] C. C. Davenport, J. App. Mech. **5**, 55 (1938).
[6] A. Nadai and J. Boyd, Proc. Fifth International Congress of Applied Mechanics, Cambridge, Massachusetts, 1938, p. 245. Special acknowledgments are due to Mr. A. D. Irwin, for design of the machine.

II. RELAXATION MACHINE

To duplicate relaxation conditions, load must be continuously removed so that the elastic shortening balances the permanent elongation. This ideal type of test is approached by having very many small steps of unloading. The required elements of the machine, therefore, are a spring loading mechanism and an accurate but sturdy extensometer. A diagram of the machine is shown in Fig. 1. See, also, Fig. 2.

The tensile specimen (*H*) is loaded through a lever arm (*B*) by springs (*C*) whose extension is measured by a follow-up mechanism (*D*). The springs are loaded and unloaded by a worm gear drive (*J*). The motor driven follow-up

device is directly coupled with the recorder so that the stress, which is directly proportional to the spring elongation, can simply be calculated from the chart.

The extensometer (K) is attached to the specimen at the gage length of 6 inches. The steel extensometer arms extend down through the bottom of the furnace and at (G) the small relative motion is mechanically amplified. An electric contact with a micrometer measuring device accurately determines the total strain. After the specimen is loaded this contact operates the unloading motion for a strain of approximately 2×10^{-6} inch per inch.

The electric furnace (A) heats the specimen and controls the temperature at any desired level below 750°C. The differential expansion of a quartz rod and a nickel tube operating another contact device is utilized to interrupt part of the heating current. In this way the specimen temperature varies no more than $\pm\frac{1}{4}$°C.

On all of the control contacts a 6-volt potential is applied which, when contacts are closed, is amplified by a thyratron tube to operate a relay. This small voltage eliminates sparking and therefore increases accuracy and decreases wear. These automatic devices have given no trouble and require attention only several times a year.

Figure 3 shows a loading curve and indicates that the small strains required to operate a loading motor are less than 1/100 of the total strain.

Figure 4 is a picture of a continuous 1100-hr. load-time record of a relaxation test on an alloy steel at 500°C. This unusually long test was used to check both the reliability of the machine and the accuracy of the extrapolation. At points B and C the pen was shifted so that the line would stay on the paper. At B the time scale was reduced to $\frac{1}{6}$ the initial scale because the stress was changing more slowly. At E a slight disturbance can be noticed; this was caused by a change in room temperature, which could not always be controlled. The disturbance was of no consequence since the stress was reduced less than 1 percent and for only a short time. For perfect test results air temperature and circulation must not be disturbed near the machine.

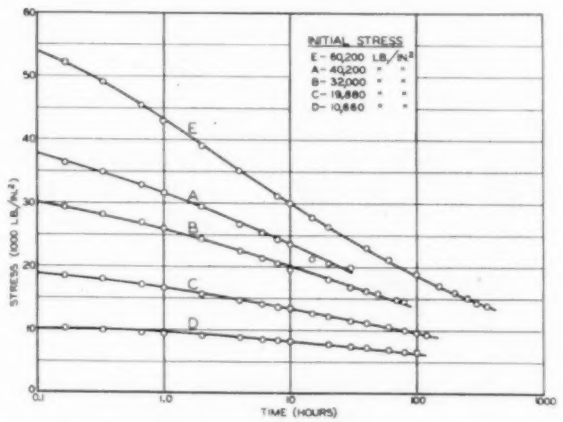

FIG. 5. Relaxation of Cr-Mo-W steel at 500°C.

III. RESULTS

Since one of the main purposes of the construction of the automatic relaxation machine was to study mechanical properties of high

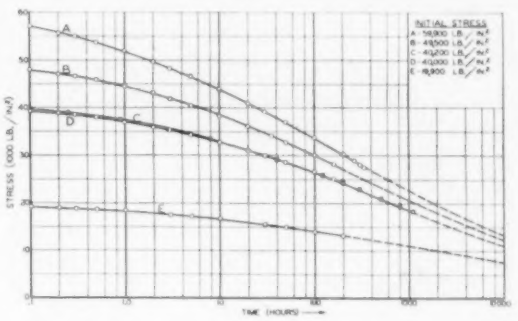

FIG. 6. Relaxation of Cr-Mo-W steel (2) at 500°C.

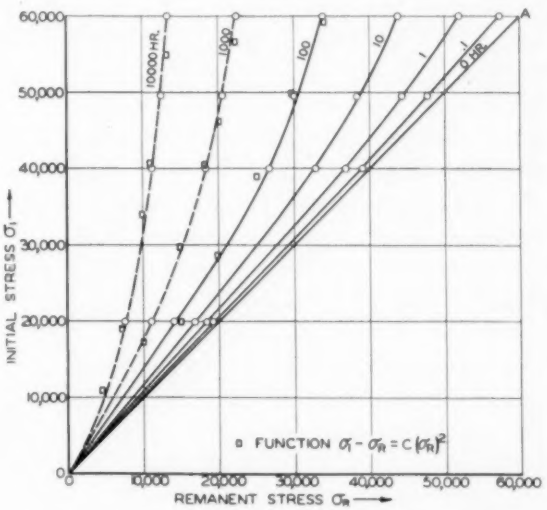

FIG. 7. Relaxation of Cr-Mo-W steel (2) at 500°C. Remanent stress *vs.* initial stress.

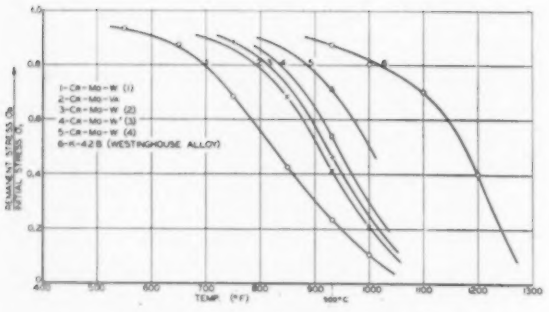

FIG. 8. Relaxation values at 1000 hr. Initial stress $\sigma_1 = 40{,}000$ lb./in.^{2}

temperature bolting materials, a great amount of data has been gathered on this subject. It was found that, usually, after one week the stress decreased very slowly and so the usual time of testing became about 150 hours.

Figures 5 and 6 show typical plots of test data. It is convenient to use the semilog plot because the logarithmic time scale fits both the rapid initial relaxation and the subsequent slow changes. Curve E of Fig. 5 has an inflection point at approximately one-half of the initial stress. This observation and the assumption that eventually the relaxation curve becomes asymptotic to the zero stress axis have been the guide for extrapolation of the relaxation data. Figure 6 is one of the extrapolated series of curves in which curve C is a replot of the record shown on Fig. 4. The original curves of this material were drawn and extrapolated before the check test was run. The check test not only agrees well with the original test whose initial stress was 40,000 lb./sq. in. but it also coincides with the extrapolation. In most cases when check tests were run starting with the same initial stress there was agreement between the observations. When more than one relaxation machine becomes available, other long tests will be run to check even further extrapolations; however those to 10,000 hours are probably fairly accurate.

A cross plot of Fig. 6, taking time as the parameter, is shown in Fig. 7. This is a useful plot for the engineer as it simplifies interpolation. It happens that a parabolic function $\sigma_1 - \sigma_R = c(\sigma_R)^2$ (where σ_1 = the initial and σ_R = the final stress) expresses the curves closely for all of the high strength materials. The parabolas are drawn through the origin O making them tangent to line OA (Fig. 7). Theoretical considerations of possible creep laws show, however, that this assumption may not be true, for the indication is that straight lines fan out from the origin O at the low stresses. For test data on very weak materials it was found that the parabola does not fit. Although we realize that this is an empirical statement and we do not know, therefore, the more exact shapes of the curves of Fig. 7, we do know that for strong materials such curves seem probable from the observations.

In order to compare the relaxation of steels at various temperatures, a comparison was made of the relaxed values at an initial stress of 40,000 lb./sq. in. and at a time of 1000 hr. Figure 8 shows readily which is the strongest material because of its resistance to creep. Materials may well be compared by means of a "creep critical temperature range" which would be the range of temperature near the point of maximum slope of this type of curve. In creep tests there is also a range of temperature at which the creep rate for a given stress increases very rapidly, but since there are no creep test data at various temperatures on the above materials it is impossible to show that these temperature ranges are identical. The significance of this critical temperature can be appreciated in that it is known from several other types of tests that the alloy K-42-B has excellent high temperature proper-

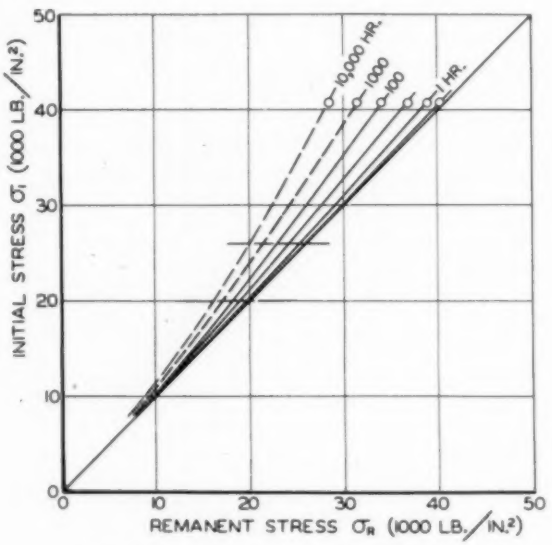

FIG. 9. Relaxation of K-42-B at 1000°F.

ties, and a glance at the critical temperature comparison brings out the order of increasing creep resistance of the steels which were compared.

Since relaxation under certain conditions is essentially an integrated creep phenomenon under variable stress, it would seem that we should be able to correlate the two types of test results. Unfortunately, no complete series of both types of test results on the same material are available, but an attempt at least to correlate several tests which were available for K-42-B at 538°C (1000°F) will be described. Figure 9 is the plot of the relaxation test at the initial stress of 40,900 lb./sq. in., and the parabolic curves used to interpolate the information required. In Fig. 10 the interpolated relaxation curves are drawn so that a range at 20,000 lb./sq. in. is covered. The assumptions for the correlation are that, given the same material at zero time, *at equal times and stresses the plastic strain rates are also equal.* As mentioned before (see Eq. (2)), the permanent strain ϵ'' is a function of the change of stress in the relaxation curve, and a creep curve $\epsilon''=f(t)$ at a constant stress can be plotted using an equivalent stress $\sigma=E\epsilon''$ as the coordinate instead of the strain. A graphical integration is made of the relaxation curve slopes at the stress of 20,000 lb./sq. in. and a creep curve is calculated. The slopes at points A to F are redrawn near the creep curve to show that this is the basis of the correlation. Both calculated and tested curves are plotted on the normal strain-time coordinates and their close correlation can be noted. Two other attempts at this type of correlation were equally successful. Although in no case was there sufficient information, all evidence so far available points in the direction that this correlation can give good results.

The relaxation test is useful beyond the direct

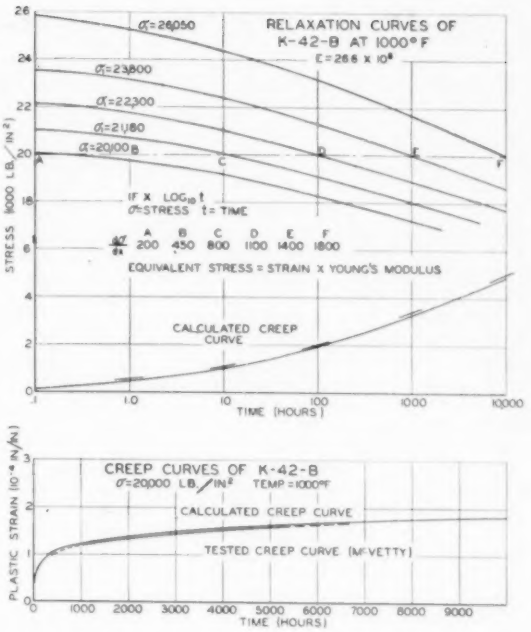

FIG. 10. Correlation diagrams.

application of information regarding the behavior of metals at constant total strains. It establishes the relative ability of a material to withstand stress at high temperatures, particularly in the applications of bolting materials. It is also valuable in that it may be used to estimate creep values in certain industrially important ranges of stress and temperature for high strength alloys. Effectively, this is a much needed short time test to predict mechanical properties of metals at high temperatures.

ACKNOWLEDGMENT

Acknowledgments are due to Dr. A. Nadai for his advice and cooperation in the work as it progressed. Also, credit is due to Messrs. G. H. Heiser and J. Boyd for running some of the tests used in this paper.

Engineering Defense Training Program

The following is a list of the engineering defense training courses which have been authorized to December 30, 1940. Courses are all of college grade. The cost of instruction will be paid by the Federal Government, but students are required to provide their own textbooks and supplies.

Alabama

Alabama Polytechnic Institute, Auburn, Alabama: (1) Construction Engineering, (2) Engineering Drawing, (3) Engineering Economy, (4) Industrial Relations, (5) Machine Design, (6) Marine Engineering, (7) Military Highway Engineering, (8) Naval Architecture, (9) Production Engineering, (10) Surveying, (11) Tool Engineering.

University of Alabama, University, Alabama: (1) Correlation Course for Ordnance Inspectors, (2) Industrial Organization and Management, Time and Motion Study, (3) Industrial Practice, Cast Iron Pipe and Fittings Industry, (4) Industrial Practice, Electric Power Industry, (5) Industrial Practice, Steel Industry, (6) Industrial Safety and Safety Administration, (7) Mechanics and Strength of Materials, (8) Mechanisms and Elementary Machine Design, (9) Physical Metallurgy and Metallurgy of Iron and Steel, (10) Tool and Die Design.

Arkansas

University of Arkansas, Fayetteville, Arkansas: (1) Engineering Drawing.

California

California Institute of Technology, Pasadena, California: (1) Production Engineering, (2) Production Supervision, (3) Radio and Electronics.

University of Southern California, Los Angeles, California: (1) Materials Inspection and Testing (Unit A), (2) Materials Inspection and Testing (Unit B), (3) Materials Inspection and Testing (Unit C).

Colorado

Colorado School of Mines, Golden, Colorado: (1) Production of Major Nonferrous Metals, (2) Theory and Application of Welding.

Colorado State College of Agricultural and Mechanical Arts, Fort Collins, Colorado: (1) Engineering Drawing, (2) Machine Design, (3) Materials Inspection and Testing.

University of Colorado, Boulder, Colorado: (1) Advanced Electronic Instruments, (2) Airplane Stress Analysis, (3) Engineering Drawing and Machine Design, (4) Machine Design, (5) Material Testing and Inspection, (6) Production Engineering, (7) Technology of Heavy Chemicals Industry, (8) Theory of Elasticity.

University of Denver, Denver, Colorado: (1) Testing of Chemicals and Other Defense Materials.

Connecticut

Yale University, New Haven, Connecticut: (1) Applied Mechanical Design, (2) Engineering Drawing, (3) Inspection of Materials, (4) Metallurgy, (5) Production Control, (6) Welding Supervision.

Delaware

University of Delaware, Newark, Delaware: (1) Motion and Time Analysis.

District of Columbia

George Washington University, Washington, D. C.: (1) Concrete Inspection and Testing, (2) Construction Materials, Properties, Tests and Specifications, (3) Map Making and Interpretation, (4) Radio Communication, (5) Ship Construction, (6) Structural Steel Design, (7) Surface and Aerial Navigation.

Howard University, Washington, D. C.: (1) Engineering Drawing.

Florida

University of Florida, Gainesville, Florida: (1) Engineering Drawing.

Georgia

Georgia School of Technology, Atlanta, Georgia: (1) Construction Materials, (2) Engineering Drawing, (3) Metal Inspection, (4) Textile Testing.

Idaho

University of Idaho, Moscow, Idaho: (1) Design Drafting, (2) Engineering Drawing.

Illinois

Bradley Polytechnic Institute, Peoria, Illinois: (1) Engineering Drawing.

Illinois Institute of Technology, Chicago, Illinois: (1) Design of Bombproof Shelters, (2) Design of Tools and Testing Equipment, (3) Diesel Engines, (4) Drafting and Elementary Design, (5) Industrial Management, (6) Inspection Methods, (7) Machine Design, (8) Metallurgy, (9) Production Planning Routing, (10) Strength of Materials and Steel Design, (11) Structural Designing and Drafting, (12) Testing and Inspection of Concrete, (13) Testing Methods, (14) Time and Motion Study, (15) Tool and Fixture Design, (16) Welding Engineering.

Indiana

Purdue University, Lafayette, Indiana: (1) Aeronautical Engineering, (2) Applications of Electronics, (3) Engineering Drafting, (4) Explosives Inspection, (5) Machine Design, (6) Materials Inspection, (7) Materials Testing and Inspection (2 courses), (8) Metallurgy, (9) Production Engineering (2 courses), (10) Production Supervision (2 courses), (11) Tool Design (2 courses).

Rose Polytechnic Institute, Terre Haute, Indiana: (1) Electrica Communication, (2) Engineering Drawing and Machine Design, (3) Illuminating Engineering, (4) Materials Inspection and Testing, (5) Production Engineering.

University of Notre Dame, South Bend, Indiana: (1) Chemical Analysis of Metallurgical Materials, (2) Production Engineering, (3) Physical Metallurgy, (4) Tool and Die Design.

Iowa

Iowa State College, Ames, Iowa: (1) Materials Inspection and Testing, (2) Tool Engineering.

Kansas

Kansas State College, Manhattan, Kansas: (1) Aeronautical Engineering, (2) Engineering Drawing, (3) Explosives, (4) Materials Inspection and Testing, (5) Tool Engineering.

University of Kansas, Lawrence, Kansas: (1) Aeronautical Engineering, (2) Engineering Drawing, (3) Machine Design, (4) Materials Inspection and Testing, (5) Production Engineering and Supervision.

Kentucky

University of Louisville, Louisville, Kentucky: (1) Aerial Photographic Mapping, (2) Applied Mechanics (Statics), (3) Elementary Unified Mathematics, (4) Ferrous Physical Metallurgy, (5) Nonferrous Physical Metallurgy, (6) Strength of Materials.

Louisiana

Louisiana Polytechnic Institute, Ruston, Louisiana: (1) Engineering Drawing.

Southwestern Louisiana Institute, Lafayette, Louisiana: (1) Engineering Drawing.

Tulane University, New Orleans, Louisiana: (1) Engineering Drawing (2 courses), (2) Machine Design.

Maryland

Johns Hopkins University, Baltimore, Maryland: (1) Electricity Applied to Aircraft, (2) Industrial Organization and Management, (3) Materials Inspection and Testing, (4) Mechanical Design for Radio Engineers, (5) Plastics, (6) Production Fundamentals, (7) Radio Engineering, (8) Time and Motion Study.

University of Maryland, College Park, Maryland: (1) Aeronautical Drafting and Design, (2) Aircraft Inspection, (3) Aircraft Tool Engineering, (4) Radio Engineering, (5) Radio Testing and Inspection.

Massachusetts

Massachusetts Institute of Technology, Cambridge, Massachusetts: (1) Aeronautical Engineering, (2) Aircraft Engines, (3) Applications of Metallography, (4) Applied Mathematics, (5) Defense Production Coordination and Expediting, (6) Dynamic Analysis of Servomechanisms, (7) Engineering Fundamentals, (8) Exterior Ballistics, (9) Instrumentation and Vibration Measurement, (10) Marine Engineering, (11) Naval Architecture, (12) Ordnance Inspection, (13) Textile Testing, (14) Vibrations and Their Applications.

Northeastern University, Boston, Massachusetts: (1) Applied Mechanics, (2) Elementary Airplane Structures, (3) Engineering Drawing, (4) Higher Mathematics, (5) Instrumentation, (6) Machine Design (2 courses), (7) Materials Inspection and Testing (2 courses), (8) Methods Engineering, (9) Production Engineering and Supervision, (10) Production Supervision.

Tufts College, Medford, Massachusetts: (1) Applied Mathematics, (2) Chemistry in National Defense, (3) Concrete Inspection and Construction, (4) Engineering Drawing, (5) Foreman Conferences and Instructor Training, (6) Machine Design, (7) Physical Metallurgy, (8) Production Engineering, (9) Radio Engineering, (10) Theory and Practice of Welding.

Worcester Polytechnic Institute, Worcester, Massachusetts: (1) Elements of Machine Design, (2) Elements of Tool Engineering, (3) Materials Testing and Inspection.

Michigan

Detroit Institute of Technology, Detroit, Michigan: (1) Machine Design, (2) Tool and Die Design.

Michigan College of Mining and Technology, Houghton, Michigan: (1) Engineering Drawing, (2) Machine Design, (3) Materials Inspection and Testing.

University of Detroit, Detroit, Michigan: (1) Aeronautical Engineering, (2) Drawing, Descriptive Geometry, and Shop Mathematics, (3) Materials Inspection and Testing, (4) Production Engineering, (5) Production Supervision.

University of Michigan, Ann Arbor, Michigan: (1) Machine Design, (2) Materials Inspection and Testing, (3) Production Engineering and Supervision, (4) Tool Engineering.

Wayne University, Detroit, Michigan: (1) Electronics Engineering I, (2) Engineering Drawing I, (3) Engineering Drawing II (Descriptive Geometry), (4) Engineering Drawing III (Freehand Drawing), (5) Industrial Organization and Factory Management, (6) Machine Design, (7) Material Testing, (8) Metallurgy, (9) Shop Processes, Mathematics and Measurements, (10) Telephone Communication.

Minnesota

University of Minnesota, Minneapolis, Minnesota: (1) Engineering Drawing, (2) Machine Design, (3) Metallurgy and Metallography, (4) Optical Engineering.

Mississippi

Mississippi State College, State College, Mississippi: (1) Engineering Drawing, (2) Materials Inspection and Testing, (3) Tool Engineering.

Missouri

Washington University, St. Louis, Missouri: (1) Machine Design, (2) Material Inspection and Testing, (3) Production Engineering, (4) Production Supervision, (5) Tool Engineering.

Nevada

University of Nevada, Reno, Nevada: (1) Civil Engineering Drawing.

New Hampshire

University of New Hampshire, Durham, New Hampshire: (1) Engineering Drawing.

New Jersey

Newark College of Engineering, Newark, New Jersey: (1) Engineering Drawing, (2) Machine Design, (3) Materials Inspection and Testing.

Rutgers University, New Brunswick, New Jersey: (1) Machine Design.

Stevens Institute of Technology, Hoboken, New Jersey: (1) Elements of Engineering Drawing, (2) Introduction to Engineering.

New Mexico

New Mexico College of Agricultural and Mechanical Arts, State College, New Mexico: (1) Engineering Drawing, (2) Machine Design, (3) Materials Inspection and Testing.

New York

Cornell University, Ithaca, New York: (1) Advanced Stress Analysis and Elastic Stability, (2) Electronics, (3) Materials Testing and Physical Metallurgy, (4) Mechanics and Elementary Aircraft Design.

New York University, New York, New York: (1) Aerial Bombardment Protection, (2) Aircraft Stress Analysis Procedure, (3) Elements of Advanced Aircraft Engine Design, (4) Food Inspection, (5) Fundamentals of Aircraft Fitting Design, (6) Gaging and Inspection Methods, (7) Heat Treatment of Aluminum Alloys, (8) Introductory Aerodynamics, (9) Marine Engineering, (10) Materials Testing with Laboratory, (11) Metallurgy and Metallography, (12) Military Sanitation, (13) Production Control, (14) Time and Operation Study.

Pratt Institute, Brooklyn, New York: (1) Engineering Drafting and Practice, (2) Production Engineering.

Union College, Schenectady, New York: (1) Chemistry of Metals, (2) Design of Highly Stressed Structures and Apparatus, (3) Drafting and Drafting Room Practice, (4) Electron Tubes and Their Applications, (5) Elementary Electrical Theory and Practice, (6) Elementary Mechanics and Strength of Materials, (7) Engineering Materials and Manufacturing Methods, (8) Engineering Problems and Their Mathematical Solution, (9) Industrial Applications of Optics, (10) Industrial Chemistry, (11) Internal Combustion Engines, (12) Methods Improvement by Motion Study, (13) Principles and Practice of Radio Communication, (14) Production and Cost Control, (15) Tool Design.

North Carolina

Agricultural and Technical College of North Carolina, Greensboro, North Carolina: (1) Materials Inspection and Testing.

Duke University, Durham, North Carolina: (1) Communication Engineering, (2) Machine Design.

North Carolina State College, Raleigh, North Carolina: (1) Aircraft Inspection, (2) Chemical Testing and Inspection, (3) Diesel Engineering, (4) Engineering Drawing, (5) Experimental Electronics, (6) Instrument Men and Topographers, (7) Machine Design, (8) Materials Inspection and Testing, (9) Production Engineering, (10) Production Supervision.

North Dakota

University of North Dakota, University, North Dakota: (1) Engineering Drawing, (2) Materials Inspection and Testing.

Ohio

Case School of Applied Science, Cleveland, Ohio: (1) Electrical Maintenance and Control, (2) Elements of Motion Economy, (3) Engineering Surveying, (4) Explosives, (5) Fundamentals of Machine Design, (6) Industrial Instrumentation, (7) Inspector and Metallurgical Technician Training, (8) Internal Combustion Engine Testing, (9) Machine Detailing.

University of Cincinnati, Cincinnati, Ohio: (1) Materials Inspection and Testing, (2) Production Supervisor.

Fenn College, Cleveland, Ohio: (1) Engineering Drawing, (2) Material Inspection and Testing, (3) Nonmetal Material Testing, (4) Production Engineering, (5) Production Supervision, (6) Stress Analysis, (7) Structural Detailing, (8) Tool Engineering.

Ohio State University, Columbus, Ohio: (1) Air Navigation, (2) Communications Laboratory Technique, (3) Design of Chemical Plant Machinery and Equipment, (4) Engineering Drawing, (5) Explosives, (6) Inspection of Materials of Chemical Industry (A. S. T. M. methods) and Chemicals, (7) Inspection of Construction Materials, (8) Inspection of Instruments, (9) Inspection and Testing of Small Electrical Power Units, (10) Inspection and Testing of Small Internal Combustion Engine Power Units, (11) Inspection of Steel and Cast Iron Products, (12) Inspection of Welded Products, (13) Machine Design, (14) Physical Metallurgy, (15) Production Engineering, (16) Production Supervision, (17) Tool Engineering, (18) Welding Engineering Design.

Oklahoma

Oklahoma Agricultural and Mechanical College, Stillwater, Oklahoma: (1) Engineering Drawing, (2) Machine Design, (3) Materials Inspection and Testing, (4) Production Engineering, (5) Tool Engineering.

University of Oklahoma, Norman, Oklahoma: (1) Aeronautical Engineering, (2) Engineering Drawing (2 courses).

Oregon

Oregon State College, Corvallis, Oregon: (1) Aeronautical Engineering.

Pennsylvania

Bucknell University, Lewisburg, Pennsylvania: (1) Engineering Drawing, (2) Materials Inspection and Testing, (3) Production Engineering.

Carnegie Institute of Technology, Pittsburgh, Pennsylvania: (1) Cost Control, (2) Elementary Industrial Chemistry, (3) Elements of Metallurgical Engineering, (4) Engineering Drafting, (5) Industrial Relations, (6) Machine Design, (7) Production Engineering, (8) Production Supervision, (9) Testing and Inspection.

Drexel Institute of Technology, Philadelphia, Pennsylvania: (1) Chemical Plant Operation, (2) Electrical Circuit Theory, Machines and Instruments, (3) Machine Design, (4) Marine Electrical Engineering, (5) Production and Tool Engineering.

Grove City College, Grove City, Pennsylvania: (1) Engineering Drawing.

Lehigh University, Bethlehem, Pennsylvania: (1) Instrument Design, (2) Machine Design.

Pennsylvania State College, State College, Pennsylvania: (1) Diesel Engineering, (2) Electronics and Electron Tubes, (3) Elementary Engineering Drafting, (4) Elementary Machine Design, (5) Elementary Tool Design, (6) Fuel Technology, (7) Operation Inspection, (8) Petroleum Refinery Control, (9) Physical Metallurgy, (10) Physical Testing of Materials (2 courses), (11) Pre-Foremanship Training in Production Supervision, (12) Production Engineering (2 courses), (13) Pyrometry, (14) Test Calculations and Instrumentation, (15) Time and Motion Study.

University of Pennsylvania, Philadelphia, Pennsylvania: (1) Chemical Engineering for Production Supervision, (2) Diesel Engineering, Design and Construction, (3) Machine Design, (4) Motion Study—Time Study—Wage Incentives, (5) Physical Metallurgy, (6) Production Engineering, (7) Production Management, (8) Production Supervision, (9) Safety Engineering.

University of Pittsburgh, Pittsburgh, Pennsylvania: (1) Engineering Materials Inspection and Testing, (2) Machine Design, (3) Machinery Inspection and Testing, (4) Mechanical Drawing and Descriptive Geometry, (5) Metallurgical Inspection, (6) Production Engineering, (7) Production Planning, (8) Spectroscopic Testing of Materials, (9) X-Ray Testing of Materials.

Rhode Island

Brown University, Providence, Rhode Island: (1) Flements of Machine Design, (2) Engineering Drawing, (3) Engineering Mathematics, (4) Jig and Fixture Design.

South Carolina

Clemson Agricultural College, Clemson, South Carolina: (1) Elementary Drafting.

South Dakota

South Dakota State College, Brookings, South Dakota: (1) Machine Design.

Tennessee

Tennessee Polytechnic Institute, Cookeville, Tennessee: (1) Engineering Drawing.

University of Tennessee, Knoxville, Tennessee: (1) Electric Communications, (2) Elementary Mathematics for In-Service Training, (3) Materials Inspection and Testing.

Vanderbilt University, Nashville, Tennessee: (1) Engineering Drawing, (2) Machine Design, (3) Materials Inspection and Testing.

Texas

Agricultural and Mechanical College of Texas, College Station, Texas: (1) Aeronautical Engineering, (2) Aircraft Inspection, (3) Camp Sanitation, (4) Engineering Drawing, (5) Material Inspection and Testing.

Southern Methodist University, Dallas, Texas: (1) Engineering Drawing, (2) Production Supervision.

Texas College of Arts and Industries, Kingsville, Texas: (1) Engineering Drawing.

Texas Technological College, Lubbock, Texas: (1) Production Engineering.

University of Texas, Austin, Texas: (1) Engineering Drawing, (2) Materials Inspection and Testing (2 courses), (3) Soil Mechanics Laboratory Technique, (4) Structural Drafting.

Utah

University of Utah, Salt Lake City, Utah: (1) Aeronautical Engineering, (2) General Metallurgy, (3) Industrial Electronics, (4) Machine Design, (5) Materials Inspection and Testing, (6) Mechanical Drawing and Descriptive Geometry, (7) Ore Dressing.

Vermont

Norwich University, Northfield, Vermont: (1) Engineering Drawing.

Virginia

University of Virginia, Charlottesville, Virginia: (1) Engineering Drawing, (2) Industrial Electronics, (3) Materials Testing and Inspection, (4) Production Supervision, (5) Principles of Radio, (6) Simple Aerodynamics and the Airplane.

Washington

State College of Washington, Pullman, Washington: (1) Engineering Drawing.

University of Washington, Seattle, Washington: (1) Advanced Mechanics of Structures, (2) Aircraft Descriptive Geometry, (3) Aluminum and Its Alloys, (4) Design and Operation of Radio Equipment, (5) Fundamentals of Aerodynamics, (6) Fundamentals of Communications, (7) Hull Fittings and Mechanical Devices in Warship Construction, (8) Junior Marine Engineer, (9) Mechanical Engineering (Heat and Ventilation), (10) Mechanics of Structures, (11) Metallography, (12) Naval Architecture, (13) Naval Architecture and Ship Drafting, (14) Naval Practice in Electrical Engineering, (15) Ordnance Design, (16) Ship Piping Design for Mechanical Engineers, (17) Technical Sketching.

West Virginia

West Virginia University, Morgantown, West Virginia: (1) Drafting and Designing, (2) Metallurgy, (3) Process Engineering (Chemical), (4) Production Supervisors, (5) Testing and Inspection.

Wisconsin

Marquette University, Milwaukee, Wisconsin: (1) Materials Inspection and Testing, (2) Production Engineering.

Wyoming

University of Wyoming, Laramie, Wyoming: (1) Engineering Drawing.

Puerto Rico

University of Puerto Rico, Mayaguez, Puerto Rico: (1) Communication Engineering.

Letter to the Editor

On the Resistance to the Uniform Motion of a Solid Through a Viscous Liquid

JOHN T. BURWELL, JR.
Lubrication Laboratory, Department of Mechanical Engineering, Massachusetts Institute of Technology, Cambridge, Massachusetts
January 17, 1941

IN a paper by Raymond B. Block of the same title appearing in this journal,[1] experiments on rolling a steel ball down an inclined tube filled with a viscous liquid were reported and it was found that the data for different liquids did not fit either Stokes' or Oseen's law for the viscous drag on a sphere. The usual assumption made in fluid mechanics is that there is no relative motion of the liquid at the surface of the sphere, but he concluded that if tangential slipping is postulated, the data can be used to calculate a coefficient of slip which varies from liquid to liquid. It is suggested following Brillié[2] that this slip should be greater with polar compounds.

The hypothesis of slip has intrigued investigators since the time of Helmholtz,[3] and many experiments have been conducted in order to prove its existence, with no positive results.[4] Hence, if the conclusions of Block's paper are justified they have very far-reaching significance, among other things the fact that any measurement of viscosity would always depend on the apparatus and the liquid under investigation.

The criticisms of the work under discussion fall into three general categories: (1) whether Stokes' or Oseen's law should apply in the present experiment even if there were no slip, (2) whether the effect of slip is also present in the measurement of viscosity and should be allowed for in reducing the data, and (3) whether glycerin itself is a polar compound.

Considering these objections in turn, the first relates to the applicability of Stokes' or Oseen's law in the present case. Both these equations, as the author points out, apply to the uniform translation of a sphere through an infinite amount of liquid and not to combined translation and rotation in a relatively small tube. The effect of the walls of a cylindrical tube, assuming the sphere symmetrically placed in the tube has been considered by Ladenburg,[6] by Faxen,[7] and by Francis.[8] For the apparatus used by Block the correction factor for the walls will be quite large and in that case will depend on the speed and the viscosity. Hence, it should be taken into account when comparing different liquids. The matter of the superimposed rotation of the sphere complicates the problem and no rigorous treatment of it has yet been given. It would have to be shown that a linear relation did exist between the drag, F, and the quantity, μvd, where μ is the absolute viscosity, d the diameter of the sphere and v its velocity. Even assuming for the moment that this is so, a more serious objection lies in the fact that both these equations were derived on the assumption that the "Reynolds' number" $\rho vd/\mu$, where ρ is the density of the liquid, must be much less than unity. Many experiments[9-13] have been performed to test this relationship. These include dropping Rose metal spheres in several vegetable oils and steel spheres in water and glycerol. A summary[14,15] of the results shows that Stokes' law is precisely obeyed if the Reynolds' number is less than 0.5 and that Oseen's law is obeyed for values of the Reynolds' number up to 0.8. Above these points the experimental values begin to deviate from the theoretical curves as would be expected. Block shows three plots in which the variable Π_2, which is the Reynolds' number as defined here, appears. For the experiments using pure glycerin Π_2 ranges from 0.012 to 0.25, for the solution containing 10 percent methyl alcohol in glycerin it ranges from 0.63 to 2.0, and for the other solutions used Π_2 is even higher. It can be seen that except in the case of pure glycerin neither of the theoretical equations are even supposed to apply to the present experiment, and hence any deviations therefrom cannot be taken as evidence of slip. The true explanation probably lies in the partial or complete neglect of the inertial terms in the equation of motion.[5]

The second criticism of the conclusions drawn in the paper under discussion is that in any investigation of the existence of slip by this method account should be taken of its effect on the measurement of viscosity by means of the modified Ostwald capillary viscosimeter. If we assume a coefficient of slip, β, then Poiseuille's equation for the discharge rate, Q, of a liquid through a tube of radius r and length l under a difference of pressure p, becomes:

$$Q=(\pi r^4 p/8\mu)(1+4\mu/\beta r).$$

Taking the values of μ and β given in Table IV of Block's paper and assuming a radius of the capillary of the viscosimeter of 0.2 cm, the factor $(1+4\mu/\beta r)$ becomes approximately equal to 4. (The end effects will modify this result only slightly.) This means that a liquid which slips on the surface will flow through the viscosimeter four times as fast as a similar liquid of the same absolute viscosity which does not show slip. This result seems highly unlikely, but if the object of the present work is to prove the existence of this phenomenon then either this factor should be taken into account in the formulae or else it should be definitely established that none of the liquids used exhibit slip on the glass walls of the viscosimeter. In this latter connection Whetham[16] found no observable deviations from Poiseuille's equation for the flow of water through either silvered or unsilvered glass tubes.

Lastly, it has been well established that glycerol is a polar compound[17-19] and the value of its dipole moment[17] has been given as 2.20×10^{-18} as compared with 1.68×10^{-18} for methyl alcohol and zero for a nonpolar substance. It appears then that one would expect both substances to behave alike even on the hypothesis suggested by Block

and that the differences observed by him are undoubtedly due to the great disparity in the viscosities with its resultant effect on the inertial terms in the equations of motion.

It should also be pointed out that Arnold[9] and Allen[11] were able to verify Stokes' law for the low range of Reynolds' number using colza oil, linseed oil, aqueous alcohol and water, all of which are or contain polar substances.

If there is still any question as to the non-existence of slip in spite of the many experiments that have been performed to find it, a few of which have been cited above, then the critical experiment should be somewhat as follows: the sphere should be allowed to fall freely in a cylinder filled with the liquid and the diameter of the cylinder should be at least thirty times that of the sphere. Two liquids of the same viscosity should be used so that any differences observed could not be ascribed to viscosity. It is known that a pure mineral oil such as Nujol is nonpolar[20] and this could be compared with some vegetable oil such as castor oil or a solution of stearic acid in caprylic acid which is known to be polar. It would be preferable to arrange the constants of the system so that the Reynolds' number is small, in order that the theoretical equations could be applied to the data. Such an experiment should answer unequivocally what Block's work fails to do.

The author is indebted to Professor J. C. Hunsaker for suggesting this comment and to Professor A. M. Gaudin for helpful discussion.

[1] R. B. Block, J. App. Phys. **11**, 635 (1940).
[2] H. Brillié, Mém. Soc. Ing. Civ. France **88**, 623 (1935); Proc. Gen. Discussion on Lubrication and Lubricants, Vol. 2 (The Institution of Mechanical Engineers, London, 1937), pp. 248–250.
[3] Helmholtz and Piotrowski, Akad. Wiss. Wien **40**, 607 (1860).
[4] For review of literature and discussion on this subject see E. C. Bingham, *Fluidity and Plasticity* (McGraw-Hill, 1922), pp. 29–35; also G. Barr, *A Monograph of Viscometry* (Oxford University Press, 1931), pp. 43–46.
[5] H. Lamb, *Hydrodynamics* (Cambridge University Press, sixth edition, 1932), articles 337, 342.
[6] R. Ladenburg, Ann. d. Physik **23**, 447 (1907).
[7] H. Faxen, Arkiv. Mat. Astron. och Fysik **17**, No. 27 (1922).
[8] A. W. Francis, Physics **4**, 403 (1933).
[9] H. D. Arnold, Phil. Mag. **22**, 755 (1911).
[10] H. Liebster, Ann. d. Physik **82**, 541 (1927).
[11] H. S. Allen, Phil. Mag. **50**, 323, 519 (1900).
[12] R. C. Lunnon, Proc. Roy. Soc. **118A**, 680 (1928).
[13] J. Schmiedel, Physik. Zeits. **29**, 593 (1928).
[14] H. Rouse, "Nomogram for the Settling Velocity of Spheres," *Report of the Committee on Sedimentation, 1936–37* (National Research Council, 1937), pp. 57–64.
[15] G. Barr, *Report of the Committee on Sedimentation, 1936–37* (National Research Council, 1937), pp. 173–180.
[16] W. C. D. Whetham, Phil. Trans. **181A**, 559 (1890).
[17] C. P. Smyth, J. Am. Chem. Soc. **46**, 2151 (1924).
[18] P. Girard and P. Abadie, Comptes rendus **195**, 119 (1932).
[19] P. Debye, *Polar Molecules* (Chemical Catalog Company, 1929), p. 99.
[20] H. Mueller, private communication.

Calendar of Meetings

March

3– 7 American Society for Testing Materials, Washington, D. C.
4– 5 Inter-Society Color Council, Washington, D. C.
13–14 Society of Automotive Engineers, Washington, D. C.
30–April 5 American Ceramic Society, Baltimore, Maryland

April

1– 3 American Society of Mechanical Engineers, Atlanta, Georgia
4– 5 Southeastern Section of American Physical Society, Vanderbilt University, Nashville, Tennessee
7–11 American Chemical Society, St. Louis, Missouri
16–19 Electrochemical Society, Inc., Cleveland, Ohio
23–25 American Society of Civil Engineers, Baltimore, Maryland
23–25 American Mining and Metallurgical Engineers, Chicago, Illinois
28–30 National Academy of Sciences, Washington, D. C.
30–May 3 American Geophysical Union, Washington, D. C.

May

1–3 American Physical Society, Washington, D. C.
5– 7 Acoustical Society of America, Rochester, New York
5– 7 Society of Motion Picture Engineers, Rochester, New York
12–13 Society of Automotive Engineers, Milwaukee, Wisconsin
12–15 American Foundrymen's Association, New York, New York
12–21 American Institute of Chemical Engineers, Chicago, Illinois
19–23 American Society for Metals, Los Angeles, California
27–29 American Society for Refrigerating Engineers, Cincinnati, Ohio

June

1– 6 Society of Automotive Engineers, White Sulphur Springs, West Virginia
2– 6 American Medical Association, Cleveland, Ohio
12–20 American Society of Mechanical Engineers—Semi-Annual, Kansas City, Missouri
16–19 American Society of Heating and Ventilating Engineers, San Francisco, California
16–20 American Institute of Electrical Engineers (Summer Convention), Toronto, Ontario
18–20 American Physical Society, Pacific Coast Meeting, Pasadena, California
19–21 National Colloid Symposium, Cornell University, Ithaca, New York
20–21 American Physical Society, Providence, Rhode Island
23–27 American Association for the Advancement of Science, Durham, New Hampshire
23–27 American Society for Testing Materials—Annual Meeting and Exhibit of Testing Apparatus and Related Equipment, Chicago, Illinois

Eastman High-Resolution Plate

. . . for graticules and other purposes requiring the resolution of a fine structure of sharp, dense lines

THIS PLATE has the extraordinarily high resolving power of more than 500 lines per millimeter—a value far greater than is attained by any normal photographic lens. It has high maximum density and good sharpness, and is clean-working. Its speed is naturally low—about that of contact printing paper.

The *Eastman High-Resolution Plate* is regularly furnished with orthochromatic (G-type) sensitizing and antihalation backing; other sensitizings, however, may be obtained on special order. Further information will be forwarded upon request.

EASTMAN KODAK COMPANY

Research Laboratories **Rochester, N. Y.**

The COMPTON CHART

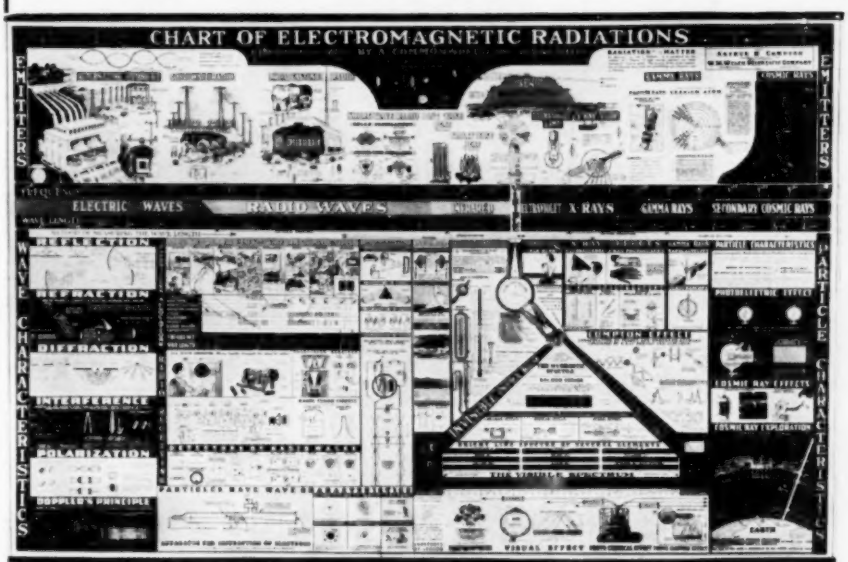

of

ELECTROMAGNETIC RADIATIONS

Edited by Professor Arthur H. Compton

Gives the complete wave gamut with significant facts regarding emitters and detectors for every section. Over 100 illustrations.

Lithographed in 8 differentiating colors

No. 4845 Size, 64 x 42 inches

on durable, cloth backed chart paper, mounted on split rollers top and bottom, complete with 32-page manual. Each, $10.00

W. M. Welch Scientific Company

Established 1880

1515 Sedgwick Street Chicago, Illinois, U.S.A.

RECERTIFICATION
of
STANDARD CELLS

Industry is continually demanding more and more accuracy from science. With proper treatment your Eppley precision type standard cells will meet this demand, but we wish to point out that according to authoritative sources the emf of cadmium cells should be redetermined at intervals of not more than two years.

In this connection we are pleased to offer the services of a finely equipped laboratory and a competent personnel. Our saturated standards, maintained in closely controlled oil baths, are regularly compared with the national standards at the National Bureau of Standards in Washington.

We will be pleased to examine and report on the condition of your cells without charge. For recertification a charge of Three Dollars ($3.00), plus postage and insurance is made. Approximately two weeks should be allowed for recertification.

EPLAB

THE EPPLEY LABORATORY, INC.
SCIENTIFIC INSTRUMENTS
NEWPORT, R.I.
U.S.A.

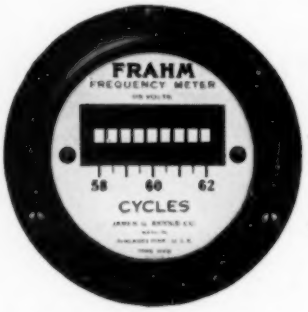

Miniature Type

Dependable Indications of Power Frequencies

Our "Frahm" Vibrating-Reed Frequency Meters are unaffected by wave form or by ordinary voltage and temperature changes. No pivots, jewels or rotating parts. Available in switchboard and wide-range portable types as well as miniature model here illustrated. Various ranges between 15 and 500 cycles per sec. *Bulletin 1555-R.*

JAMES G. BIDDLE CO.
ELECTRICAL INSTRUMENTS
1211-13 ARCH STREET PHILADELPHIA, PA.

POLAROID*
Announces A New All-Purpose Kit
$9.75 COMPLETE

This new Polaroid Experimental Kit may be used by hand, on an optical bench, with a common horizontal projector, or with a vertical projector for all kinds of demonstrations. It includes accessories for all the basic demonstrations so important in acquainting students with the principles of the new applied science of polarized light.

As a holder for the polarizing filters, the kit contains a slotted metal V-block screwed to a 10 mm support rod which may be held by hand, or in the carriages of optical benches, or mounted in a projection lantern with laboratory clamps.

Price: Polaroid Experimental Kit, No. 420, with Laboratory J-Filters (set of 2), $9.75. 48-page text and instruction manual included.

For new, complete catalog write your laboratory supply house or Division 43

POLAROID CORPORATION
730 Main Street, Cambridge, Mass.

*T. M. Reg. U. S. Pat. Off.

THREE OUTSTANDING NEW BOOKS

ELECTROMAGNETIC THEORY

By J. A. STRATTON, Massachusetts Institute of Technology. *International Series in Physics.* 615 pages, 6 x 9. $6.00

In this advanced text and reference book the author places primary emphasis on dynamic rather than static field theory, and the greater part of the book is devoted to the propagation of plane, cylindrical, and spherical waves, the theory of radiation, and representative boundary-value problems. The m.k.s. system is used throughout.

WEATHER ANALYSIS AND FORECASTING. A Textbook on Synoptic Meteorology

By SVERRE PETTERSSEN, Massachusetts Institute of Technology. 505 pages, 6 x 9. $5.00

Unique in scope, this distinctive new book presents a complete, authoritative treatment of modern methods of weather analysis and forecasting. The author discusses in detail the underlying theories and their application to weather charts and upper air charts and offers numerous examples of correct analysis and forecasts.

PHYSICS OF THE AIR. *New third edition*

By W. J. HUMPHREYS, United States Weather Bureau (Retired). 676 pages, 6 x 9. $6.00

As before, the author of this book presents a thorough discussion of the mechanics and thermodynamics of the atmosphere, of meteorological acoustics, of atmospheric optics, and of the factors involved in climatic control.

Send for copies on approval

McGRAW-HILL BOOK COMPANY, Inc.

330 West 42nd Street **New York, N. Y.**

GAERTNER

INFRA-RED SPECTROGRAPH (Littrow Type)

Range .5461 to 15 microns

with

Bilateral Slits of 40 mm clear aperture and provided with micrometer, reading from 0.01 to 3 mm width of opening.

Rocksalt or Potassium Bromide Prisms of best optical quality.

Mirrors are parabolized 10° off axis, focal length 1 m, figured to high accuracy.

Baffled to eliminate stray light.

Cover is air tight except for the breather tubes. All adjustments of slits, wavelength, etc., are made from outside of case.

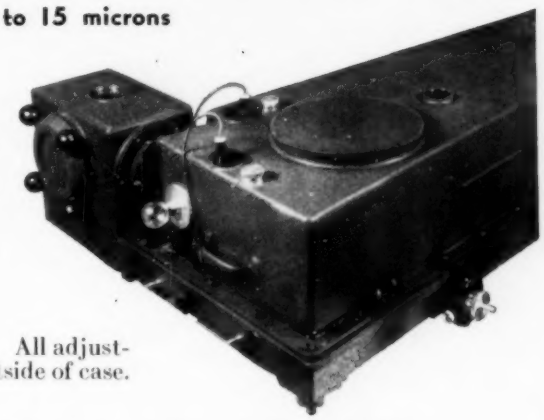

THE GAERTNER SCIENTIFIC CORPORATION

1212 Wrightwood Ave. **Chicago, U.S.A.**

LOW REFLECTION SURFACES

We are now prepared to produce low reflecting surfaces on a commercial basis by the high-vacuum distillation of metallic fluorides.*

By reducing the usual 4% reflection loss at each glass-air surface, a substantial improvement can be made in the light transmission and image forming characteristics of any optical system.

NATIONAL RESEARCH CORPORATION
100 BROOKLINE AVENUE
BOSTON, MASS.

*U. S. Pat. 2,207,656

IMPROVED "SPOTLIGHT" GALVANOMETERS

Rubicon MULTIPLE REFLECTION galvanometers have recently been improved through a redesign of the optical system. The definition of the line-image is now so sharp that readings can be estimated to .1 of a millimeter division.

These sturdy, self-contained galvanometers are available with sensitivities as high as .0006 microampere per millimeter. The scales, which are 100 mm. long, are remarkably proportional. Send for Bulletin 320.

RUBICON COMPANY
ELECTRICAL INSTRUMENT MAKERS
Ridge Ave. at 35th Street Philadelphia, Pa.

INDEX TO ADVERTISERS

The following firms have shown their interest in the advancement of physics through their support of the journals and other services of the American Institute of Physics and its Founder Societies. This should entitle them to consideration by physicists whenever possible.

Name *Page*

BAUSCH & LOMB OPTICAL COMPANY .....Cover 3
Makers of Microscopes, Microtomes, Colorimeters, Refractometers, Spectrometers, Baloptícons, Photomicrographic and Microprojection Apparatus and related instruments. Also makers of Orthogon Eyeglass Lenses for Better Vision.

JAMES G. BIDDLE COMPANY iv
"Jagabi" Rheostats; Adam Hilger and Kipp & Zonen Optical Instruments; "Pointolite" Lamps; Electrical Testing and Speed-measuring Instruments.

CENTRAL SCIENTIFIC COMPANY .....Cover 4
Manufacturers of Cenco Physical Apparatus and Instruments to meet all requirements of University, College and High School Physics Laboratories. Specializing in high vacuum pumps and development of instruments and apparatus for various sciences.

EASTMAN KODAK COMPANY iii
Purified Organic Chemicals for research purposes; Plates for Photography, Photomicrography, Spectroscopy, Photometry, Astronomy; Wratten Light Filters; Cameras and Films.

THE EPPLEY LABORATORY, INC. iv
Standards of e.m.f. (standard cells). Precision electrical instruments; potentiometers, bridges, temperature bridges, volt boxes. Thermopiles and pyrheliometers.

GAERTNER SCIENTIFIC CORPORATION v
Spectroscopes, Spectrometers, Spectrographs, Spectrophotometers, Heliostats, Measuring Microscopes, Comparators, Cathetometers, Reading Telescopes, Interferometers, Chronographs, Dividing Machines, etc.

GENERAL RADIO COMPANY ii
Manufacturers of electronic measuring instruments; vacuum-tube voltmeters, amplifiers and oscillators; wave analyzers, noise meters and analyzers, stroboscopes; laboratory standards of capacitance, inductance and frequency; impedance bridges, decade resistors and condensers; air condensers and variable inductors; rheostats, Variacs, transformers; other laboratory accessories.

LEEDS & NORTHRUP COMPANY i
Manufacturers of Galvanometers, Resistors, Bridges, Condensers, Inductances, Potentiometers, Testing Sets; Temperature Measuring, Recording and Controlling Apparatus; Instruments for Measuring and Controlling Conductivity of Electrolytes and Hydrogen Ion Concentrations.

McGRAW-HILL BOOK COMPANY, INC. v

NATIONAL RESEARCH CORPORATION vi
Specialists in industrial applications of high vacuum in the fields of physics and chemistry; research, design, consulting; low reflecting glass surfaces, special products produced under low pressure.

POLAROID CORPORATION iv
Polaroid experimental kit for demonstrating Polarized light. Hand book.

RUBICON COMPANY vi
Galvanometers, electrometers, potentiometers, Wheatstone and Kelvin bridges, resistance boxes, hydrogen ion and conductivity apparatus.

W. M. WELCH SCIENTIFIC COMPANY iii
Scientific instruments—laboratory apparatus. Catalog lists 10,000 items.